



PART I:

**Synthesis and Characterization of Alkalides
and Electrdes that Contain 15-Crown-5.**

PART II:

Alkali Metal NMR Studies of Alkalides.

By

Mary L. Tinkham

A DISSERTATION

**Submitted to Michigan State University
in partial fulfillment of the requirements
for the degree of**

DOCTOR OF PHILOSOPHY

Department of Chemistry

1985

ABSTRACT

**PART I: Synthesis and Characterization of Alkalides
and Electrides that Contain 15-Crown-5.**

PART II: Alkali Metal NMR Studies of Alkalides.

By

Mary L. Tinkham

Ten crystalline compounds that contain alkali metal ions and 15-crown-5 (15C5) were synthesized and analyzed. These compounds were precipitated from solutions of alkali metals and 15-crown-5 in mixtures of dimethyl ether (Me_2O) and either diethyl ether or trimethylamine. Analyses were in good agreement with the expected stoichiometries of $\text{K}^+(\text{15C5})_2 \cdot \text{Na}^-$, $\text{K}^+(\text{15C5})_2 \cdot \text{Rb}^-$, $\text{Rb}^+(\text{15C5})_2 \cdot \text{e}^-$, $\text{Rb}^+(\text{15C5})_2 \cdot \text{Na}^-$, $\text{Rb}^+(\text{15C5})_2 \cdot \text{Rb}^-$ and $\text{Cs}^+(\text{15C5})_2 \cdot \text{Na}^-$ but deviated somewhat from $\text{K}^+(\text{15C5})_2 \cdot \text{e}^-$, $\text{K}^+(\text{15C5})_2 \cdot \text{K}^-$, $\text{Cs}^+(\text{15C5})_2 \cdot \text{K}^-$ and $\text{Cs}^+(\text{15C5})_2 \cdot \text{Rb}^-$.

Pressed powder D.C. conductivity measurements indicated that these compounds are extrinsic semiconductors with apparent band gaps of 0.5 to 1.7 eV. EPR spectra of $\text{K}^+(\text{15C5})_2 \cdot \text{e}^-$ and $\text{Rb}^+(\text{15C5})_2 \cdot \text{e}^-$ showed a narrow line at $g = 2.003$ for each electride. Magnetic susceptibilities showed that a high fraction of electrons are unpaired in each compound. A "jump" in the electronic χ_m of $\text{Rb}^+(\text{15C5})_2 \cdot \text{e}^-$ between 120 and 140 K may indicate a phase transition.

Tinkham, Mary L.

Solid state alkali metal NMR was used to identify alkalides that were synthesized both by the author and by others. Magic angle spinning (MAS) spectra were obtained for ^{23}Na , ^{39}K , ^{87}Rb and ^{133}Cs NMR. Eleven compounds were identified as sodides and each had the $^{23}\text{Na}^-$ NMR peak of in the range of -56 to -63 ppm. The NMR signal of the complexed cation was observed for the homonuclear sodides $\text{Na}^+\text{C}_{222}\cdot\text{Na}^-$ and $\text{Na}^+(\text{12C}_4)_2\cdot\text{Na}^-$. ^{39}K MAS-NMR studies of potassides provided the first NMR observation of K^- chemical shifts at -105 to -115 ppm. Quadrupolar broadening prevented the observation of a complexed cation signal both for K^+ and for Rb^+ . The Rb^- anion had a frequency dependent NMR peak at -187 to -199 ppm. ^{133}Cs MAS-NMR was used to identify three alkalides and each had a ^{133}Cs NMR peak at +24 to +29 ppm which corresponded to $\text{Cs}^+(\text{15C}_5)_2$. Some samples had additional peaks which corresponded to $\text{Cs}^+(\text{15C}_5)_2\cdot\text{e}^-$ at +505 ppm and Cs^- at -263 ppm. ^{39}K and ^{87}Rb solution NMR spectra of alkalides in Me_2O are also reported.

ACKNOWLEDGMENTS

The author wishes to express her sincere gratitude to Professor James L. Dye for his guidance, encouragement and support throughout this study. I would like to thank the members of Dr. Dye's research group, both past and present, for their cooperation, suggestions and aid. In particular, I wish to acknowledge Zexia Barnes, Steven Dawes, Margaret Faber, Odette Fussá, Rui Huang, Stephan Jaenicke and Iraj Behbahani for their help and moral support. Thanks are also extended to the newer members of the group, Lauren Hill, Jineun Kim, Mark Kuchenmeister and Joseph Skowyra. I also wish to thank Dr. Dye and his group for the fishing trips, the great Asilomar adventure and other group outings which helped to make working together much more enjoyable.

Thanks go to the glass blowers Scott Bancroft, Manfred Langer and Keki Mistry for their speedy and excellent service. The secretaries, Naomi Hack, Carol Zink and especially Margy Lynch, are also acknowledged for their help. The cheerfulness and the helpful attitude of Dorothy Boettger is also greatly appreciated. I also wish to thank the members of the electronics and machine shops.

Special thanks go to Kermit Johnson for his help with the solid state NMR work at Michigan State University. Drs. Klaas Hallenga and Long Dinh Le are also gratefully acknowledged. A special "thank you" goes to Dr. Pat Smith at Dow Chemical Corporation at Midland, Michigan for his initial aid and continuing help in magic angle spinning NMR studies. Thanks go to Professor Eric Oldfield and his group at the University of Illinois for their aid in the ^{87}Rb high field NMR work.

Financial support is gratefully acknowledged from the Department of Chemistry, Michigan State University and from the National Science Foundation (grants DMR 79-21979 and DMR 84-14154).

I would like to thank my family, in particular, my sister Linda, for their faith and encouragement throughout this study. Finally, I would like to thank my friends, Ruby Freed, Bob Kean and especially N.R. Nirmala, for their patience, understanding and support; for without their friendships, this road would have been impossible to travel.

PREFACE

The work covered by this dissertation can be divided into two areas -- each heavily dependent on the other. The first is the synthesis and characterization of new inorganic salts that have either an alkali metal anion (alkalide) or a trapped electron (electride) as the negative species. In both cases the positive ion is an alkali metal cation complexed by macrocyclic organic ligands. Species identification is essential in the characterization of alkalides and electriles to correctly distinguish between pure compounds, mixtures and "junk". Historically, alkalides and electriles have been identified via stoichiometry and optical spectroscopy. Although these techniques have proved satisfactory for most cases, some ambiguity arose for others.

The second portion of this work describes the application of alkali metal NMR as an identification tool for alkalides and electriles. This nuclear specific technique was applied to all alkali metals except lithium. For the most part, it was restricted to the solid state where the "magic angle" sample spinning technique was employed, although some solution experiments were also performed.

Because of the major differences in the background required to understand these two facets of this research, the material is presented in two separate sections, Parts I and II. Each section has historical, experimental and results chapters. A final chapter is used to relate the conclusions that can be drawn from these two sections and to present suggestions for further work.

TABLE OF CONTENTS

	PAGE
List of Figures.	viii
List of Tables.	xi
Part I: Synthesis and Characterization of Alkalides and Electrudes that contain 15-crown-5.	1
Chapter One: Introduction.	1
A. Metal Ammonia Solutions.	1
B. Alkali Metals in Amines and Ethers.	8
C. Properties of Alkalides and Electrudes.	18
Chapter Two: Experimental.	30
A. Reagent Preparation.	30
1. Metals.	30
2. 15-crown-5.	30
3. Solvents.	32
a. Dimethylether and trimethyl- amine.	32
b. Diethylether.	32
B. Synthesis Techniques.	32
1. Glassware preparation.	33
2. Improved synthesis technique.	33
C. Analysis.	38
1. Hydrogen evolution.	40
2. pH titration.	42
3. Flame emission.	43
4. Proton NMR.	43
D. Optical Spectra.	44
E. Pressed Powder Conductivity.	47
F. Electron Paramagnetic Resonance.	48
G. Magnetic Susceptibility.	48
Chapter Three: Results and Discussion.	50
A. Synthesis.	51
B. Analysis.	55
C. Optical Spectra.	60
D. Pressed Powder Conductivity.	73
E. Electron Paramagnetic Resonance.	82
F. Magnetic Susceptibility.	87

	PAGE
G. Results from other Sources.	94
1. Differential Scanning Calorimetry.	94
2. X-ray Diffraction.	95
3. EXAFS and XANES.	97
PART II: Alkali Metal NMR Studies of Alkalides.	102
Chapter One: Introduction.	102
A. Nuclear Properties of Alkali Metals.	103
B. NMR of Alkali Metal Anions in Solution.	105
C. Solid State NMR.	108
D. Identification of a Ceside and an Elec- tride by ^{133}Cs MAS NMR.	115
Chapter Two: Experimental.	120
A. Sample Preparation.	120
1. Solution Samples.	120
2. Model Salts.	121
3. Solid State Samples.	121
B. Instrumentation.	121
1. At Michigan State University.	122
2. At Dow Chemical Corporation.	123
3. At the NSF Regional NMR Center.	124
Chapter Three: Results and Discussion.	125
A. ^{23}Na NMR Spectra.	125
B. ^{39}K NMR Spectra.	132
1. Solution studies.	133
2. MAS studies.	135
C. ^{87}Rb NMR Spectra.	140
1. Solution studies.	141
2. MAS studies.	143
D. ^{133}Cs NMR Spectra.	152
Summary and Suggestions for Future Work.	157
List of References.	164

LIST OF FIGURES

FIGURE		PAGE
1	Models for Species of Stoichiometry M^-7
2	Optical Spectra of Alkali Metals in Ethylenediamine.11
3	Cryptand-2,2,2 and 18-crown-6.14
4	Log K versus Cation Radius in Methanol at 25°C.16
5	Packing of Na^+C222 and Na^- (solid circles) in the crystalline Solid $Na^+C222 \cdot Na^-$19
6	Born-Haber Cycle for Formation of $M^+L \cdot N^-$	20
7	Vacuum Distillation Apparatus for 15-Crown-5 Purification.31
8	Synthesis Apparatus: H Cell.	34
9	Analysis Scheme for Alkalides (A) and Electrides (B).	39
10	Hydrogen Evolution Apparatus.	41
11	Optical Absorption Apparatus.	45
12	Optical Absorption Spectra of Thin Dry Films Made From Solutions of $K^+(15C5)_2 \cdot K^-$ (A) and $K^+(15C5)_2 \cdot e^-$ (B and C) in Methylamine.	62
13	Optical Absorption Spectrum of a Thin Dry Film Made From a Solution of $K(15C5)_{1.3}$ in Methylamine.63

FIGURE		PAGE
14	Optical Absorption Spectra of Thin Dry Films Made From Solutions of $\text{Rb}^+(\text{15C5})_2 \cdot \text{Rb}^-$ (A) and $\text{Rb}^+(\text{15C5})_2 \cdot \text{e}^-$ (B) in Methylamine.65
15	Optical Absorption Spectra of Thin Dry Sodide Films Made From Solutions of $\text{Cs}^+(\text{15C5})_2 \cdot \text{Na}^-$ (A), $\text{Rb}^+(\text{15C5})_2 \cdot \text{Na}^-$ (B), and $\text{K}^+(\text{15C5})_2 \cdot \text{Na}^-$ (C) in Methylamine.66
16	Optical Absorption Spectrum of a Thin Dry Film Made From a Solution of Crystals with Stoichiometry $\text{KRb}(\text{15C5})_2$ in Methylamine.69
17	Optical Absorption Spectra of Thin Dry Films Made From a Solution of $\text{Cs}^+(\text{15C5})_2 \cdot \text{K}^-$ in Methylamine.72
18	$-L_n$ (current) versus $1/T$ for $\text{Rb}^+(\text{15C5})_2 \cdot \text{e}^-$79
19	EPR Spectrum of $\text{Rb}^+(\text{15C5})_2 \cdot \text{e}^-$ at -103°C84
20	EPR Spectrum of $\text{K}^+(\text{15C5})_2 \cdot \text{e}^-$ at -97°C85
21	$1/\chi_m$ versus Temperature for $\text{Rb}^+(\text{15C5})_2 \cdot \text{e}^-$90
22	$1/\chi_m$ versus Temperature for $\text{K}^+(\text{15C5})_2 \cdot \text{e}^-$92
23	DSC Trace for $\text{Rb}^+(\text{15C5})_2 \cdot \text{Na}^-$96
24	K-edge X-ray Absorption Spectrum of $\text{Rb}^+(\text{15C5})_2 \cdot \text{Na}^-$98
25	Diagram Illustrating the Motion of a Typical Internuclear Vector, r_{ij} , when a Solid is Rotated with an Angular Velocity, ω_r , about an Axis Inclined at Angle β^r to H_o111
26	^{133}Cs MAS-NMR Spectra of the Two Crystalline Compounds, $\text{Cs}^+(\text{18C6})_2 \cdot \text{Cs}^-$ and $\text{Cs}^+(\text{18C6})_2 \cdot \text{e}^-$ at 44.24 MHz.118
27	^{23}Na NMR Spectra of Crystalline $\text{Na}^+\text{C222} \cdot \text{Na}^-$ at 52.94 MHz.127
28	^{23}Na MAS-NMR Spectrum of $\text{Na}^+(\text{12C4})_2 \cdot \text{Na}^-$ at 47.61 MHz.129

FIGURE	PAGE
29	^{39}K NMR Spectrum of $\text{K}^+(\text{15C5})_2\cdot\text{K}^-$ in Dimethylether (0.06 M) at 220 K and 8.40 MHz. 134
30	^{39}K NMR Spectra of Polycrystalline $\text{K}^+(\text{15C5})_2\cdot\text{K}^-$ at 180 K. 136
31	^{87}Rb NMR Spectrum of $\text{Rb}^+(\text{15C5})_2\cdot\text{Rb}^-$ in Dimethylether (0.068 M) at 235 K. 142
32	^{87}Rb NMR Spectra of Polycrystalline $\text{Rb}^+(\text{15C5})_2\cdot\text{Rb}^-$ at 65.4 MHz. 150
33	^{133}Cs MAS-NMR Spectrum of an Impure Sample of $\text{Cs}^+(\text{15C5})_2\cdot\text{K}^-$ 153
34	^{133}Cs MAS-NMR Spectrum of $\text{Cs}^+(\text{15C5})_2\cdot\text{K}^-$ at 23.62 MHz. 155

LIST OF TABLES

TABLE		PAGE
I	Alkali Metal Solubilities in Various Solvents.	10
II	Crystallization Conditions and Relative Stabilities of 15-Crown-5 Alkalides and Electrides.	54
III	Analysis Results of Alkalides and Electrides.	57
IV	Results of Optical Absorption Studies of Thin Dry Films.	68
V	Results of Pressed Powder DC Conductivity Measurements.	77
VI	Relative Areas of Rubidium K-Edge Absorption Threshold Resonances.	99
VII	Nuclear Properties of Alkali Metals.	104
VIII	Calculated Chemical Shifts for Gaseous Alkali Metal Atoms and Anions and Observed Chemical Shift of M ⁻ in Solution.	109
IX	Results of ²³ Na MAS-NMR Studies.	128
X	Results of ³⁹ K MAS-NMR Studies.	138
XI	Results of ⁸⁷ Rb MAS-NMR Studies at Three Frequencies.	144
XII	Results of ⁸⁷ Rb NMR With and Without Proton Decoupling.	149
XIII	Results of ¹³³ Cs MAS-NMR Studies.	156

PART I:

**Synthesis and Characterization of Alkalides
and Electrudes that Contain 15-Crown-5.**

PART I

CHAPTER 1 -- INTRODUCTION

The synthesis of crystalline alkalides and electrides is a direct outgrowth of attempts by Dye and coworkers to extend the study of alkali metal-ammonia solutions to other solvents. This chapter will cover a brief history of the development of alkalide and electride chemistry starting with metals in liquid ammonia. The use of macrocyclic complexing agents to increase the solvent range will be discussed as well as the effect of these complexants on general properties. Finally, the synthesis and characterization of alkalides and electrides, prepared as powders or thin films, as well as precipitated crystals, will be reviewed.

A. Metal Ammonia Solutions

The unpublished notebooks of Sir Humphrey Davy show that alkali metal-ammonia solutions were prepared as early as 1808 [1]. These solutions were first described in the open literature by Weyl in 1864 [2]. Since that time, many papers have been written on the properties of metal-ammonia

solutions. The proceedings of six international conferences [3-8] and a number of review articles [9-20] have been published. Although metal-ammonia solutions have been studied rather intensely, several questions remain unanswered. The area of metal-ammonia chemistry is still a very active field both on the fundamental and applied level. For example, the high reducing power of such solutions has been utilized to create new organic and organo-metallic intermediates [21].

Discussions of metal-ammonia solutions are usually restricted to one of three concentration ranges: dilute (infinite dilution to ~1.0 mole percent metal (MPM)), intermediate (1-8 MPM) and concentrated (>8 MPM). These distinctions are drawn on an arbitrary basis since the properties of the solutions change gradually with concentration. In general, dilute solutions have electrolyte behavior and concentrated solutions are metallic. There is a gradual transition from electrolyte to non-metal to metal as the metal concentration is increased. These transitions are usually seen in the intermediate range since the non-metal to metal transition is usually complete at a concentration of 8 mole percent metal.

Liquid ammonia dissolves the following metals: Li, Na, K, Rb, Cs, Ca, Sr, Ba, Yb and Eu. It is universally agreed that the major species in dilute solutions are solvated electrons and metal cations. Indeed, one may avoid most of the cationic effects by introducing electrons by means of

ionizing radiation from an accelerator. The majority of metal ammonia solution studies involve alkali metals. This review will be restricted to such studies.

Metal-ammonia solutions may be studied over a wide range of temperatures and concentrations. Even at the normal boiling point of NH_3 , -33°C , very concentrated solutions of the alkali metals can be made. Solubilities range from 15 MPM for potassium to 65 MPM for cesium for saturated solutions at -33°C . The saturation concentrations change very little with temperature, with the exception of that of cesium, which is found to be completely miscible with NH_3 near 25°C and above. There are miscibility gaps in the phase diagram for the other alkali metals. It has been speculated that all alkali metals would be completely miscible with liquid ammonia at the melting point of the metal. However, most metal-ammonia work is carried out at temperatures at or below the normal boiling point of ammonia. Even with this as a high temperature limit, the temperature range available is quite large. The eutectic temperature of lithium in NH_3 is -184.6°C -- a freezing point depression of over 100 degrees! The concentration is surprisingly high at the eutectic temperature (20 MPM).

The electrical conductivity of a saturated solution of lithium in liquid ammonia exceeds that of liquid mercury at room temperature. The other alkali metals in NH_3 have conductivities almost as high. In concentrated solutions, the

electrical conductivity increases approximately as the cube of the metal content. The conductivity also increases in a nearly linear fashion with temperature, except for the most concentrated solutions of lithium and cesium. In these solutions a slight decrease is observed as the temperature increases.

A second similarity of concentrated metal ammonia solutions and metals occurs in the plasma absorption edge observed by optical reflectance studies. This plasma edge occurs at approximately $10,000 \text{ cm}^{-1}$ at the metal-nonmetal transition but shifts to the blue as the concentration is increased. The color (by reflectance) of concentrated metal solutions is a polished bronze.

Magnetic data for $M\text{-NH}_3$ solutions give rather confusing results. The static magnetic susceptibility shows a weak temperature dependence even in the most concentrated solutions. The derivatives of the EPR signal show an asymmetry of the low field maximum compared to the high field minimum. The change in the A/B ratio is reminiscent of metallic systems. A and B are the respective amplitudes of the low and high field lobes of the first derivative EPR spectra. These changes are observed at relatively low concentrations. The magnetic behavior of metal-ammonia solutions, at any concentration, has not been explained in a satisfactory manner, although Thompson has put forth several models [19].

Dilute solutions (concentrations < 1 MPM) have a characteristic blue color at concentrations of 10^{-6} molar or more. The optical maximum for the solvated electron lies in the near infrared region at 6900 cm^{-1} , but has an asymmetric high energy tail into the visible. This line is completely unaffected by the type of solute at low concentrations. The absorption band is also observed when electrons are produced by ionizing radiation or when ND_3 is substituted for NH_3 . The spectrum is affected by concentration and temperature, and shifts to lower energies as either is increased. Because of the concentration dependence, pulse radiolysis is the preferred method for optical studies of isolated solvated electrons in liquid ammonia.

The specific conductance of M-NH_3 solutions increases with the metal concentration. In very dilute solutions ($< 10^{-2}$ M), the equivalent conductance decreases as expected for a solution that can form ion pairs. One can infer that the cation and electron are truly separated only at concentrations below about 10^{-4} M. Other properties such as susceptibility, activity coefficient and density are nearly the same from one metal to another when compared at the same concentrations. The EPR spectrum of a very dilute solution features a very narrow line with a g -value near the free electron value of 2.0023. As the concentration is increased some interaction between the cation and solvated electron can be observed by the paramagnetic shift in the

alkali metal NMR. Although several models have been postulated for the species in dilute $M-NH_3$ solutions, only one is in reasonable agreement with the various properties mentioned above. This model proposes the formation of ionic aggregates which retain the basic characteristics of M^+ and e_{solv}^- . Species with stoichiometries such as M , M^- and M_2 could form without changing the optical spectrum or molar volume of the solution. This model would then allow for the spin pairing observed in the static susceptibility and EPR measurements as the concentration is increased. Figure 1 gives three models that have been proposed for species of stoichiometry M^- . The first is an example of the ion aggregate model and is EPR active.

Perhaps the most interesting properties of metal-ammonia solutions are found in the intermediate concentration range. In this range, a transition from non-metallic to metallic behavior is observed as the metal concentration is increased. The phase diagram for sodium ammonia solutions shows a liquid-liquid phase separation at 4 MPM sodium at temperatures below 230 K. The more concentrated, less dense metallic phase floats on top of the dark blue, less concentrated electrolytic phase. As the temperature is increased, these phases become miscible. This phase separation has been compared to the liquid vapor phase separation of a metal near its critical point. A review article by Edwards and Sienko [22] discusses the results of supercritical alkali metal studies and the onset of metal-

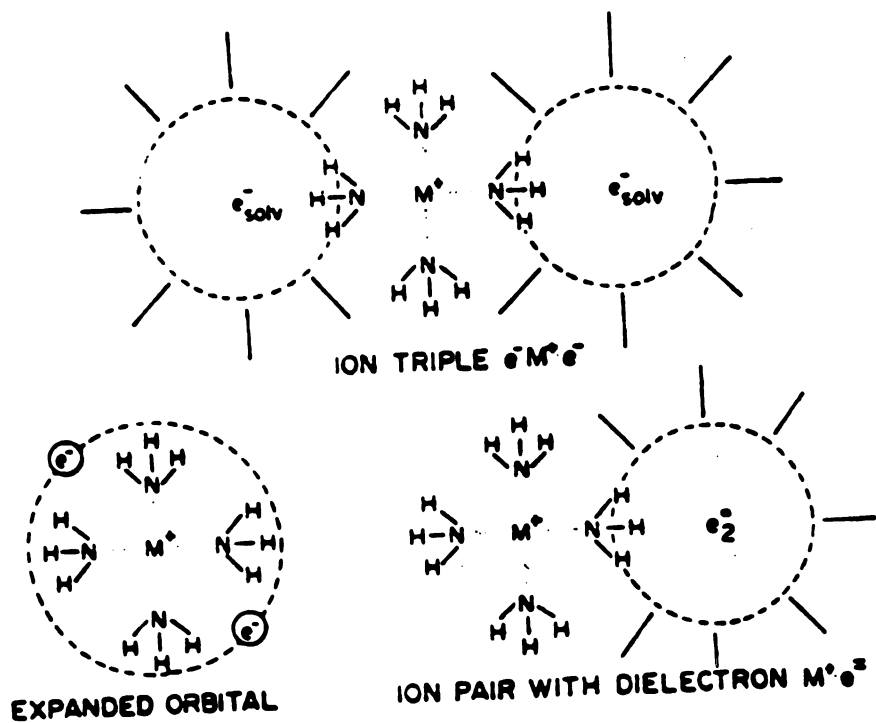


Figure 1. Models for Species of Stoichiometry M^- .

lization. For a very general but thorough discussion on the metal to non-metal transition, the reader is referred to Thompson [19].

As a final note on metal-ammonia solutions, the compounds isolated from concentrated solutions will be discussed. In general, these compounds retain the golden color of the concentrated solution. $\text{Li}(\text{NH}_3)_4$ is the only truly crystalline alkali metal-ammonia compound that has been isolated. The others are of the general formula, $\text{M}(\text{NH}_3)_6$, and contain Ca, Sr, Ba, Eu or Yb. Structures of the hexamines show that the metal atom is octahedrally situated among the six nitrogens. Powder neutron diffraction spectra show that not all N-D distances are equal in $\text{M}(\text{ND}_3)_6$ and the pseudo trigonal axis of rotation of the ND_3 is 13° from being colinear with the M-N bond. $\text{Li}(\text{NH}_3)_4$ has at least two crystalline forms with a solid-state phase transition at 82 K. Both structures are body-centered cubic. Magnetic susceptibility measurements also confirm a structural change at 82 K and suggest magnetic ordering at low temperatures. The 82 K phase transition was not present in $\text{Li}(\text{ND}_3)_4$.

B. Alkali Metals in Amines and Ethers

The range of solvents available for nonaqueous metal solutions is limited by low solubilities and by solvent reduction [5-8,19,20]. Only with lithium in methylamine

can metal concentrations be obtained that are on the order of those obtained in liquid ammonia. For other solvents, concentrations range from millimolar to undetectable. As an example, the solubility of sodium in ethylenediamine is only 2.4×10^{-3} M at 25°C. Table I gives the solubilities of alkali metals in various solvents [23].

The characteristic blue color of dilute metal-ammonia solutions is also observed in metal-amine solutions with concentrations of 10^{-6} M or greater. The optical absorption spectra of these solutions feature either one or two maxima. One of these bands may be attributed to the solvated electron, as in liquid ammonia. The second is shifted to higher energy, and is strongly metal dependent but only moderately dependent on the solvent. The species responsible for the second absorption band has been identified as an alkali metal anion. This species is not simply one of those shown in Figure 1 but rather a true anion with no solvent molecules between the nucleus and the valence electrons. The optical spectra of alkali metals in ethylenediamine solutions are given in Figure 2 [24]. Except for that of lithium, these spectra all show the metal dependent peak attributed to M^- . In the case of lithium, only a solvated electron peak at 7810 cm^{-1} is observed. The spectra of K, Rb and Cs show the maximum due to M^- and a shoulder due to e_{solv}^- . Sodium solutions show only the peak of Na^- .

TABLE I. Alkali Metal Solubilities in Various Solvents.

Metal	Solvent	Solubility (M)	Temperature (°C)
Li	ethylenediamine	0.29	25
	methylamine	$x_{Li} = 0.15$	--
Na	ethylenediamine	2.4×10^{-3}	25
	methylamine	$>2 \times 10^{-4}$	-50
K	ethylenediamine	1.04×10^{-2}	25
	tetrahydrofuran	5×10^{-6}	24
Rb	ethylenediamine	1.31×10^{-2}	25
Cs	ethylenediamine	0.054	25
	methylamine	$>2 \times 10^{-3}$	-50

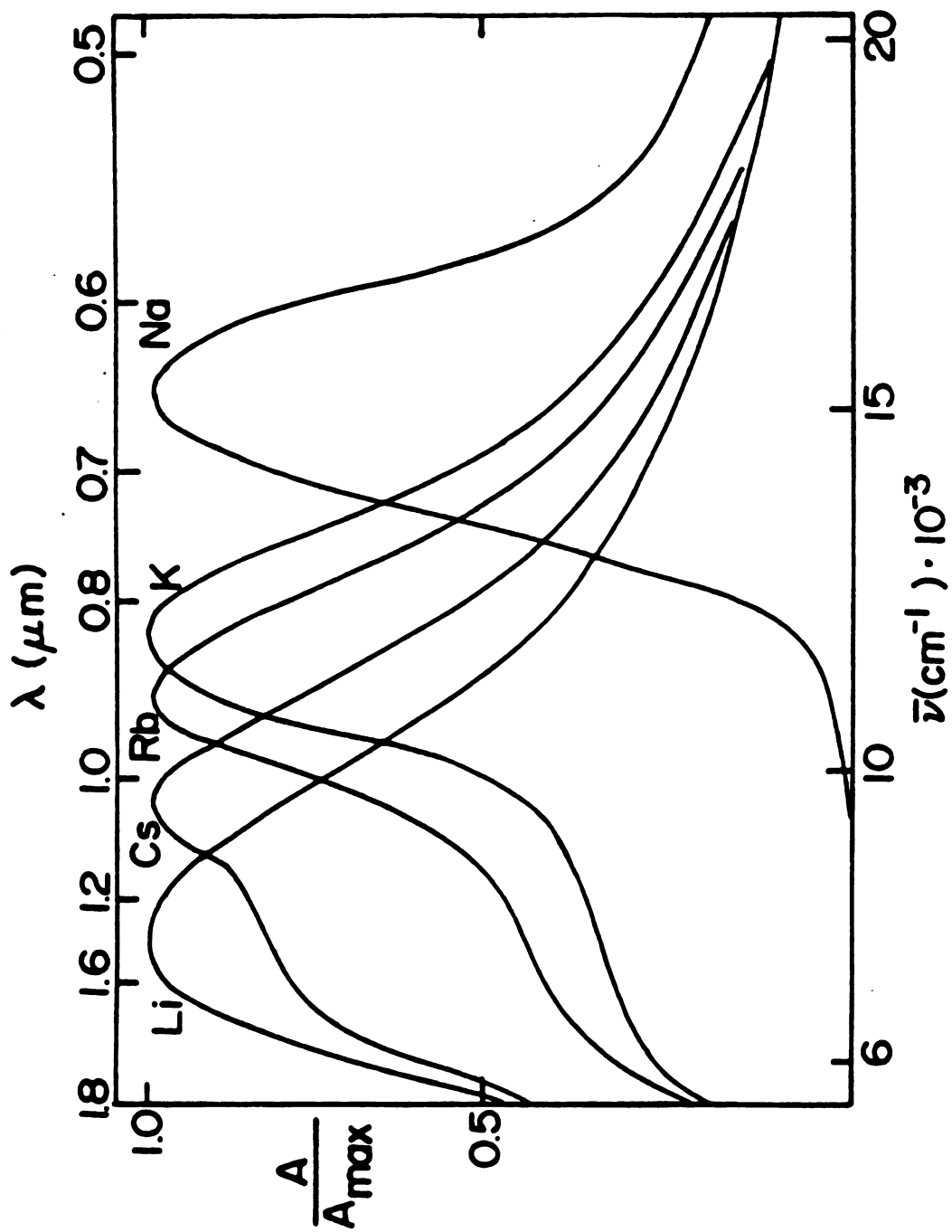


Figure 2. Optical Spectra of Alkali Metals in Ethylenediamine.

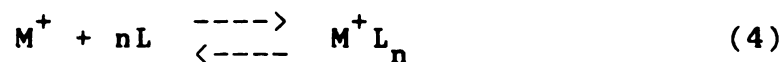
Further evidence of the existence of M^- is found in the EPR spectra of solutions which contain only the metal dependent optical band. In contrast to the strongly paramagnetic ammonia solutions, these solutions were diamagnetic with very weak EPR signals. The filled ns^2 orbital of M^- would satisfy the conditions necessary to give these spectra.

Other evidence is found in the oscillator strength, electrical conductivity and solubility studies. The oscillator strength has been measured for Na in ethylenediamine (EDA) and was found to be twice that of e_{solv}^- . The conductance of these solutions decrease with increasing concentration as expected for electrolytes. Although this behavior indicates ion pairing as with normal salts, the extent is less than expected. This would occur for ions with large closest approach values. The distance for sodium in methylamine (MA) exceeds 6 Å, an indication that Na^- is a large ion. Solubility studies show that sodium metal will not dissolve in 1,2-methoxyethane alone. However, the equimolar Na-K alloy does dissolve. This can readily be explained by the formation of K^+ and Na^- . The most conclusive evidence for M^- is found in the alkali metal NMR spectra of these solutions. The NMR spectra feature a peak with a chemical shift that corresponds well to the theoretical value of M^- . Further background and the results of alkali metal NMR studies are deferred until Part II of this dissertation.

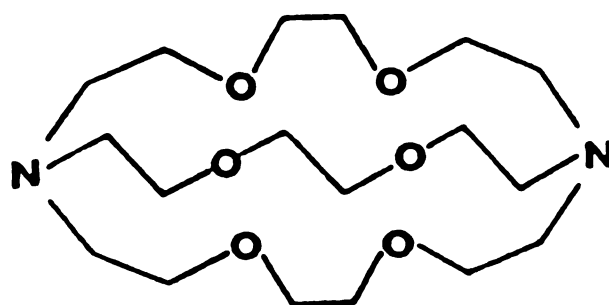
Solvation of alkali metals in amines and ethers may be described by the following equilibria:



where M_{solv} is the "monomer" and probably represents a contact ion pair between M^+ and e_{solv}^- [25]. This species has a characteristic EPR signal with alkali metal hyperfine coupling, and is observed to be present only in very low concentrations. To increase the solubilities of alkali metals, organic complexing agents were used. These ligands, L, introduce a fourth equilibrium



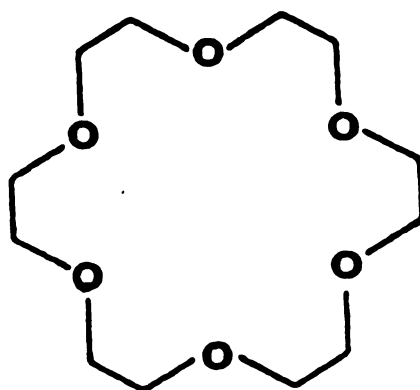
which drives equations (1) and (3) to the right. Two main classes of complexants have been used for this purpose, crown ethers and cryptands, originally developed by Pedersen [26] and Lehn and coworkers [27], respectively. Figure 3 features a representative molecule from each class. Most commonly, crown ethers are cyclic ethers with alternating $-\text{CH}_2-\text{CH}_2-$ groups and oxygens. Their abbreviated names reflect the ring size and number of oxygens. For



1

2,2,2 Cryptand

(C₂₂₂)



2

18-Crown-6

(18-C-6)

Figure 3. Cryptand-2,2,2 and 18-Crown-6.

example, 18-crown-6 (18C6) is an eighteen member ring containing 6 oxygen atoms. The crown ethers may also have alkyl or benzo groups attached to the ring. The cryptands are three dimensional complexants that consist of ethyl ether linkages between two tertiary nitrogens. The generic abbreviation for cryptands is C-m,n,o where m, n and o are numerical representations of the number of $-\text{CH}_2\text{CH}_2\text{O}-$ groups in each strand between the two nitrogens. Crown ethers have been used not only to increase alkali metal solubility but also as solvents for alkali metals. Sodium was found to dissolve in 12-crown-4 to form stable, dark blue solutions. Potassium, rubidium and cesium form metastable solutions in 12-crown-4 [28]. Edwards and coworkers studied Na^- and Rb^- in these two component metal solutions [29].

Crown ethers and cryptands have ion selectivity based largely on their cavity sizes. The hole diameter of 18-crown-6 is large enough to accommodate either Na^+ or K^+ but 18-crown-6 shows a preference for K^+ . X-ray diffraction studies of the complexes of alkali halides show a ring distortion and loss of symmetry as one goes from K^+ to Na^+ . The larger cations, Rb^+ and Cs^+ , are unable to enter the cavity and can give metal:complexant ratios other than 1:1. The complexation constant as a function of cavity size is graphically represented in Figure 4 [30]. Because of their larger complexation energies, cryptands show a higher degree of cation specificity than the crown ethers. The

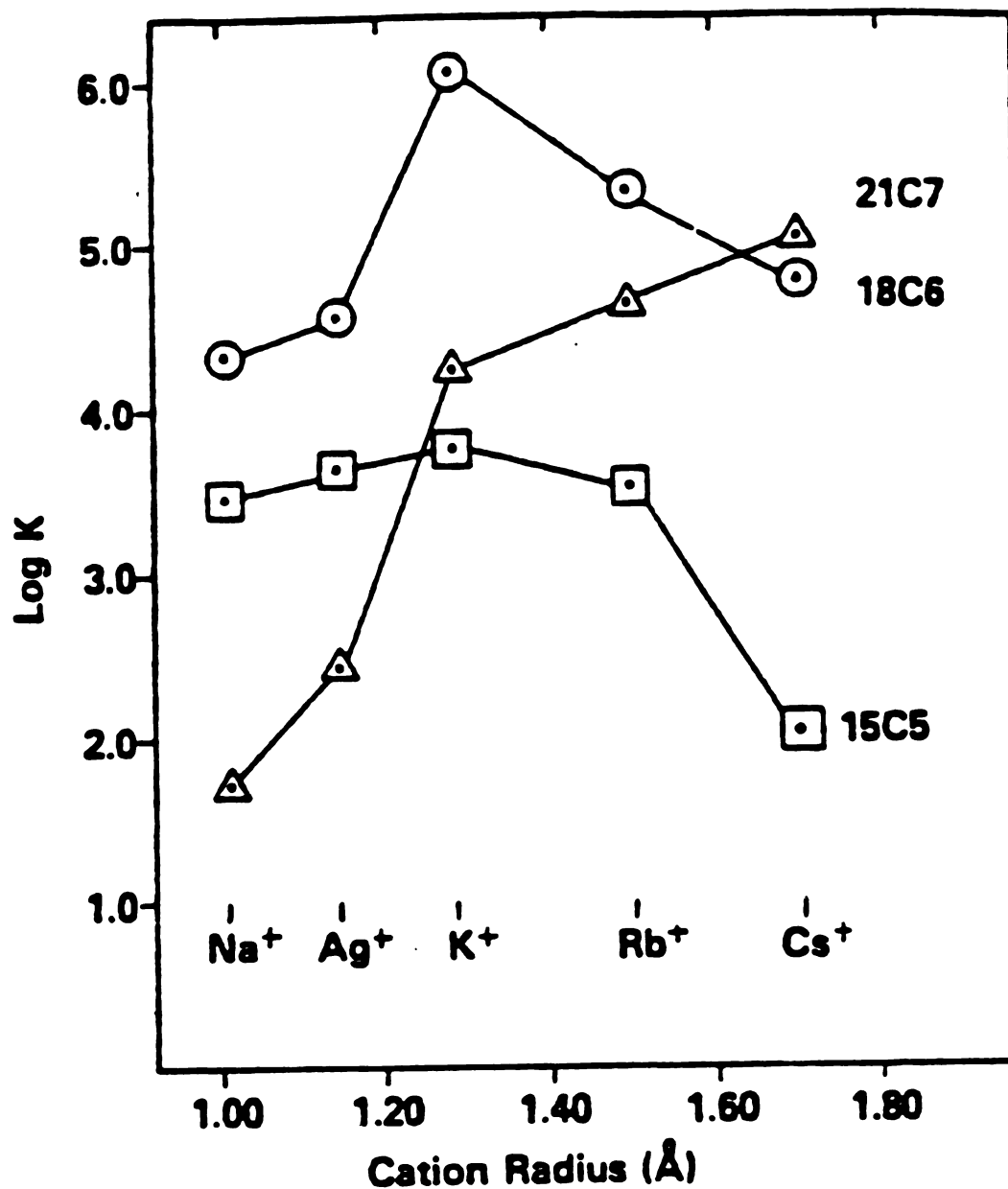


Figure 4. Log K versus Cation Radius in Methanol at 25°C.

formation constants ($\log K$) for cryptands range from 1.8 to almost 10 in methanol. The maximum for crown ether in methanol is slightly more than 6 for K^+18C6 . Since the cryptands have 3-dimensional cavities they tend to form only 1:1 complexes. However, in some cases, more than one ion can occupy a single cavity.

The optical absorption spectra of metal solutions with crown ethers or cryptands present are temperature dependent. The absorption maxima shift to higher energies as the temperature is decreased as for dilute metal-ammonia solutions. The cryptand or crown ether concentration also influences the observed spectra. In solvents where the metal is insoluble, addition of complexant gave M^- and/or e_{solv}^- optical bands. When the concentration of complexant exceeded the amount of dissolved metal, the e_{solv}^- band increased. The conditions needed for this observation are described by equilibria 1-4.

The use of complexing agents in nonaqueous metal solutions not only provided accessibility to new solvent systems but also opened up the possibility of the formation of new compounds. When a solution of a pure metal in ammonia or other solvent is evaporated, the electrons recombine with the cation to form metal films or powders. The presence of a complexing agent inhibits this reaction because of the energy required to break the cation-ligand bonds. The synthesis and characterization of compounds of this type are discussed in the next subsection.

C. Properties of Alkalides and Electrides

A golden precipitate forms from a solution of sodium and cryptand-2,2,2 (C222) in ethylamine as it is cooled below -15°C [31,32]. The precipitate, which was first observed in 1974, was the first crystalline compound which contained an alkali metal anion and has the formula $\text{Na}^+\text{C222}\cdot\text{Na}^-$. The parent compound has been fully characterized; even the crystal structure has been determined. The packing of $\text{Na}^+\text{C222}$ and Na^- is represented in Figure 5 [32]. The sodium cation is located in the center of the cryptand, which has its three strands twisted to give an antiprismatic arrangement and to allow a closer fit to the sodium cation. These "expanded" cations are closest-packed in ABCABC repeating layers. The sodium anions are located in the pseudo-octahedral holes of the lattice. The van der Waals contact distances in the crystal suggest that the radius of Na^- is about 2.6 Å. Since $\text{Na}^+\text{C222}\cdot\text{Na}^-$ forms isothermally at 0°C from sodium and C222 in solution, the Gibbs free energy must be negative for the following reaction:



Estimates of the enthalpy, free energy and entropy were made based upon a modified Born-Haber cycle [33]. The cycle is diagrammed in Figure 6 and initial calculations

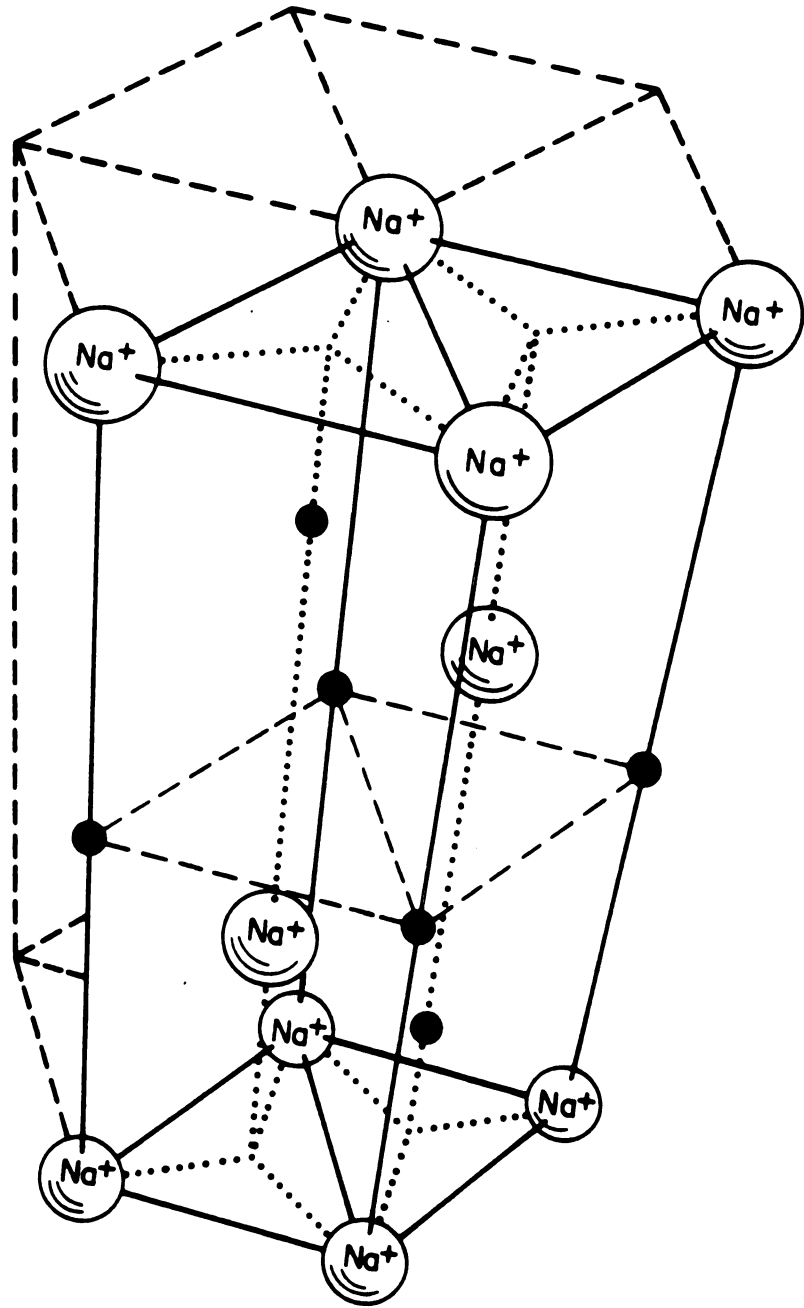


Figure 5. Packing of Na^+ C222 and Na^- (solid circles) in the Crystalline Solid Na^+ C222 \cdot Na^- .

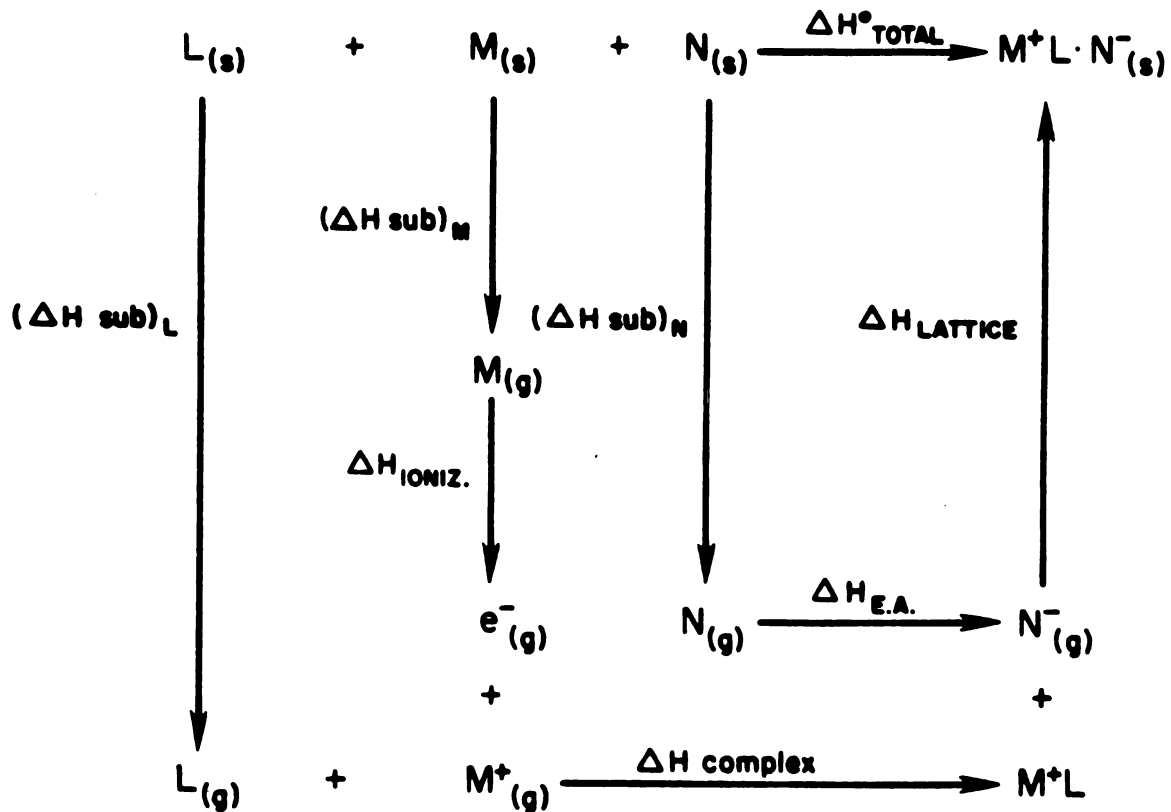


Figure 6. Born-Haber Cycle for Formation of $M^+L \cdot N^-$.

suggested that $\text{Na}^+\text{C222}\cdot\text{Na}^-$ is unstable to disproportionation to sodium metal and cryptand by 22 kJ mol^{-1} , a measure of the error in these estimates, since the compound is stable. Schindewolf and coworkers developed a sodium electrode [34-36] which permitted the cell potential of reaction (5) to be measured directly. It was found that the estimated entropy value was $100 \text{ J mol}^{-1} \text{ K}^{-1}$ too low, probably due to errors in the estimation of the solvation or crystal entropy [37]. The observed value of ΔG_{298}° was -7.1 kJ mol^{-1} .

Estimates of thermodynamic stabilities were made for several alkalides which utilize cryptands [23] or crown ethers [38]. Cation radii were estimated by Lehn's method using the ligand thickness so that the Kapustinskii equation could be used to calculate the lattice energies. Because of errors in the method, these stability estimates serve only as guidelines for synthesis rather than as hard and fast predictions. For example, $\text{Li}^+(\text{12C4})_2\cdot\text{Cs}^-$ is calculated to be twice as stable as $\text{Cs}^+(\text{12C4})_2\cdot\text{Li}^-$. Therefore, if a lithide is desired, a different complexing agent and cation should be chosen.

Subsequent alkalides were prepared by one of three different methods [25,39]. The first is the gradual cooling with or without a solvent composition change to precipitate crystals [39-44]. The stoichiometry of the resultant crystals was not necessarily the same as that of the solution. The second method is slow solvent evapora-

tion to yield powders and films with the same stoichiometry as the solution [45]. The third method is direct vapor deposition of the metal and complexant onto a substrate [49,50]. The latter method requires either a solid state reaction or a gas phase reaction near the surface of the substrate. By increasing the complexant to metal ratio, electrides may be made by any of these methods.

Films for optical absorption spectra of alkalides and electrides were first made by flash evaporation of solutions of metals and complexant in stoichiometric amounts. Later, crystalline compounds were introduced directly into the optical apparatus and redissolved [51-53]. Films were made by flash evaporation as before. There exists the possibility that the films do not contain the same species as the crystals that are dissolved to produce the solution. The maxima of the resultant spectra were compared to the spectra of pure alkali metals in solution. Films from $\text{Na}^+\text{C222}\cdot\text{Na}^-$ solutions yield spectra featuring an absorption band at $15,000\text{ cm}^{-1}$ with a pronounced shoulder at $18,900\text{ cm}^{-1}$. A small but distinct peak at $24,500\text{ cm}^{-1}$ was also observed. Decomposition of the films resulted in the loss of all spectral features. Films of potassium, rubidium or cesium with C222 were prepared and are considerably less stable. The spectrum of each of these films consisted of a single asymmetric peak and showed neither a high energy shoulder nor an additional high energy peak. The absorption maxima were at $11,900$, $11,600$, and $10,500\text{ cm}^{-1}$ for K^- ,

Rb⁻, and Cs⁻, respectively. These locations correspond well to the M⁻ bands in ethylenediamine (EDA) at 12,000, 11,200 and 9,800 cm⁻¹. Na⁻ in EDA solutions has an absorption band at 15,400 cm⁻¹ but no other band or shoulder. The similarity between the homonuclear alkali films and the solution spectra lead to the utilization of optical spectra as an identification tool for heteronuclear alkali films.

Films from solutions of K-Na-18C6 in methylamine gave a broad absorption band at 13,300 cm⁻¹ with a shoulder at 9,000 cm⁻¹ [52]. The main band lies intermediate to the expected locations of Na⁻ and K⁻. The crystals were found to have up to 18% solvent content. This system was resynthesized by the author to produce solvent-free crystals with 1:1:1 stoichiometries [51]. Films made from solutions of the pure crystals had a narrower optical maximum at 14,000 cm⁻¹ with no low energy shoulder. Although this compound was presumed to be a sodide, a clear assignment could not be made. The position of the maximum required a 1000 cm⁻¹ red shift of Na⁻ from the homonuclear C222 film or an 1100 cm⁻¹ blue shift for K⁻. The maximum position is even further shifted from the 16,700 cm⁻¹ peak observed for films made from solutions of sodium 18-crown-6 in a 2:1 mole ratio. The compound was presumed to be a sodide because of the selectivity of 18-crown-6 for potassium rather than sodium and the greater stability of Na⁻ compared with K⁻.

Other heteronuclear alkalides also have changes in the position of the absorption maxima from those in solution. $\text{Cs}^+(\text{18C6})_2\cdot\text{Na}^-$ has a sharp peak at $14,600\text{ cm}^{-1}$ while $\text{Rb}^+\text{18C6}\cdot\text{Na}^-$ has a maximum at $13,800\text{ cm}^{-1}$. These compounds were also thought to be sodides. In the case of rubidium and cesium with 18-crown-6, two peaks are observed. One covers a 1000 cm^{-1} range with its maximum at $11,500\text{ cm}^{-1}$. This band is asymmetric with the center at $12,000\text{ cm}^{-1}$. The second peak occurs at 9000 cm^{-1} and was assigned to trapped electrons. Neither Rb^+ nor Cs^+ can enter the crown ether cavity completely and the anion assignment cannot be made without ambiguity. Shifts in the absorption maxima may be due to cation-anion interaction. Crown ether complexes can have axial symmetry, which would allow exposure of the cation above and below the ring. Cations complexed with 2 crown molecules should be more shielded and may disturb the anion environment less. That this is not necessarily the case is seen with 12-crown-4 sandwich sodides. Dry films of $\text{K}^+(\text{12C4})_2\cdot\text{Na}^-$ showed two maxima at $13,100$ and $17,000\text{ cm}^{-1}$ [38]. Films prepared from $\text{Na}^+(\text{12C4})_2\cdot\text{Na}^-$ also had two absorption peaks but these were slightly shifted from the heteronuclear peaks at $13,500$ and $17,500\text{ cm}^{-1}$ [54]. The origin of the higher energy peak is unknown, but it is reminiscent of the shoulder seen with $\text{Na}^+\text{C222}\cdot\text{Na}^-$.

The cation-anion interaction should be less for cryp-
tated cations than for those salts with the cations

complexed by crown ethers. Since in the former case the cation is complexed by a three dimensional complexant, one would expect less interaction of the cation with its surroundings and smaller shifts in the absorption maximum location of the anion for these salts. However, this is not the case as seen in the $M^+C222 \cdot Na^-$ compounds. The peak location for $K^+C222 \cdot Na^-$ is red-shifted 300 cm^{-1} from that of $Na^+C222 \cdot Na^-$ while in $Rb^+C222 \cdot Na^-$ the absorption is shifted to $14,000 \text{ cm}^{-1}$.

The first optical absorption spectrum of an electrider was that of a film made from a solution of potassium and cryptand-222. The maximum at 7400 cm^{-1} was in the near infrared, as expected for a trapped electron. As the potassium/cryptand mole ratio increased from 1 to 2, a second band corresponding to K^- appeared. At a mole ratio of 2 only the K^- peak was observed [55]. Since that time a number of electrider films have been prepared. The observed spectra fall into one of two categories -- localized or "metallic" behavior. The localized electrideres have absorption maxima which correspond to traps of at least 0.4 to 0.6 eV depth. These absorption bands tend to be broad, indicative either that electron-electron interactions may be important or that the excited state is delocalized. These electrons may also undergo fast exchange with adjacent trapped electrons but not on the optical time scale. The "metallic" electrideres give absorption spectra similar to those of concentrated metal-ammonia solutions.

The absorbance remains high in the infrared, out to at least 3000 cm^{-1} . This suggests electron delocalization or at least shallow traps. This behavior has been observed from certain $\text{K}^+\text{C}_{222}\cdot\text{e}^-$ films and films from solutions with stoichiometries of $\text{Li}_2\text{C}_{211}$ and $\text{Cs}_2 \text{ 18C6}$. It has not been possible yet to verify the "metallic" behavior of crystalline electrides by D.C. conductivity measurements because of their instability. However, powders of these stoichiometries have large microwave power absorptions that would be expected for conducting samples.

The golden appearance of $\text{Na}^+\text{C}_{222}\cdot\text{Na}^-$ suggested that it may be metallic. However, a plot of log resistance versus $1/T$ had a slope that corresponded to a semiconductor with a band gap of 2.4 to 2.5 eV. Extrapolation to infinite temperature gave a specific conductivity greater than $10^6 \text{ ohm}^{-1} \text{ cm}^{-1}$, an indication that $\text{Na}^+\text{C}_{222}\cdot\text{Na}^-$ is an intrinsic semiconductor. D.C. conductivity measurements of pressed powders indicate that all alkalides behave as semiconductors. Reported band gaps range from 0.89 to 2.6 eV. However, most alkalides have much lower specific conductivities of 10^{-2} to $10 \text{ ohm}^{-1} \text{ cm}^{-1}$ at infinite temperature than expected for intrinsic semiconductors. The observed electrical conductivity is probably due to defect electrons which are trapped at energies much closer to the conduction band rather than from the valence electrons in M^- , thereby giving extrinsic semiconductor behavior. Electrides, prepared as powders by solvent evaporation, also behave as

semiconductors with band gaps of 0.5 to 0.8 eV. The conductivity of electrider samples may also arise from "defect electrons" rather than from the bulk of trapped electrons in the sample. The first crystalline electrider, $\text{Cs}^+(\text{18C6})_2 \cdot \text{e}^-$, had a specific conductance intercept at infinite temperature of $\sim 10^2 \text{ ohm}^{-1} \text{ cm}^{-1}$ with a band gap of $0.9 \pm 0.1 \text{ eV}$. Therefore, $\text{Cs}^+(\text{18C6})_2 \cdot \text{e}^-$ has characteristics that lie between extrinsic and intrinsic semiconductivity [42,53].

The ns^2 electronic configuration of alkalides predicts that they are EPR inactive. Samples of $\text{Na}^+\text{C222} \cdot \text{Na}^-$ are indeed diamagnetic and have no appreciable EPR signal. Some samples of $\text{K}^+\text{18C6} \cdot \text{Na}^-$ [51] and $\text{Rb}^+\text{18C6} \cdot \text{Na}^-$ [53] showed comparable strong EPR signals with the presence of fine structure. This structure is due to the hyperfine splitting of the signal by the interaction of trapped electrons with the K^+ or Rb^+ nucleus. The presence of hyperfine splitting is preparation-dependent and is not evident in all samples. In most cases the EPR spectrum of an alkalide sample consists of a single, narrow line near the free electron g-value. Sometimes a second broader band is superimposed on the first, indicating the presence of two or more trapping sites. In general, the EPR spectra of alkalides appear to arise from trapped electrons rather than from intrinsic structural features of the crystals.

In contrast to alkalides, most electrides have very strong EPR signals. Powders of $\text{Li}^+\text{C211} \cdot \text{e}^-$ had microwave

power absorption similar to those of powdered metals [56]. The $\text{Cs}^+(\text{18C6})_2 \cdot \text{e}^-$ EPR spectra featured a single Dysonian line at $g = 2.0023$. The line became more symmetrical at lower temperatures. The width of the line was only 0.48 G, which indicated well-defined local trapping of the electrons [53]. Samples of crystalline $\text{K}^+\text{C222} \cdot \text{e}^-$ and $\text{Rb}^+\text{C222} \cdot \text{e}^-$ gave such strong EPR signals that only a very few crystals would saturate the detector of the spectrometer [50].

Magnetic susceptibility measurements of alkali crystals also show that alkalis are diamagnetic. Some paramagnetism of defect electrons is usually evident at low temperatures. The electrides show a wide range of magnetic properties. $\text{Cs}^+(\text{15C5})_2 \cdot \text{e}^-$ has low temperature deviations from the Curie-Weiss law that allow it to be classified as an antiferromagnetic material [57]. Crystalline $\text{K}^+\text{C222} \cdot \text{e}^-$ is best described as a Pauli paramagnetic compound. At low temperature there is some adherence to the Curie law but the susceptibility quickly goes to a metal-like temperature-independent value as the temperature is increased. $\text{Rb}^+\text{C222} \cdot \text{e}^-$ behaves very much like the potassium electride but the Curie-Weiss behavior extends over a larger temperature range. The electrical conductivities of these two salts were too high to measure by the available methods, a further indication that $\text{K}^+\text{C222} \cdot \text{e}^-$ and $\text{Rb}^+\text{C222} \cdot \text{e}^-$ are either metallic or near the metal-nonmetal borderline [50].

The object of Part I is to describe the synthesis and characterization of new alkali and electride salts. Characterization techniques include elemental analysis and optical absorption spectroscopy as identification tools and D.C. conductivity measurements for all compounds. Magnetic susceptibility measurements and EPR spectra were recorded for those compounds thought to be electrides. The results of these studies for 10 new alkali metal-crown ether systems are reported.

PART I

CHAPTER TWO -- EXPERIMENTAL

A. Reagent Preparation

1. *Metals* - Sodium, potassium and rubidium under argon were purchased from Alpha Ventron Products in 5 gram break-seal ampules. Total purity was 99.95% for each metal. Cesium metal was obtained as a gift from Dow Chemical Corp. and had been previously transferred into ~5 gram sealed glass ampules. Each metal was further distributed to smaller tubing following the procedure outlined by Issa [52]. Desired quantities of metal were obtained by isolating calculated lengths of metal inside of tubing that had premeasured inner diameters.

2. *15-Crown-5* - (15C5 or IUPAC 1,4,7,10,13-pentaoxacyclopentadecane) was distilled at 85-90°C under dynamic vacuum. The apparatus for the distillation is given in Figure 7. The crown ether was pipetted into the bottom of the apparatus without further purification. The apparatus was evacuated to $\sim 2 \times 10^{-5}$ torr before submerging the lower half into a preheated oil bath at the desired temperature. The cold finger was cooled by flowing dry nitrogen gas

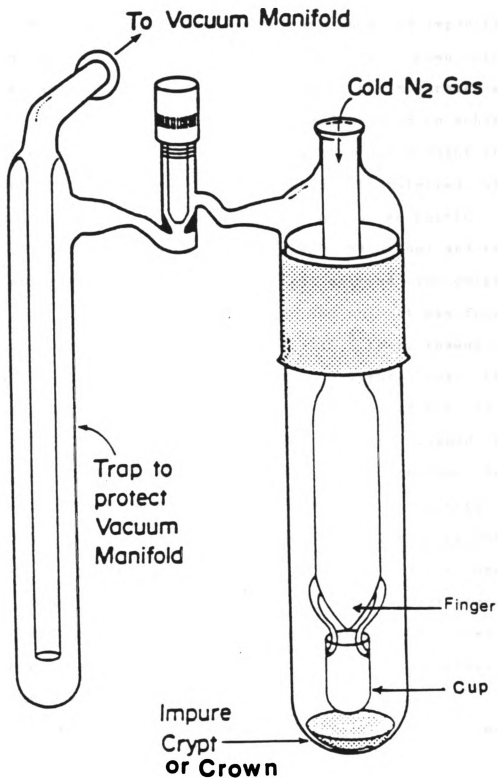


Figure 7. Vacuum Distillation Apparatus for 15-Crown-5 Purification.

at 0°C. The temperature of the nitrogen should be warm enough to avoid condensation of any unwanted impurities (such as H₂O) onto the cold finger. When the crown ether had completely distilled into the bucket, the apparatus was closed, removed from the oil bath and allowed to achieve thermal equilibrium. The entire apparatus was brought into an inert atmosphere box and the crown was transferred with a disposable pipet from the bucket to a storage bottle.

3. *Solvents* - a. Dimethyl ether (Me₂O; Matheson) and trimethylamine (TMA; Matheson) were first stirred over calcium hydride at -20°C for several hours. The solvent was frozen in liquid nitrogen, pumped to $<4 \times 10^{-5}$ torr, thawed and stored at -78°C overnight. The solvent was then transferred to flasks containing an excess of NaK₃ alloy and about 0.5 gram diphenyl ketone, frozen, pumped and stored overnight, before transferring to another NaK₃ bottle. After the solution maintained the characteristic blue color of the benzophenone dianion-ketyl mixture for 2 consecutive cycles, the solvent was transferred to heavy walled glass storage bottles or stainless steel storage tanks. The solvent was then subjected to several freeze-pump-thaw cycles until the initial pressure at pumping was less than 1×10^{-4} torr.

b. Diethyl ether (ethyl ether, anhydrous, Mallinckrodt, Inc.) was treated in the same manner as dimethyl ether and trimethylamine. Final storage was over NaK₃ alloy without diphenylketone.

B. Synthesis Techniques

1. *Glassware* - All glassware was first rinsed with a hydrofluoric acid cleanser solution (5% HF (28M), 33% HNO₃ (16M) and 62% deionized water, by volume) then immediately rinsed six times with deionized water. The glassware was filled with freshly prepared aqua regia (3 HCl:1 HNO₃, by volume) and left overnight. The aqua regia was discarded and glassware was rinsed six times with deionized water followed by six rinses with conductance water (house deionized water which had been further deionized with a Crystalats Deeminizer and distilled through a high reflux ratio column to less than 1 ppm impurity) and dried in a 450°F oven overnight.

2. *Improved synthesis technique* - The general synthesis scheme for the preparation of alkalides and electriles has been fully described [51]. This section is used to point out the improvements made over this general scheme by the use of a simpler apparatus called an H-cell (Ace Glass) and a new solvent system. The H-cell, shown in Figure 8, was modified from the factory issue to better accommodate the low temperature synthesis of alkalides and electriles. First, the angle between chambers A and B was increased from 90° to about 120° with respect to the horizontal connection. Second, the distance between the stopcock and horizontal was increased by 7-8 cm to allow complete

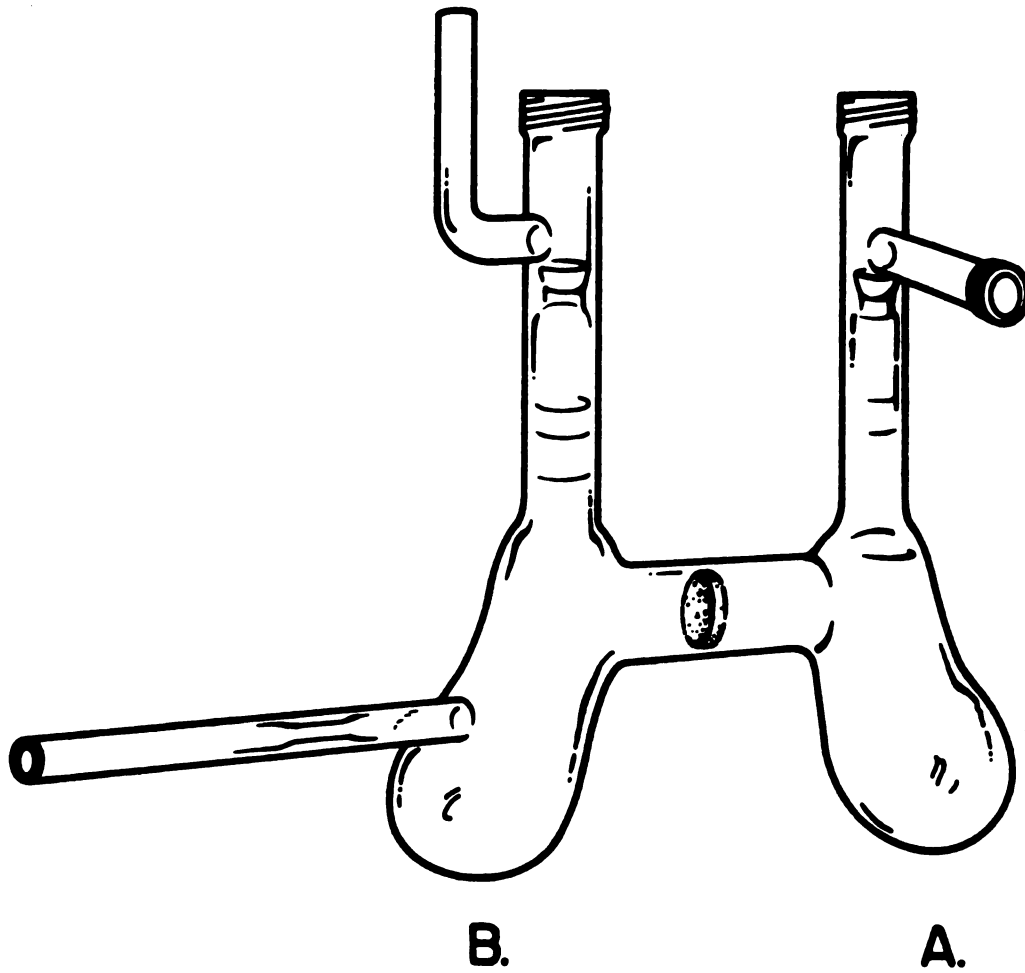


Figure 8. Synthesis Apparatus: H Cell.

cooling of the frit without cooling the stopcocks. Lastly, a 9 mm OD side arm was added to one of the chambers for metal introduction. The size of the H-cell is its main advantage. H-cells are small enough to allow entry into the inert atmosphere box so that the complexants are never exposed to atmosphere but can be loaded into the synthesis apparatus under the dry helium atmosphere. Syntheses involving lithium are also greatly simplified by direct loading of the lithium in an inert atmosphere box [50].

The 15-crown-5 was loaded through the stopcock into chamber A with a disposable pipet. The amount of crown ether was determined by mass difference of the storage vial. A premeasured amount of metal, sealed in a 3 or 4 mm OD scribed glass tubing was broken and placed in the metal sidearm. The H-cell was closed and sidearm capped with a 3/8" Ultra-torr Union (Cajon) and a closed end glass cap. The H-cell could then be removed from the dry box and evacuated to 2×10^{-5} torr. The Ultra-torr union and glass cap were removed by making a vacuum seal on the sidearm. A metal mirror was made in chamber B by gently heating the remaining sidearm until all metal had distilled into B. A final seal was made at the constriction and the H-cell allowed to thermally equilibrate.

The use of dimethyl ether instead of methylamine improved the stability of the alkali and electride solutions. Working temperatures were increased from -40°C with MA to -10° to 0°C with Me_2O . This allowed for faster dis-

solution of the alkali metal and generally shorter synthesis times. Chamber A of the H-cell was cooled to $<-30^{\circ}\text{C}$ and ~10 ml dimethylether was distilled onto the now frozen 15-crown-5. The apparatus was closed and warmed to -10°C in a dry ice-isopropanol bath. When the crown was completely thawed and dissolved, the solution was poured onto the metal mirror in B. Me_2O was distilled from B to A and then poured back into B several times to insure complete solution of the crown. The metal mirror was dissolved by gentle agitation of the H-cell. Complete dissolution took 0.5 to 3 hours at -10°C . When no trace of the metal mirror could be seen, the entire solution was poured into chamber A. The total volume of the solution was reduced to a small viscous puddle (~1-3 ml) by distilling the excess Me_2O to a waste bottle. The cell was cooled to less than -30°C . If there was any precipitation of material, more Me_2O was added to yield a homogeneous solution.

Diethyl ether (DEE) or trimethylamine (TMA) were added as co-solvents for crystallization. It is important to keep the DME solution temperature well below the DME boiling point of -27°C to avoid reverse distillation. The co-solvent was distilled, a small portion at a time, with the H-cell being shaken between additions to insure proper mixing. Total volume of co-solvent did not exceed 7 ml. The H-cell was then packed in dry ice for 3 to 12 hours.

The H-cell was then checked for the formation of crystals. If no crystals were present, the solution was further concentrated by removal of the solvent to a waste bottle. The H-cell would again be stored at -78°C for several hours. After the formation of crystals had stopped, the mother liquor was poured into B and then distilled into a waste bottle.

The wash solvent for the crystals was the same as the co-solvent. Fresh solvent was distilled onto the crystals, the cell shaken to insure mixing and the solvent decanted to chamber B. The solvent was then distilled from B to A and decanted to B to remove any soluble impurities from the crystals. This distill-decant procedure was repeated several times until the solvent became colorless. Finally the solvent was distilled from B to a waste bottle until the H-cell was solvent free. The crystals were further dried by dynamic pumping to 2×10^{-5} torr. If the crystals had sufficient thermal stability, the H-cell was allowed to warm to ambient temperature for several minutes while pumping. During pumping, the cell was repetitively shaken and tapped to free crystals from adherence to the walls.

Crystals were harvested by transferring into either evacuable storage tubes or glass vials. The most stable compounds could be taken into the inert atmosphere box and stored at -40°C in the freezer that is located in the box. Compounds with greater temperature sensitivity were transferred to evacuable storage tubes in a nitrogen glove

bag. The storage tubes were evacuated and individual sample fingers were sealed off. These compounds were stored at -80°C .

Some syntheses were made in the more complex synthesis apparatus called the "cow" which features an additional sample storage tube chamber. This apparatus has the advantage of keeping the crystals under vacuum until characterization studies were performed. The synthesis procedure is identical to the H-cell preparation with the exception that the crystals are moved to the storage chamber prior to washing. After the crystals are washed, the wash solvent is frozen in one of the other chambers. The apparatus is evacuated to $<4 \times 10^{-5}$ torr, as in the case of the H-cell, and the storage chamber is sealed off. A detailed discussion of the final stage has been given elsewhere [51].

C. Analysis

The general analysis scheme for determining the stoichiometry of alkalides is given in Figure 9A. The crystals were first allowed to react with water to yield a basic residue and hydrogen gas. The volume of the hydrogen is directly proportional to the reducing power of the crystals. A calculated excess of HCl (at least three times the number of moles of OH^-) was added to the decomposed material. The resultant solution was divided into 3 portions; one for flame emission spectroscopy, one for pH

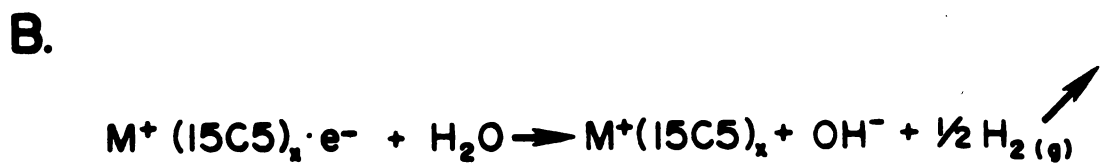
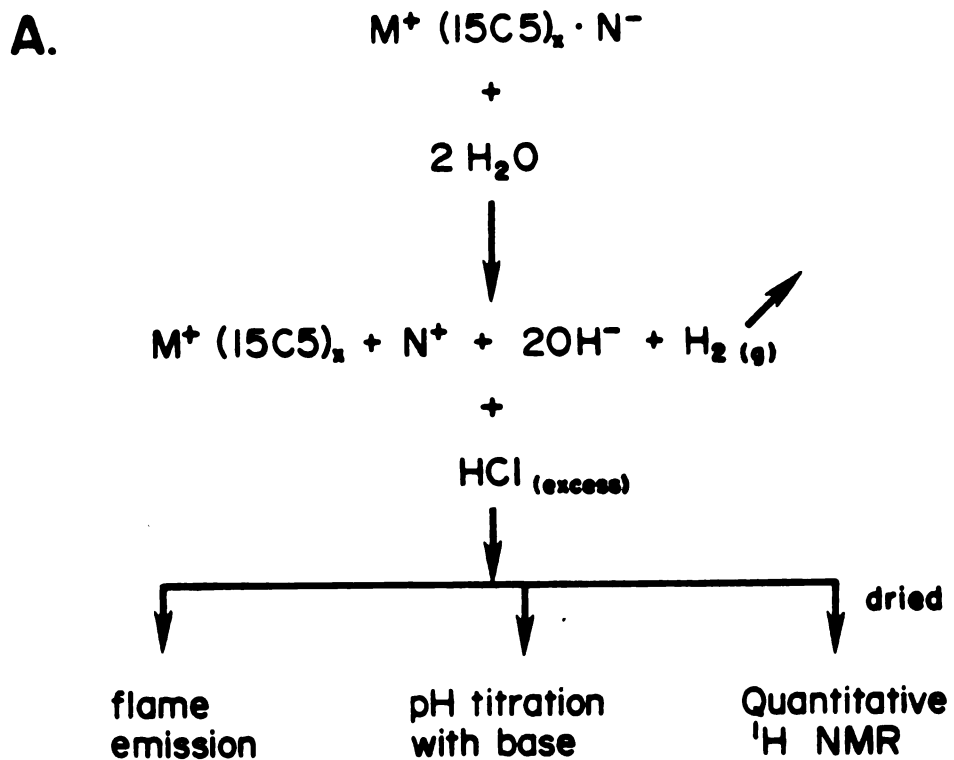


Figure 9. Analysis Scheme for Alkalides (A) and Electrides (B).

titration with base and the third for quantitative proton NMR measurements. Figure 9B gives the equation for the reaction of an electride with water. Note that the amount of hydrogen gas evolved is exactly half the amount of electride used. The same analysis scheme was used for electrides. This procedure gives three checks for the metal content and one for the crown content of the crystals.

1. *Hydrogen evolution* - Care was taken that the crystals decomposed only according to the equations given in Figure 9. Sample tubes were scribed with a glass knife and weighed quickly to avoid thermal decomposition. The hydrogen evolution apparatus is shown in Figure 10. Crystals were loaded under a dry nitrogen atmosphere by breaking the scribed sample tube open and placing both pieces through the 1/2" tubing at the top of the apparatus. The bottom surface was precooled in liquid nitrogen to avoid thermal shock of the crystals. The 1/2" opening was then capped with a sealed glass tube and an Ultra-torr union. The apparatus was evacuated to $\sim 10^{-5}$ torr on the vacuum system designed for hydrogen collection. This system consists of a gas buret and a modified Toeppler pump and is described by Van Eck [23]. The entire system had been previously evacuated to less than 2×10^{-5} torr. Conductance water which had been degassed several times was used for the decomposition reaction. The water was allowed to distill through the hydrogen collection system and freeze on the walls above the crystals. The vessel was warmed spot-by-

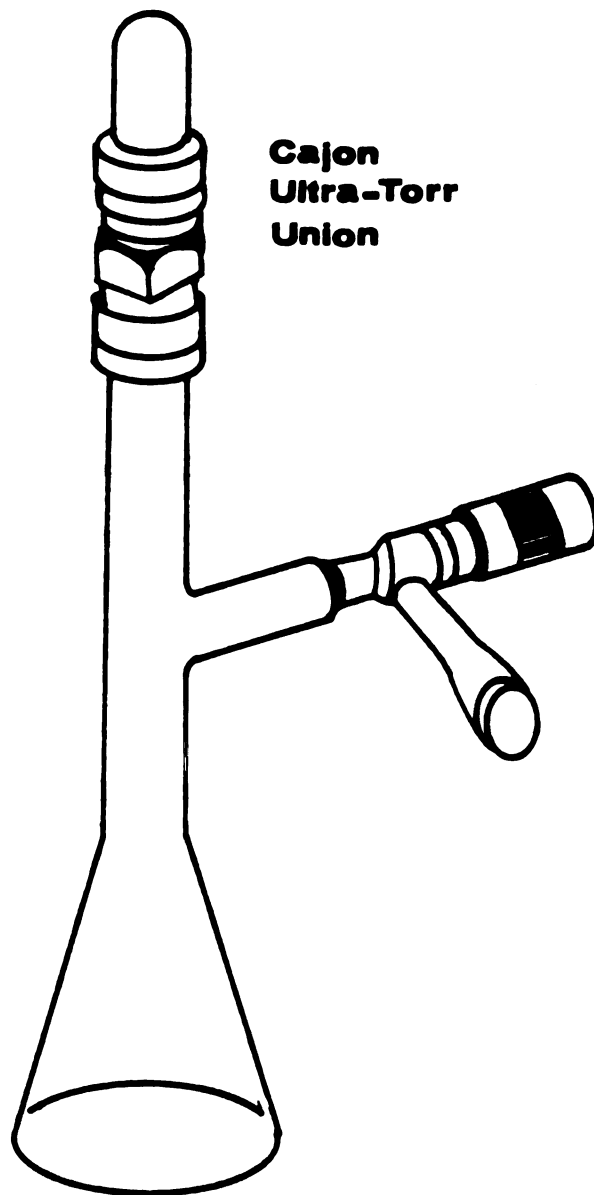


Figure 10. Hydrogen Evolution Apparatus.

spot to melt the ice and allow only a small amount of liquid water to contact the crystals at any time. After the reaction began, a dry ice-isopropanol bath was used to cool the vessel in order to slow or halt any further reaction. By repeating this thaw-quench procedure, the crystals were slowly decomposed without thermal decomposition to yield a white residue. At this time, additional water was rapidly distilled onto the decomposition product to form a solution and insure complete reaction. The evolved hydrogen was pumped through a double liquid nitrogen trap into a chamber of known volume by means of a manual Toeppler pump. After several cycles, the pressure of the hydrogen was measured by noting the height of the mercury in a U tube opened on one side to atmosphere and the other side to the known volume of hydrogen. The end point was determined to be the pressure at which five additional pump cycles did not change the mercury level. By noting the temperature of the hydrogen chamber and the atmospheric pressure, the ideal gas law could be employed to calculate the moles of hydrogen evolved. The pump cycles also served to evaporate the basic solution to yield a dry residue.

2. *pH titration* - The residue from the hydrogen evolution was dissolved in a known amount of HCl and conductance water under a nitrogen atmosphere, to give a solution of pH ~3. The number of moles of hydrogen evolved was used to estimate the number of equivalents of base present. The

solution was divided into 3 portions, as described above. The pH titration portion was further divided into 2 or 3 parts. Each part was titrated with an NaOH solution that had been freshly standardized with HCl. Phenolphthalein was used to indicate the titration endpoint. To prevent CO₂ absorption by the base, the titration buret had a glass sheath allowing dry nitrogen gas to flow over the solution. The results of the different titrations were averaged to give the number of equivalents.

3. Flame emission - A Jarrel-Ash Atomic Absorption/Flame Emission spectrometer was used to determine the alkali metal content of the compound. Only the flame emission feature was used. The flame emission portion of the residue solution was further diluted to give solutions of ~35 ppm for each metal. Standard solutions of each metal in the 10-100 ppm range were used to obtain the calibration curve. The reading obtained with conductance water was noted between each standard in order to give a baseline correction. Calibration curves of ppm vs digital output of the amplifier circuit were used to find the concentration of the unknown.

4. Proton NMR - The third portion of the hydrogen evolution residue solution was neutralized by adding the appropriate amount of the NaOH solution. The solution was covered with tissue and allowed to air dry at room temperature. When dry, the resultant residue was further dried in a vacuum desiccator for 30-60 minutes. More rigorous pumping

resulted in evaporation of crown and led to errors in the early determinations. A known amount of dry sodium acetate and ~0.5 ml D₂O were added to the residue and the solution was transferred to a 5 mm OD NMR tube. The sodium acetate served as an internal standard. A 1:1 ratio of acetate protons to crown protons was approximated by using the amount of hydrogen evolved as an estimate of the number of moles of 15-crown-5. Spectra were taken with a Bruker 250 MHz Fourier Transform NMR spectrometer equipped with an Aspect 2000 computer. Individual peaks were isolated and fitted to either a Lorentzian or Gaussian curve by a line fitting program provided by Bruker [58]. This program gives the amplitude, full width at half height and the standard deviation for the frequency of the fitted curve. A ratio of the area under the curves gave the ratio of acetate to crown protons.

D. Optical Spectra

Optical transmission spectra were taken of films made from solutions of crystals dissolved in methylamine. Figure 11 shows the apparatus used for optical studies. Crystals were loaded through the stopcock into the pre-cooled optical cell under a dry nitrogen atmosphere. The apparatus was closed and evacuated to 2×10^{-5} torr. Methylamine was distilled onto the crystals to fill the optical cell. Films were made by two methods. The first

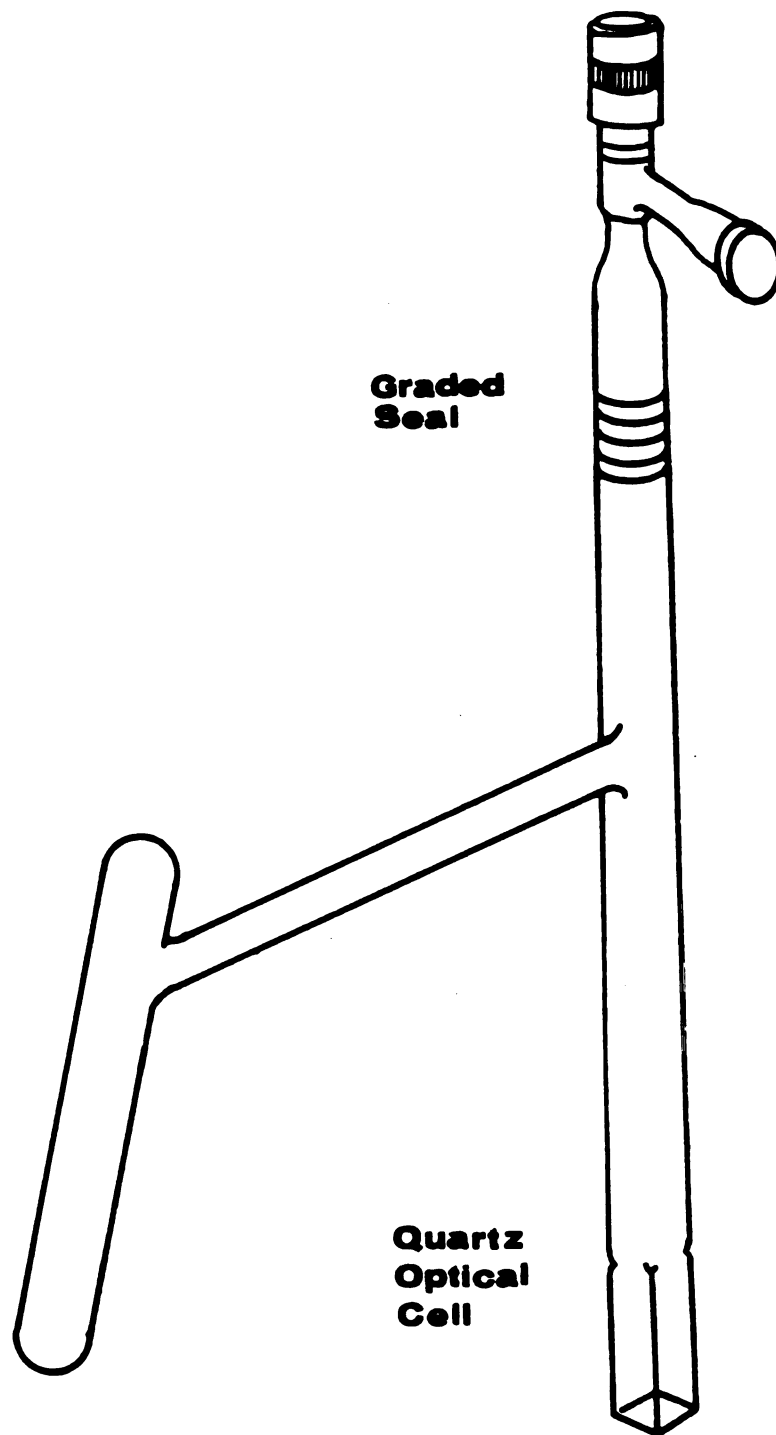


Figure 11. Optical Absorption Apparatus.

method consists of pouring the solution from the cell to the side chamber which is held at liquid nitrogen temperature. The solution must be concentrated enough to leave a good film with one pour. The resultant films were fairly uniform to the naked eye. The second method is flash evaporation. The solution was poured into the side chamber leaving 1 or 2 ml in the optical cell. The side chamber was frozen in liquid nitrogen while the apparatus was vigorously shaken to spread the solution over the walls of the cell. These films were not as homogeneous as those made by the first method but less concentrated solutions could be used. Spectra were recorded on a Beckman DK-2 double beam recording spectrophotometer that had been modified to permit temperature control of the sample compartment between 0° and -130°C. Rough temperature control was achieved by adjusting the flow rate of nitrogen gas that had passed through a cooling coil immersed in liquid nitrogen. A copper-constantan thermocouple was placed in the cell compartment to monitor the temperature. Spectra were recorded in the 2800 to 400 nm range with the reference beam passing through air. The spectra were normalized by subtracting the baseline correction of an empty cell and then rescaling the lowest absorbance to zero and the maximum to 1.0. Temperature dependence of the optical transmission spectra was also studied.

E. Pressed Powder Conductivity

Powder conductivity measurements were made under pressure in an apparatus designed by J.L. Dye and M.R. Yemen [20,59]. Under a dry nitrogen atmosphere, a sample was loaded into a precooled 2 mm inner diameter heavy-walled fused silica tube which rested on a stainless steel electrode. A second stainless steel electrode was inserted into the top of the tube and was used to compress the sample by means of a spring with a measured force constant. The sample cell was loaded into a cryostat which was cooled by controlled liquid nitrogen boil-off. Ohm's law obedience was checked by measuring the current as a function of voltage. At a constant voltage, the crystals were slowly cooled to less than -50°C and warmed again to 0°C . The current was read at approximately two degree intervals during the temperature cycle. The apparatus was then disassembled to check for decomposition. If the crystals had maintained a dark blue color, the system was reassembled and taken through another temperature cycle. For some samples a check was made for polarization by reversing the current flow. After completion of the second temperature cycle the height of the pressed powder was measured so that the specific resistivity could be estimated.

F. Electron Paramagnetic Resonance

The samples for EPR spectra were loaded into evacuable 4 mm OD quartz tubes in a dry nitrogen atmosphere. Each tube was evacuated to 4×10^{-5} torr and sealed. Spectra were recorded on an X-band spectrometer (Bruker model 200). Temperature regulation was unavailable except by reduction of the flow rate of cold nitrogen gas. To avoid condensation of water onto the sample tube, the gas flow was maintained at a high rate. Spectra were taken at -105 to -90°C. A copper-constantan thermocouple with a digital readout (Doric model DS-350) was placed under the sample tube to observe the temperature.

G. Magnetic Susceptibility

The magnetic susceptibilities of the electriles were measured by an S.H.E. Corp. computer controlled variable temperature susceptometer equipped with a superconducting quantum interference device (SQUID). Samples were loaded under a dry nitrogen atmosphere into thin wall Delrin buckets with snap-on lids. The buckets had an overall height of 10 mm and 6 mm outer diameter. The buckets were stored in liquid nitrogen until loading into the airlock of the susceptometer. The airlock was evacuated to ~500 millitorr and flushed with helium gas. This evacuate-flush process was repeated 2 or 3 times and the sample bucket was

visually checked to be sure no frost remained before the sample was lowered into the SQUID at 5 K. The magnetic moment of each sample was measured at various temperatures between 1.7 and 240 K. The apparent "susceptibility", χ' , was given as the magnetic moment in emu divided by the field strength in gauss. Ten readings were taken at each temperature. The software automatically discarded any data points that had more than a preselected percentage difference between two successive moments. This value was usually chosen to be 10%. After a complete temperature cycle, the sample was ejected and allowed to thermally decompose in the helium atmosphere of the air lock. The apparent susceptibility of the decomposed sample was measured at the same temperatures.

Mass determinations of the decomposed sample and empty bucket were made so that the molar susceptibility, χ_M , could be calculated. If the sample mass was known prior to the measurement of the moments, the S.H.E. computer could calculate χ_M directly. However, the weighing procedure introduces the chance of premature decomposition of the sample. The electronic contribution to the molar susceptibility was then calculated by the following equation:

$$\chi_M = \frac{\chi'_{\text{sample+bucket}} - \chi'_{\text{decomposed sample+bucket}}}{\text{moles of sample}} \quad (6)$$

PART I

CHAPTER THREE -- RESULTS AND DISCUSSION

The utility of any new compound is dependent on the ease of preparation and total cost. Electrides and alkalides are excellent reducing agents with one or two electrons readily available to donate. Although the environment must be rigidly controlled to avoid decomposition of these salts prior to reaction, the use of alkalides and electrides as electron donors for difficult reduction reactions seems feasible. Some of the problems encountered in the economical utilization of alkalides and electrides are the length of the synthesis procedure, decomposition of the solutions during synthesis, the cost of complexants and the thermal stability of the crystals.

The major goal of Part I of this dissertation is to describe the synthesis and characterization of new alkalides and electrides. A new solvent system was implemented for the synthesis, and the synthesis procedure was modified to reduce total time. The use of dimethylether as a dissolution solvent greatly increased the stability of the solutions so that fewer reactions decomposed. A new complexant, 15-crown-5, is relatively inexpensive compared

to most crown ethers and to all cryptands was tried. The success achieved with 15-crown-5 as a complexant is reported in this chapter. In all, 10 crystalline systems were isolated and characterized.

A. Synthesis

Due to the ease of preparation and thermal stability of $\text{Na}^+\text{C222}\cdot\text{Na}^-$, the first system to be attempted with 15-crown-5 was $\text{Na}^+(\text{15C5})_2\cdot\text{Na}^-$. The sodium cation, with a radius of 1.02 Å, is slightly too large to enter the cavity of 15-crown-5 which is estimated to be 1.7 to 2.2 Å in diameter. Several syntheses attempts were made with crown ether to sodium mole ratios ranging from 0.88 to 1.14 in the hope that we could mimic the 18-crown-6 systems. Cesium forms "sandwich" complexes with 18C6 in a 1:2, Cs^+ to 18C6 mole ratio [53] whereas rubidium forms compounds with metal to crown ether mole ratios ranging from 0.5 to 2.0. Both cations are too large to enter the 18-crown-6 cavity. In the case of sodium with 15-crown-5, no crystalline precipitates could be isolated from any of the synthesis attempts. One problem was difficulty in dissolving sodium metal in dimethylether (Me_2O). Even in the presence of 15-crown-5, dissolution took from several hours to two days. Methylamine (MA) was used either alone or with Me_2O to decrease the dissolution time. Although, the solubility of sodium was increased in the presence of

MA, the solution stability decreased. Lithium was used to give solution stability in those synthesis in which methylamine was a dissolution solvent. The second problem was the precipitation of metal at the time of the addition of the crystallization solvent. Although the presence of lithium reduced the chance of decomposition, its presence compounded the metal precipitation problem. In one synthesis which utilized MA and lithium, long, flat, golden crystals were observed. These crystals appeared to be highly reflective and were reminiscent of the $K^+18C6 \cdot Na^-$ crystals which had ~14% solvent content [51]. The sodium 15-crown-5 crystals decomposed before they could be isolated and analyzed.

The next system attempted was $K^+(15C5)_2 \cdot Na^-$. The potassium cation with $r = 1.38 \text{ \AA}$ is too large to fit into the 15-crown-5 cavity even if one uses the largest size estimate. The metal mirror of K-Na dissolved readily in dimethylether 15-crown-5 solution at -10°C to form a dark blue solution. The solution left bronzy-red films on the surface of the reaction vessel. Crystallites began to form immediately when diethylether was added to the concentrated Me_2O solution. Precipitation of crystals continued for several hours at 78°C . The crystals are brick red in color and are stable at room temperature for several hours.

Five other heteronuclear systems were tried and the attempts resulted in similar success. In addition, precipitates formed from potassium or rubidium solutions that

had a metal to 15-crown-5 mole ratio of 0.5 or 1.0. Dimethylether was used as the dissolution solvent for all of the syntheses and complete solvation of the metal required 30 minutes to 4 hours. Diethylether (DEE) was initially tried as the co-solvent for crystallization. In these syntheses in which no precipitate formed in the presence of diethylether (DEE), trimethylamine (TMA) was used as the co-solvent. The initial stoichiometry, crystallization conditions and general comments on color and stability of 10 metal 15-crown-5 systems are given in Table II. In general, the precipitates were polycrystalline or clusters of crystallites and the morphology cannot be described.

Several generalizations may be made for these systems. First, the heteronuclear compounds which contain sodium are easier to prepare than those without sodium. Precipitation began with the addition of the co-solvent even at temperatures as high as -30°C . The formation of crystals was complete within 30 minutes for the systems with initial stoichiometries of $\text{RbNa}(\text{15C5})_2$ and $\text{CsNa}(\text{15C5})_2$. These precipitates were microcrystalline rather than clumps of crystallites. Second, the thermal stability of the compounds that contained sodium was greater than that of the other compounds which did not. The precipitate of presumed stoichiometry $\text{RbNa}(\text{15C5})_2$ was stable for over 24 hours at 25°C . Third, the precipitates from solutions with metal stoichiometry of K15C5 and Rb15C5 were more stable than

TABLE II. Crystallization Conditions and Relative Stabilities of 15-crown-5 Alkalides and Electrides.

Initial Stoichiometry	Crystallization ^a Conditions	cosolvent, time, temperature	color, stability	Comments
K(15C5) ₂	TMA, 2-6 hours, -78°C			Blue-black, stable at -10°C for 10 min.
K(15C5)	DEE, 10-12 hrs., -78°C			Dark bronze, stable at room temperature for 10 min.
KNa(15C5) ₂	DEE, immediate, -78°C			Brick red, stable at 25°C for several hours.
KRb(15C5) ₂	TMA, 5 hours, -78°C			Blue-red, stable at 25°C for 30 minutes.
Rb(15C5) ₂	TMA, 3-6 hours, -78°C			Blue-black, stable at -10°C for 30 minutes.
Rb(15C5)	DEE, 6 hours, -78°C			Dark bronze, stable at 25°C for 2 hours.
RbNa(15C5) ₂	DEE, immediate, -30°C			Red bronze, stable at 25°C for 24 hours.
CsNa(15C5) ₂	DEE, immediate, -30°C			Dark red-bronze, stable at 25°C for 2 hours.
CsK(15C5) ₂	TMA, 10-12 hours, -78°C			Dark red-bronze, stable at 25°C for 20 minutes.
CsRb(15C5) ₂	TMA, 10-12 hours, -78°C			Dark blue-bronze, stable at 25°C for 10 minutes.

^a Conditions required for precipitation of crystals to begin.

those of the compounds from solutions with a higher 15-crown-5 content. The colors of $K(15C5)_2$ and $Rb(15C5)_2$ were deep blue-black whereas those of $K15C5$ and $Rb15C5$ were dark bronze. Apparently two distinctive compounds are prepared from solutions with metal to 15-crown-5 mole ratios of 0.5 and 1.0. Fourth, the ease of preparation and relative stability of $RbNa(15C5)_2$ indicate that this compound is the best candidate for use as a reducing agent for other reactions.

B. Analysis

Precipitates which form during the synthesis of alkylides and electrides may or may not have the same stoichiometry as the solutions from which they form. An elemental analysis scheme has been used which has three checks for metal content and one test for crown ether content. This scheme has been reviewed in Chapter Two of this dissertation. Two main problems were encountered with the use of this scheme. First, premature decomposition caused low amounts of hydrogen to be evolved. Decomposition would occur for the more thermally sensitive compounds during the determination of the mass of the scribed sample tube. Great care was taken to prevent decomposition before reaction with water but in most cases, the amount of hydrogen evolved was low in comparison to that predicted on the basis of OH-titrations and M flame emission studies.

Second, 15-crown-5 is volatile and is removed by rigorous drying of the analysis residue for ^1H NMR studies. The crown ether ring can also be destroyed during thermal decomposition and low crown ether content is often encountered.

To avoid these problems some samples were analyzed by a shortened scheme. The weighed, scribed sample tube was opened in a nitrogen atmosphere and the crystals were sprinkled into a dilute solution of HCl. Portions of the solution were titrated and the rest of the analysis scheme was followed as described in Chapter Two. The large volume of water ensured that the decomposition occurred via the reaction with water rather than by thermal pathways.

The results of the analysis of the precipitates are give in Tables IIIA and B. Thermodynamic calculation have been made for compounds of the formula $\text{M}^+(\text{15C5})_2\cdot\text{N}^-$ and can be used to estimate the relative stabilities of the potential salts [38]. These estimations have been used to predict the species within the compounds from the stoichiometries. The analytical results have been divided into two categories. The first category is comprised of those results which have a high degree of consistency among the number of moles obtained by the various techniques. The second category contains those compounds whose stoichiometries can be attributed to a unique compound. Sample sizes were determined by the OH^- titration results based on the presumed stoichiometry. The percent deviation from the

TABLE III. Analysis of Alkalides and Electrides^a.

% Deviation from Presumed Stoichiometry

Presumed Stoichiometry	Sample Size ^b mole x 10 ⁴	Mass	H ₂	M ₁ Flame	N ₁ Flame	15-crown-5 by ¹ H NMR
A. Pure Compounds						
K ⁺ (15C5) ₂ ·Na ⁻	1.80	0	+5.6	+5.6	+5.6	+3.9
K ⁺ (15C5) ₂ ·Rb ⁻	2.616	-5.7	---	+9.8	+8.8	+3.6
Rb ⁺ (15C5) ₂ ·e ⁻	1.255	---	-38.8	-3.6	---	+4.9
Rb ⁺ (15C5) ₂ ·Na ⁻	0.95	---	-1.3	-3.3	-10.3	-0.3
Rb ⁺ (15C5) ₂ ·Rb ⁻	2.642	+7.0	---	+1.0	+1.0	-5.0
Cs ⁺ (15C5) ₂ ·Na ⁻	2.625	+8.2	---	-8.3	-10.6	-7.4

B. Mixtures

K ⁺ (15C5) ₂ ·e ⁻	4.532	-23.0	---	-9.7	---	-27.9
K ⁺ (15C5) ₂ ·K ⁻	0.75	+26.7	-21.1	-12.1	-12.1	-11.2
Cs ⁺ (15C5) ₂ ·Na ⁻	1.559	+6.8	-6.2	-0.3	+6.0	-48.3 ^c
Cs ⁺ (15C5) ₂ ·K ⁻	1.68	+6.0	---	-4.2	+4.2	-11.0
Cs ⁺ (15C5) ₂ ·Rb ⁻	2.75	+17.8	---	+6.5	-2.2	+23.2

^aBased on the reaction of either M⁺(15C5)_n·N⁻ + 2H₂O --> M⁺(15C5)_n + N⁺ + 2OH⁻ + H₂ or M⁺(15C5)_n·e⁻ + H₂O --> M⁺(15C5)_n + OH⁻ + 1/2 H₂.

^bSample size determined by titration of OH⁻.

^cSample dried under dynamic vacuum.

titration results is given for each of the other techniques.

In general, the amount of hydrogen is lower than expected based on the OH^- titration and flame emission results. The deviation increases with decreasing thermal stability which is indicative of premature decomposition of the sample. The mass determinations indicate that there is more compound present than is indicated by the other techniques. Loss of sample during transfer or loss of glass chips from the sample tubes would give higher than actual results from the mass determinations.

The presence of an electroneutral complex is presumed from the stoichiometry $\text{Rb}(\text{15C5})_2$. The assignment of $\text{Rb}^+(\text{15C5})_2 \cdot e^-$ also is supported by the blue-black color of the crystals and the isolation of crystals with stoichiometry corresponding to $\text{Rb}^+(\text{15C5}) \cdot \text{Rb}^-$. All compounds listed in Table IIIA have stoichiometries which suggest that the cation is complexed by two 15-crown-5 molecules as expected from the size of the 15-crown-5 cavity and cation radii.

Four of the compounds appear to be mixtures or have slight deviations from a strict $\text{M}^+(\text{15C5})_2 \cdot \text{X}^-$ stoichiometry. The expected stoichiometries were $\text{K}^+(\text{15C5})_2 \cdot e^-$, $\text{K}^+(\text{15C5})_2 \cdot \text{K}^-$, and $\text{Cs}^+(\text{15C5})_2 \cdot \text{Rb}^-$, and the analysis results are given in Table IIIB. In addition, Table IIIB contains the analysis results for a sample of $\text{Cs}^+(\text{15C5})_2 \cdot \text{Na}^-$ which was dried under dynamic vacuum before the ^1H NMR determination of the crown ether content. The homonuclear potassium

compounds appear to be mixtures of $K^+(15C5)_2 \cdot e^-$ and $K^+(15C5)_2 \cdot K^-$ but any one synthesis yields predominantly either the electrone or alkali with only a slight contamination of the other compound. The crown ether content greatly exceeded the expected value in $Cs^+(15C5)_2 \cdot Rb^-$ and trapped electrons may be present in this sample so that the concentrations of $Cs^+(15C5)_2 \cdot e^-$ and/or $Rb^+(15C5)_2 \cdot e^-$ may be significant. Several preparations of this compound were made and the crown ether to metal ratio varied with the preparation. The tendency to form mixtures may also be present in $Cs^+(15C5)_2 \cdot K^-$ where the cesium and potassium content deviate ~9% with respect to one another and the 15-crown-5 content is 11% low compared to that expected from the OH-titration results. Nuclear specific characterization techniques are needed to correctly identify the compounds.

In addition to the tendency to form mixtures, the vacuum drying of the analysis residue before the determination of 15-crown-5 content can give misleading results. Compare the results obtained for $Cs^+(15C5)_2 \cdot Na^-$ with and without vacuum drying, Tables IIIB and IIIA, respectively. The sample dried by dynamic vacuum has a crown ether content which is 48.3% lower than expected. The sample analyzed by the abbreviated scheme has a crown ether content which is within the acceptable range of the number of moles calculated from the OH^- titration and flame emission results.

The result of the analyses indicate that eight new alkalides and two electrides were synthesized. Exact identification of the species within these compounds has been attempted by optical absorption spectroscopy and is reported in the following section. The elimination of the hydrogen evolution step in the analysis scheme and the slow drying of the analysis residue has simplified the analysis and gives acceptable results. There is a tendency to form mixtures of electride and homonuclear alkalides when the synthesis of either is attempted. The tendency is greater for the potassium systems than for those salts which contain rubidium. The levels of contamination are low, however, which is suggestive that the compounds may be treated as pure compounds in the characterization studies.

C. Optical Spectra

The "pour" method, rather than the flash evaporation method, was preferred for making films for optical studies. Uniform films could be made much more easily by pouring the solution from the optical cell to the side chamber. Solution stability was sufficient to allow the pouring to be done with the apparatus immersed in a dry ice-isopropanol bath. Films left on the walls above the cell and on the side arm of the apparatus showed no signs of decomposition during the time period of the experiment with the exception of $K^+(15C5)_2 \cdot e^-$ and $Rb^+(15C5)_2 \cdot e^-$. Decomposition of these

films occurred within 30 minutes so that films had to be made quickly and kept cold.

The optical spectrum of the film with stoichiometry $K \cdot 15C5$ is given in Figure 12A. A single maximum at 12000 cm^{-1} with a low energy shoulder was observed. The optical absorption maximum for K^- in ethylenediamine occurs at 12000 cm^{-1} and the assignment of this film is $K^+(15C5)_2 \cdot K^-$ rather than $K^+(15C5) \cdot e^-$. The low energy shoulder indicates the presence of some trapped electrons but the major species is seen to be K^- . The assignment of a potasside for this compound is further supported by the spectrum of $K(15C5)_2$ films shown in Figure 12B-C. The maximum at 7800 cm^{-1} corresponds to trapped electrons and therefore the assignment of this compound is $K^+(15C5)_2 \cdot e^-$. The two spectra of $K^+(15C5)_2 \cdot e^-$ were obtained from different films made from the same solution. The extreme narrowness of the spectrum in Figure 12C would require very narrow bands for the initial and final states. It is likely that this peak is an artifact. Spectrum B is more typical of electrider spectra with a width that corresponds to wider energy bands.

Mixtures of $K^+(15C5)_2 \cdot K^-$ and $K^+(15C5)_2 \cdot e^-$ were easily obtained in the preparations of the electrideres. A typical spectrum is given in Figure 13. The peaks, located at 11000 and 6900 cm^{-1} , correspond to K^- and e^- , respectively. In general, the excited state energy bands of an alkalide metal anion are narrower than those of electrons. Analysis

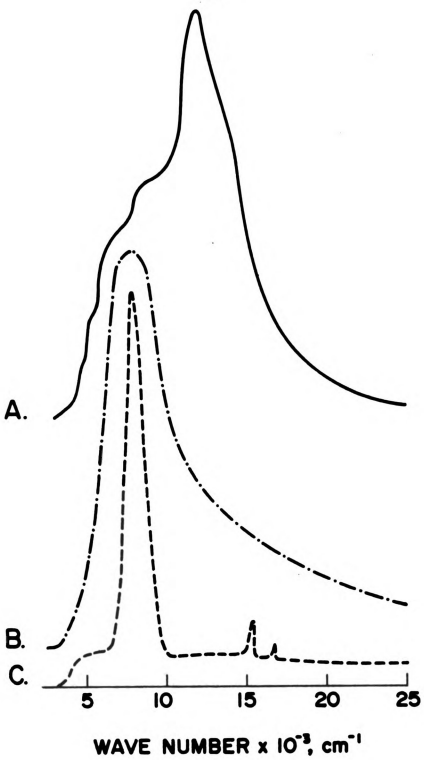


Figure 12. Optical Absorption Spectra of Thin Dry Films Made From Solutions of $\text{K}^+(\text{15C5})_2 \cdot \text{K}^-$ (A) and $\text{K}^+(\text{15C5})_2 \cdot \text{e}^-$ (B and C) in Methylamine.

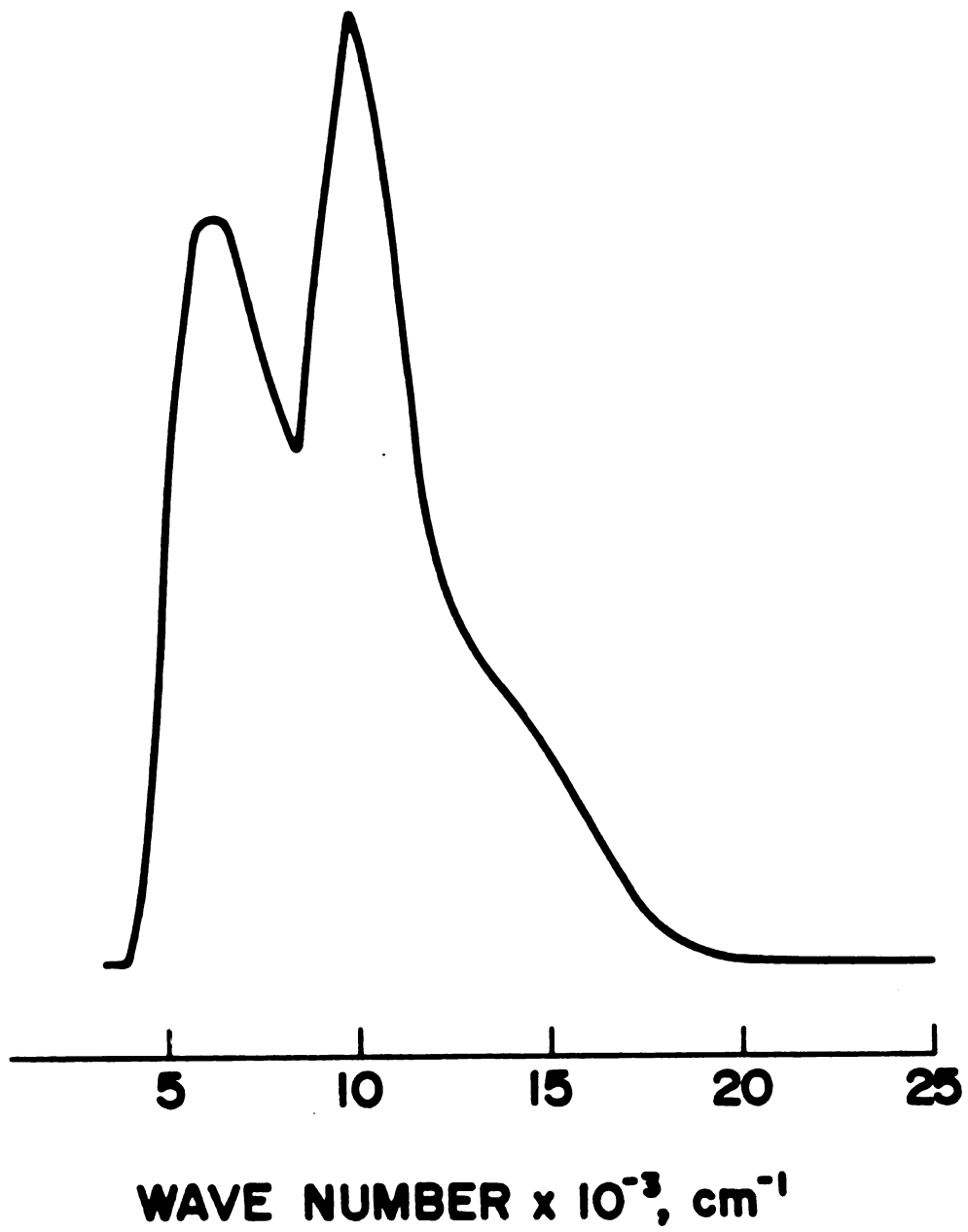


Figure 13. Optical Absorption Spectrum of a Thin Dry Film Made From a Solution of $K(15C5)_{1.3}$ in Methylamine.

of the residue left from the optical absorption studies showed that the stoichiometry was $K_1(15C5)_{1.3}$.

The compounds of rubidium with 15-crown-5 had spectra similar to those of the potassium compounds. Crystals of stoichiometry $Rb15C5$ yielded spectra that featured a single sharp absorption maximum at 9600 cm^{-1} as shown in Figure 14A. These crystals were identified as $Rb^+(15C5)_2 \cdot Rb^-$. However, crystals of stoichiometry $Rb(15C5)_2$ did not yield the simple trapped electron spectrum seen in the analogous potassium system. The spectra from several $Rb(15C5)_2$ syntheses were recorded and all featured peaks at both 9600 and 6500 cm^{-1} which correspond to Rb^- and e^- , respectively. The relative amplitudes of the two peaks were sample- and film-dependent. A typical spectrum of $Rb(15C5)_2$ is shown in Figure 14B. Decomposition of films on the walls above the optical cell led to decomposition of the solution when attempts were made to produce additional films. The assignment of these films is tentatively $Rb^+(15C5)_2 \cdot e^-$ with some Rb^- present.

The heteronuclear salts were more difficult to identify with optical absorption spectroscopy. Those salts which contain sodium could be confidently identified as sodides due to the close proximity of their maxima. $K^+(15C5)_2 \cdot Na^-$, $Rb^+(15C5)_2 \cdot Na^-$ and $Cs^+(15C5)_2 \cdot Na^-$ had absorption maxima at 14300 , 13900 , and 13900 cm^{-1} , respectively. The spectra of these films are given in Figure 15A,B and C. In addition to the main peaks, the spectrum of $Cs^+(15C5)_2 \cdot Na^-$ featured

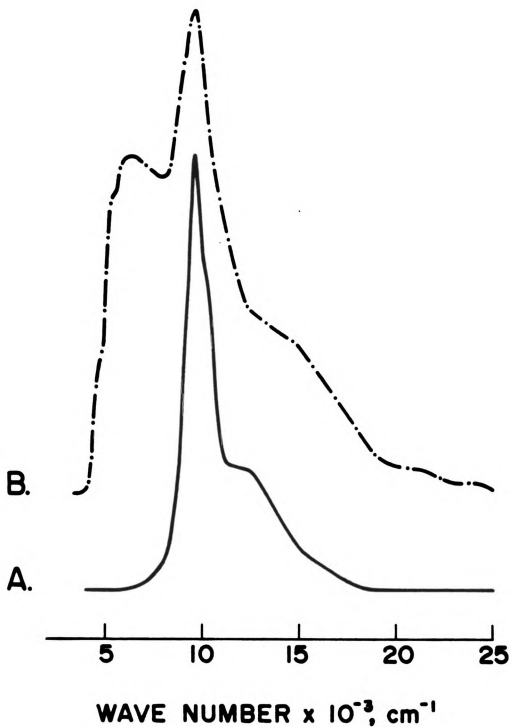


Figure 14. Optical Absorption Spectra of Thin Dry Films Made From Solutions of $\text{Rb}^+(\text{15C5})_2 \cdot \text{Rb}^-$ (A) and $\text{Rb}^+(\text{15C5})_2 \cdot \text{e}^-$ (B) in Methylamine.

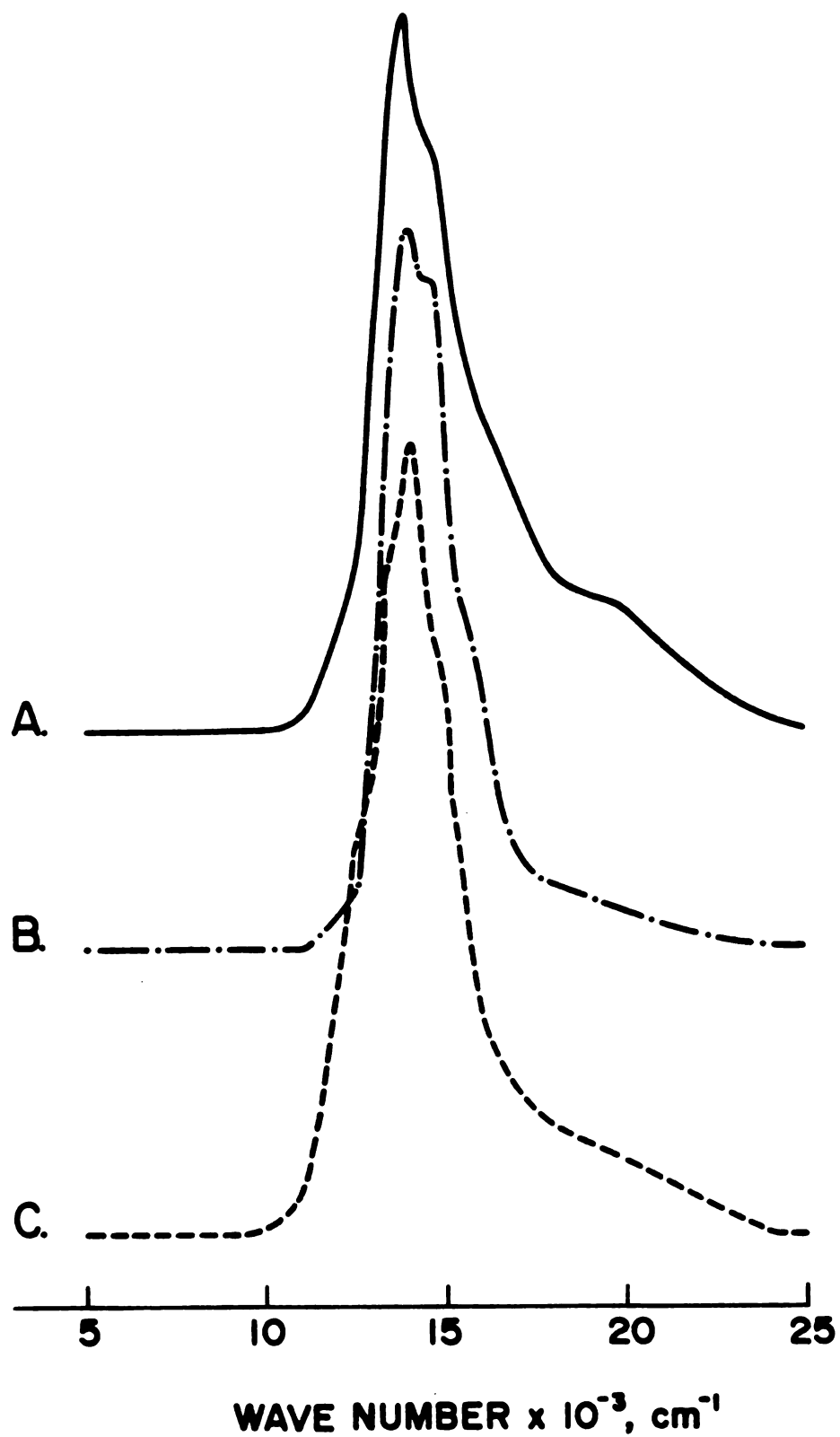


Figure 15. Optical Absorption Spectra of Thin Dry Sodide Films Made From Solutions of $\text{Cs}^+(\text{15C5})_2\cdot\text{Na}^-$ (A), $\text{Rb}^+(\text{15C5})_2\cdot\text{Na}^-$ (B) and $\text{K}^+(\text{15C5})_2\cdot\text{Na}^-$ (C) in Methylamine.

a shoulder at 15400 cm^{-1} . This shoulder was barely discernible at -40° but became more distinct as the temperature decreased. The lowest temperature achieved was -106°C and the shoulder did not completely resolve into a separate peak. The presence of the shoulder suggests there may be two or more sites for Na^- with perhaps an exchange mechanism at high temperatures. The shoulder became less distinct as the temperature was increased from -106°C . Only one temperature cycle was done and it is not known if the appearance of the shoulder is reversible.

The results of the optical studies are given in Table IV. Assignments were made based on the peak location, stoichiometry and thermodynamic estimations. The main ambiguity lies in the identification of Rb-K-15C5_2 whose optical absorption spectrum is shown in Figure 16. The thermodynamic estimations predict $\text{K}^+(\text{15C5})_2 \cdot \text{Rb}^-$ to be slightly more stable than $\text{Rb}^+(\text{15C5})_2 \cdot \text{K}^-$. These calculations assume that the enthalpy change for the complexation of the second crown ether with potassium is equal to that with rubidium. The optical spectrum of films made from solutions of these crystals featured a main peak at 10200 cm^{-1} with a 12300 cm^{-1} shoulder. As in the $\text{Cs}^+(\text{15C5})_2 \cdot \text{Na}^-$ spectrum, the shoulder became more distinct as the temperature was decreased. The main peak lies between the locations observed for the maxima of the two homonuclear salts. The peak could either be a composite of K^- and Rb^- peaks or represent a fast exchange of electrons between the two

TABLE IV. Results of Optical Absorption Studies of Thin Dry Films.

Compound Stoichiometry	Peak Location, cm^{-1}	Description	Assignment
$\text{K}(\text{15C5})_2$	7800	sharp	$\text{K}^+(\text{15C5})_2 \cdot \text{e}^-$
$\text{K}(\text{15C5})$	12000	low energy shoulder	$\text{K}^+(\text{15C5})_2 \cdot \text{K}^-$
$\text{KNa}(\text{15C5})_2$	14300	sharp	$\text{K}^+(\text{15C5})_2 \cdot \text{Na}^-$
$\text{KRb}(\text{15C5})_2$	10200	main peak, very broad	$\text{K}^+(\text{15C5})_2 \cdot \text{Rb}^{-\text{a}}$
	12300	shoulder develops at $T = -60$ to -135	or mixture
$\text{Rb}(\text{15C5})_2$	9600 and 6500	relative amplitudes of peaks vary from sample to sample.	$\text{Rb}^+(\text{15C5})_2 \cdot \text{e}^-$
$\text{Rb}(\text{15C5})$	9400	sharp	$\text{Rb}^+(\text{15C5})_2 \cdot \text{Rb}^-$
$\text{RbNa}(\text{15C5})_2$	13900	sharp	$\text{Rb}^+(\text{15C5})_2 \cdot \text{Na}^-$
$\text{CsNa}(\text{15C5})_2$	13900 15400	main peak shoulder	$\text{Cs}^+(\text{15C5})_2 \cdot \text{Na}^-$
$\text{CsK}(\text{15C5})_2$	7250 12700	main peak T independent shoulder	$\text{Cs}^+(\text{15C5})_2 \cdot \text{K}^-$
$\text{CsRb}(\text{15C5})_2$	8070	broad	$\text{Cs}^+(\text{15C5})_2 \cdot \text{Rb}^-$ (a) or mixture

a) Assignment based on thermodynamic arguments rather than optical spectra.

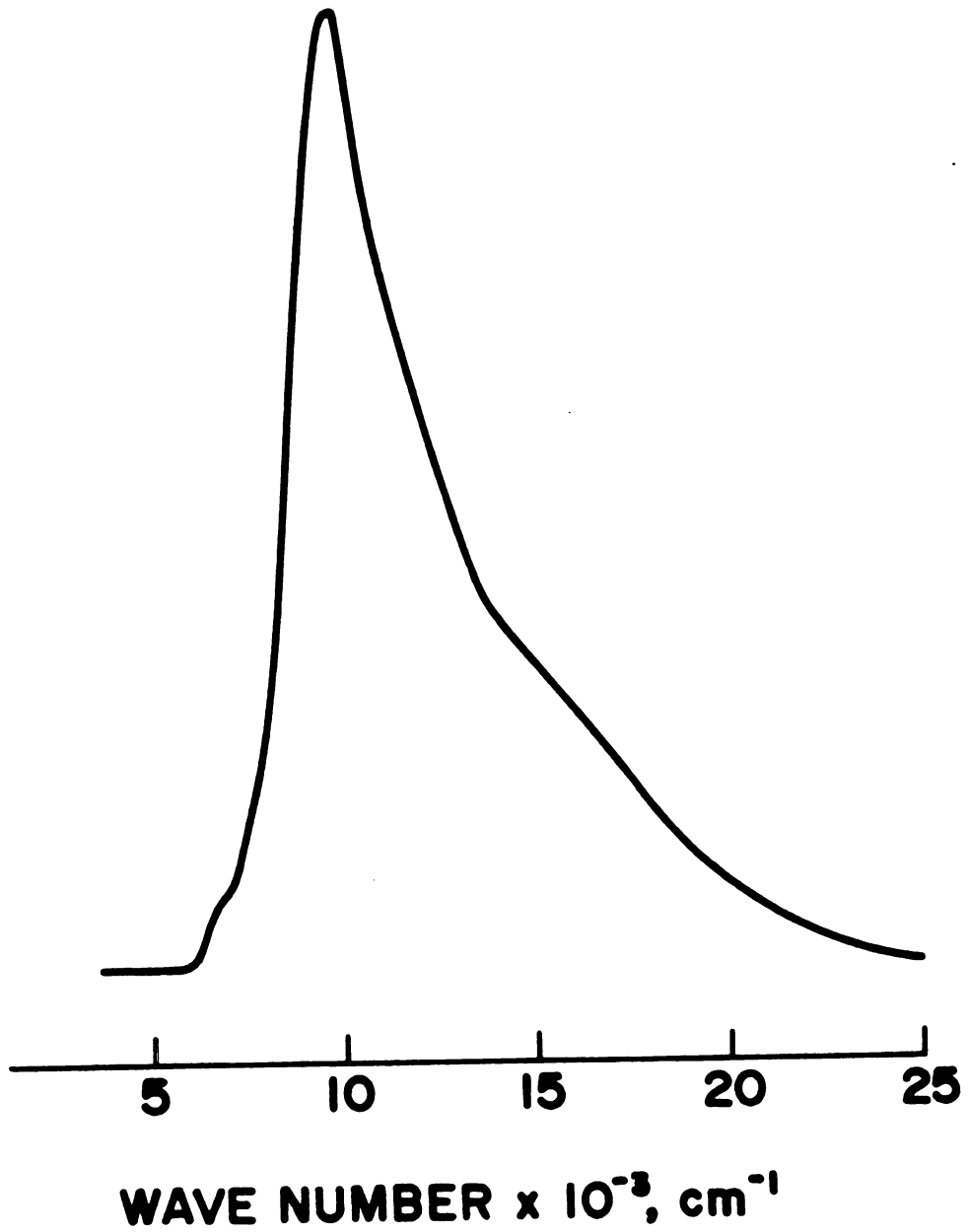
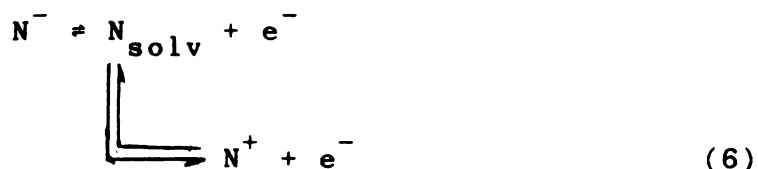


Figure 16. Optical Absorption Spectrum of a Thin Dry Film Made From a Solution of Crystals with Stoichiometry $\text{KRb}(\text{l5C5})_2$ in Methylamine.

nuclei. If the peak were due to only one of these anions, the cation would have a much larger effect on the Rb^- or K^- environment than is the case for Na^- . The Na^- optical absorption maximum shifts to lower energies by only 400 cm^{-1} as the cation is changed from $\text{K}^+(\text{15C5})_2$ to $\text{Rb}^+(\text{15C5})_2$ and there is no change in its location as the cation is changed from rubidium to cesium. The observed maximum for $\text{RbK}(\text{15C5})_2$ would require an 1800 cm^{-1} blue shift for K^- or an 800 cm^{-1} red shift for Rb^- . This compound is most likely a mixture of $\text{K}^+(\text{15C5})_2 \cdot \text{K}^-$ and $\text{Rb}^+(\text{15C5})_2 \cdot \text{Rb}^-$ and/or the heteronuclear salts. Only a nuclear-specific technique can remove this ambiguity in the identification of this system.

One of the problems associated with the use of optical absorption spectroscopy as an identification tool is the effect of the solvent. The anion in the film may or may not be the same as the anion in the crystals used to make the solutions. This is because the time scale of crystallization is much longer than that of film preparation so that a kinetically more favored species may be present in the films. For example, a metal anion may dissociate in solution to form the solvated monomer or cation and electrons according to:



Films made from these solutions would have absorption maxima corresponding to trapped electrons if reaction (6) lay far to the right and if the kinetics of metal anion formation in the solid state is slow. Anions with low electron binding energies would be more likely to undergo this type of dissociation. For example, films made from solutions of $Cs^+(15C5)_2$ in the presence of either rubidium or potassium had absorption maxima that corresponded to trapped electrons rather than alkali metal anions. Films of $Cs^+(15C5)_2 \cdot K^-$ showed the presence of both K^- and e^- . Figure 17 represents two spectra of dry films made from the same solution. The first film, shown as Figure 17A, has a single peak at 12700 cm^{-1} with a low energy shoulder. This film was prepared shortly after the solution was made. The second film was prepared after a one hour time interval. The main absorption occurs at 7250 cm^{-1} . Presumably, decomposition of the solution or precipitation of metal upon standing caused pronounced changes in the nature of the films produced by solvent evaporation. The relative amplitudes of the K^- and e^- maxima were independent of time and temperature which suggests that the processes in solution are more important than the solid state reactions. Equilibria such as those given by Equation (6) probably are

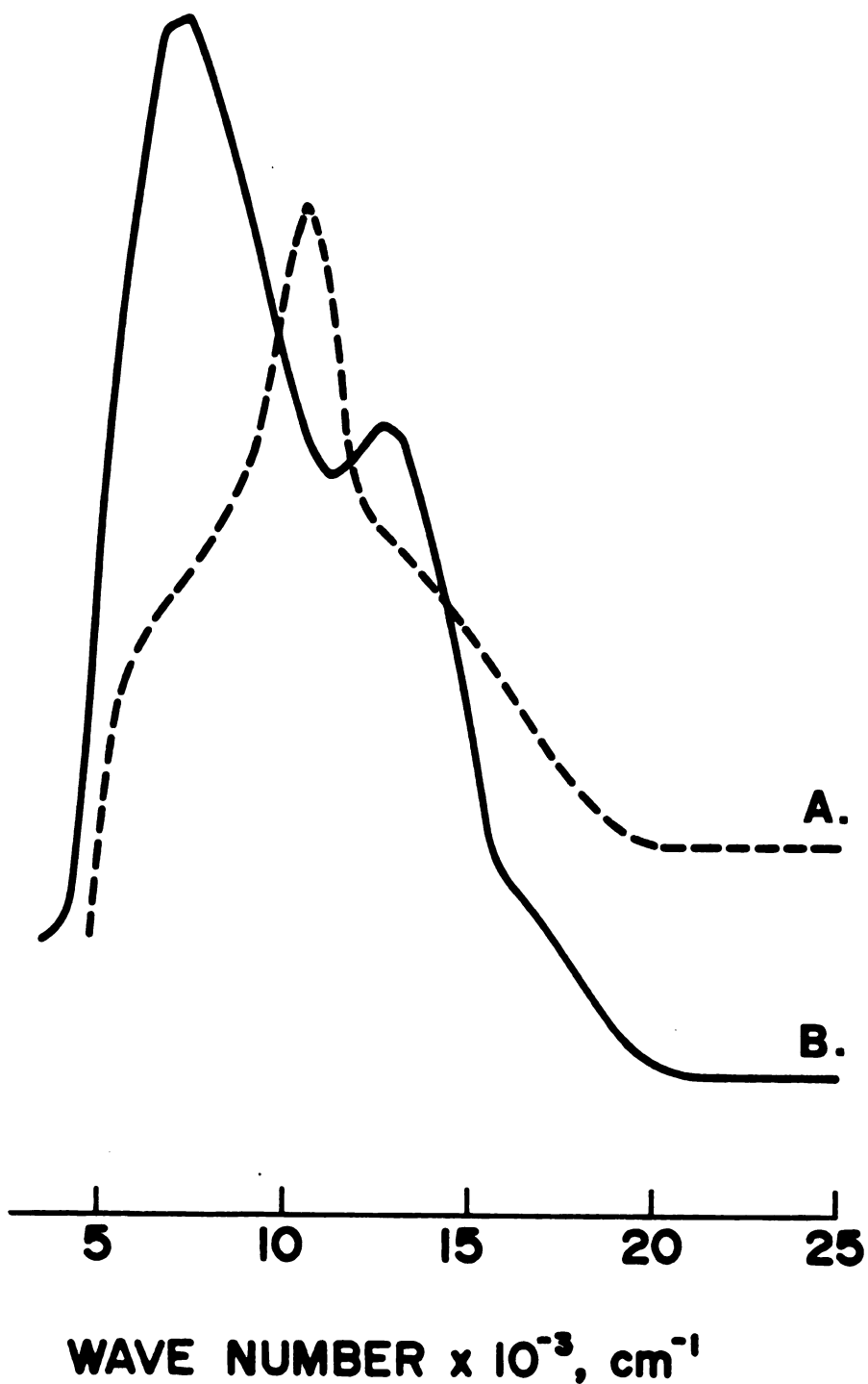


Figure 17. Optical Absorption Spectra of Thin Dry Films Made From a Solution of $\text{Cs}^+(\text{15C5})_2 \cdot \text{K}^-$ in Methylamine. (A) spectrum of film prepared shortly after solution was made; (B) spectrum of film prepared one hour later.

the cause of the broad, ambiguous peak seen for the RbK-(15C5)₂ system.

Three conclusions may be drawn from the optical absorption studies. First, electrides may be distinguished from the homonuclear alkalides but not without some uncertainty. Second, sodides can be easily identified by the location of the optical absorption maximum. Third, dissolving the crystals may introduce dissociation (or association) reactions and thereby yield films that have different anionic species than those present in the crystals. To provide clearer identification of compounds, a technique is needed which does not alter the crystalline state of the alkalides and electrides.

D. Pressed Powder Conductivity

Intrinsic semiconductors have temperature dependent electrical conductivities. The temperature dependence may be described by

$$\sigma = A \exp[-E_g/2k_B T] \quad (7)$$

where σ is the conductivity, A is the conductivity at infinite temperature and k_B is the Boltzman constant. The band gap, E_g , can be calculated from the temperature dependence of the conductivity. the resistivity, ρ ($\rho = 1/\sigma$) ranges from 10^{-6} ohm cm for copper to 10^{18} ohm cm for fused silica

at room temperature. The resistivity for intrinsic semiconductors is of the order of 10^{-3} to 10^9 ohm-cm.

Extrinsic semiconductors also show temperature dependent conductivities but usually over a much shorter temperature range. The conductivity arises from an impurity band which can either donate or accept electrons and lies between the valence and conduction bands of the bulk material. Electrons may be thermally excited either from the donor band to the conduction band or from the valence band to the acceptor band. At sufficiently high temperatures, saturation is reached and the conductivity returns to intrinsic behavior. Extrapolation to infinite temperature generally yields resistivities which are much lower than those expected for an intrinsic semiconductor.

The current flow at constant voltage was measured at several temperatures for each of the new compounds. Adherence to Ohm's law was checked by measuring the current at different voltages at constant temperature. This insures that the voltage used for subsequent measurements was in the linear region of the current versus voltage plot. Substantial polarization has been observed in single crystal conductivity studies of $\text{Na}^+\text{C}_{222}\cdot\text{Na}^-$. The polarization is due to conductivity from ionic mobility followed by electrochemical reactions at the electrodes rather than from electronic conductivity. The contribution was observed to "freeze out" at temperatures below -24°C where the conductivity for the single crystal behaved as in the

pressed powder studies for $\text{Na}^+\text{C}_{222}\cdot\text{Na}^-$ [60]. All of the new 15-crown-5 compounds obeyed Ohm's law with the exception of $\text{Cs}^+(\text{15C5})_2\cdot\text{K}^-$. The plot of current versus voltage in this case had a nonzero intercept of 1×10^{-8} amp at zero volts. This deviation from Ohm's law could be due to many reasons such as 1) Polarization of the powder by ionic conductivity followed by electrochemically produced current; 2) Offset of the zero by 1×10^{-8} amp; or 3) Temperature variation during the measurements. The plot was linear and the most likely cause of the deviation is a zero error. In the case of $\text{Cs}^+(\text{15C5})_2\cdot\text{K}^-$, a voltage comparable to that used for other alkalides was chosen for the current measurements.

Previous conductivity measurements required two full temperature cycles for a complete experiment. The data from the second cycle were used to calculate the band gap and resistance at infinite temperature in order to avoid packing effects that could be present in the first temperature cycle [51]. In this study, the entire loaded cell assembly was cooled to $<-150^\circ\text{C}$ by immersion in liquid nitrogen and then allowed to warm up to -10°C before measurements were taken. This procedure had the effect of packing the crystals as in the first temperature cycle of the previous experiments. In addition to this process, for most compounds the current was measured through one complete temperature cycle and then measured again as the temperature decreased to insure that the packing density

did not change. For five of the compounds, the polarity of the electrodes was then reversed and the current as a function of temperature was measured. The data were fit by the equation

$$I = \frac{V}{R_{\infty}} e^{-E_g/2k_B T} \quad (8)$$

where I is the current at temperature T , V is the voltage, E_g and k_B are the band gap and Boltzman's constant as before, and R_{∞} is the resistance at infinite temperature. In this procedure the nonlinear, least squares program KINFIT [61] was used. The least-squares estimates of E_g and R_{∞} are given in Table V. Each direction of the change of temperature was treated as a separate data set. For example, $K^+(15C5)_2 \cdot Na^-$ has four values listed for E_g . These values, presented in order of measurement, correspond to: 1) current as temperature decreases, 2) current as temperature increases, 3) current as temperature decreases and 4) current as temperature decreases with reverse polarity of the electrodes. An estimate of the room temperature resistivity was made for each data set and is also presented in Table V. A representative plot of \log_{10} current versus $1/T$ for $Rb^+(15C5)_2 \cdot e^-$ is given in Figure 18.

The band gaps calculated for the alkalides and electrides correspond to those typical of semiconductors. The resistivity at 298 K is however, much higher than that expected for intrinsic semiconductors with such small band

TABLE V. Results of Pressed Powder DC Conductivity Measurements.

Compound	E_g , eV	R_∞ , ohm	ρ_{298} , ohm cm
$K^+(15C5)_2 \cdot e^-$	1.06 ± 0.02	$8 \pm 3 \times 10^{-4}$	1.55×10^5
	1.02 ± 0.01	$2.1 \pm 0.6 \times 10^{-3}$	4.62×10^4
	1.05 ± 0.02	$5.2 \pm 2 \times 10^{-4}$	8.28×10^4
$K^+(15C5)_2 \cdot Na^-$	1.39 ± 0.03	$8 \pm 7 \times 10^{-6}$	1.14×10^5
	1.66 ± 0.09	$4 \pm 8 \times 10^{-8}$	1.15×10^5
	1.37 ± 0.03	$1.4 \pm 0.9 \times 10^{-5}$	1.42×10^5
	1.33 ± 0.03	$6.3 \pm 5 \times 10^{-5}$	2.93×10^5
$K^+(15C5)_2 \cdot K^-$	1.06 ± 0.02	$1.8 \pm 0.4 \times 10^{-2}$	5.23×10^5
	1.06 ± 0.005	$1.4 \pm 0.1 \times 10^{-2}$	4.07×10^5
	1.11 ± 0.01	$3.7 \pm 0.1 \times 10^{-3}$	2.84×10^5
	1.04 ± 0.009	$4.6 \pm 0.9 \times 10^{-2}$	9.05×10^5
$K^+(15C5)_2 \cdot Rb^-$	0.87 ± 0.02	$3 \pm 1 \times 10^{-1}$	2.57×10^5
	1.07 ± 0.006	$5.8 \pm 0.9 \times 10^{-3}$	1.71×10^5
	0.84 ± 0.02	$6 \pm 2 \times 10^{-1}$	1.87×10^5
$Rb^+(15C5)_2 \cdot e^-$	1.26 ± 0.03	$2 \pm 1 \times 10^{-5}$	5.75×10^4
	1.50 ± 0.06	$2 \pm 3 \times 10^{-7}$	8.45×10^4
	1.14 ± 0.03	$2 \pm 1 \times 10^{-4}$	5.52×10^4
$Rb^+(15C5)_2 \cdot Na^-$	1.10 ± 0.03	$1.0 \pm 0.1 \times 10^{-4}$	1.57×10^4
	1.14 ± 0.02	$4 \pm 2 \times 10^{-2}$	5.64×10^6
	0.93 ± 0.03	$3 \pm 2 \times 10^0$	5.88×10^6

Table V Continues.

Table V Continued.

Compound	E_g , eV	R_∞ , ohm	ρ_{298} , ohm cm
$Rb^+(15C5)_2 \cdot Rb^-$	0.89 ± 0.07	$7 \pm 1 \times 10^{-2}$	8.47×10^4
	0.90 ± 0.05	$5.4 \pm 0.7 \times 10^{-2}$	7.72×10^4
	0.96 ± 0.04	$2 \pm 2 \times 10^{-2}$	1.06×10^5
	1.19 ± 0.04	$9 \pm 8 \times 10^{-5}$	3.81×10^4
$Cs^+(15C5)_2 \cdot Na^-$	1.07 ± 0.01	$3 \pm 1 \times 10^{-2}$	1.15×10^6
	1.29 ± 0.02	$9 \pm 6 \times 10^{-5}$	3.43×10^5
	1.30 ± 0.03	$8 \pm 5 \times 10^{-6}$	3.38×10^4
$Cs^+(15C5)_2 \cdot K^-$	0.76 ± 0.004	$1.3 \pm 0.1 \times 10^0$	1.08×10^5
	0.93 ± 0.008	$9 \pm 2 \times 10^{-2}$	2.08×10^5
	0.85 ± 0.005	$4.4 \pm 0.5 \times 10^{-1}$	2.14×10^5
$Cs^+(15C5)_2 \cdot Rb^-$	0.64 ± 0.03	$2 \pm 2 \times 10^1$	1.43×10^5
	0.56 ± 0.01	$1.3 \pm 0.7 \times 10^2$	1.86×10^5
	0.88 ± 0.02	$1.1 \pm 0.5 \times 10^{-1}$	7.99×10^4

=====

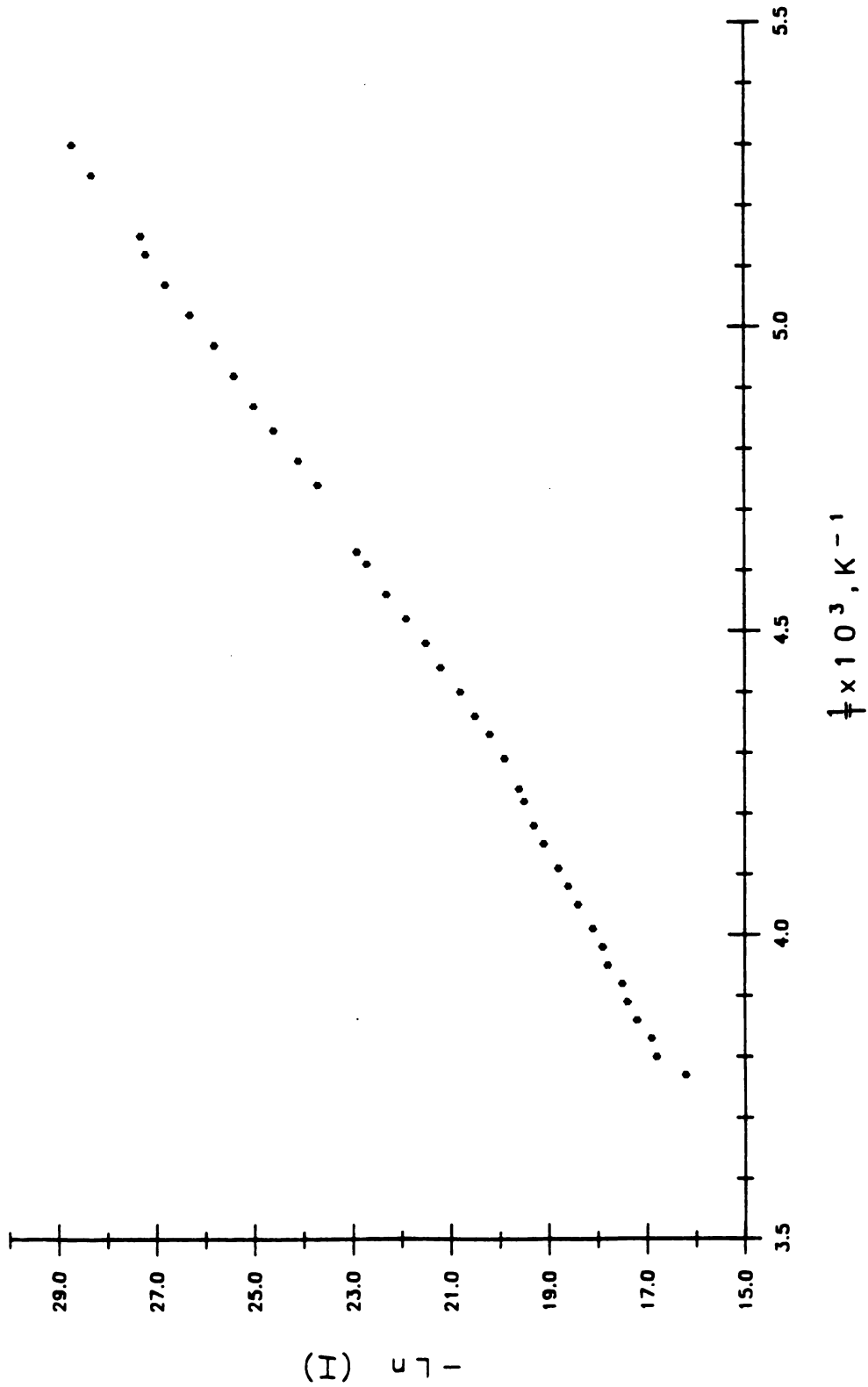


Figure 18. $-L_n$ (current) versus $1/T$ for $Rb^+(15C5)_2 \cdot e^-$.

gaps. This indicates that the conductivity of these samples is an extrinsic property. Electrons trapped in shallow traps would give rise to the small band gaps and high resistivities. The resistivities at 298 K for these electrides are an order of magnitude lower than those for the alkalides which indicates that there are more carriers in electrides. The band gaps of the electrides are not significantly different from those of the alkalides. The electrides may, however, still be extrinsic semiconductors with the most important carriers trapped in shallower wells compared with the wells for the majority of the trapped electrons. In support of this picture, the optical spectrum of $\text{Rb}^+(\text{15C5})_2 \cdot \text{e}^-$ for example, also indicated the presence of electrons at many energy levels because of the breadth of the optical absorption peak.

There is a general trend for many of the compounds to have an increase in the apparent energy gap as the experiment proceeds. This increase of E_g may be due to a "bleaching" of the shallow traps by the current flow or by an annealing or decomposition. The results for $\text{Cs}^+(\text{15C5})_2 \cdot \text{Na}^-$ indicate that electrons from the shallow traps are removed by the first set of measurements and that the conductivity observed for subsequent temperature runs is due to electrons in deeper traps. There is very little change in the band gap calculated for the second and third data sets. This explanation does not hold for other compounds in which the E_g values remain fairly constant,

(e.g., $K^+(15C5)_2 \cdot e^-$), or which have erratic values from one temperature run to the next, e.g. $Rb^+(15C5)_2 \cdot e^-$.

One of the problems encountered in the estimation of the band gap by conductivity measurements is the available temperature range. The conductivity of many materials can be measured over a wide range of temperatures. However, in alkalides and electrides thermal instability of the crystals prevents current measurements above $-10^\circ C$. Low current readings limit the low temperature value so that a 100° span is the maximum obtainable range. Slight variations in the energy gap estimation can result in wild deviations for the estimates of resistance at infinite temperature. The values of R_∞ for $Cs^+(15C5)_2 \cdot Na^-$ differ by a full order of magnitude between two temperature runs even though both have the same calculated energy gap. Data from the KINFIT output show a strong correlation between E_g and R_∞ as expected from Equation (8). Small errors in either estimation result in errors for the other. These errors may be plainly observed by the randomness of the R_∞ values. The computer-calculated curves fit the data very well as reflected by the small error in the individual estimates of E_g for each data set. However, the correlation of E_g with R_∞ is too strong and the temperature range too small to use the calculated uncertainty for E_g as the true error of the calculated values. A much more realistic value for the uncertainty of the band gaps should be ± 0.1 eV or more.

In conclusion, all the compounds measured behaved as extrinsic semiconductors with relatively small band gaps. The conductivities for $K^+(15C5)_2 \cdot e^-$ and $Rb^+(15C5)_2 \cdot e^-$ were higher than those of the alkali salts which indicates the presence of more carriers in the electrides. The temperature range covered by the conductivity experiments is too small to give accurate estimations of the band gap for such extrinsic semiconductors. It would be interesting to measure single crystal conductivities for these crystals to see if any ionic conductivity occurs and perhaps obtain more reliable values for the band gaps.

E. Electron Paramagnetic Resonance

Electron paramagnetic resonance (EPR) spectra give information about the environment of unpaired electrons. Pure alkali electrides have an ns^2 valence electron configuration and would be EPR inactive. Indeed, $Na^+C_{222} \cdot Na^-$ has no appreciable EPR signal. Paramagnetic impurities, such as F centers or metal atoms, would give EPR signals. Previous studies of alkali electride systems yielded EPR spectra of trapped electrons that featured hyperfine splitting [51,53]. The splitting of the signal was due to the interaction of the trapped electron with the nucleus of the cation. The amount of interaction and extent of the splitting were preparation-dependent for each compound.

Preliminary EPR studies were made for $K^+(15C5)_2e^-$ and $Rb^+(15C5)_2 \cdot e^-$ to determine the line shape and g-value for each compound. Both electriles had very strong microwave power absorption. A very small amount of sample was used to avoid saturation of the microwave receiver. Even so, power studies showed distortion of the EPR line at power levels of 800 nanowatt or higher. The g-values were calculated from the equation

$$h\nu = g \cdot \mu \cdot H \quad (9)$$

where h is Planck's constant, ν is the spectrometer frequency, μ is the Bohr magneton and H is the field of the resonance in gauss. $Rb^+(15C5)_2 \cdot e^-$ and $K^+(15C5)_2 \cdot e^-$ had very similar spectra and are shown in Figures 19 and 20 respectively. Both compounds have g-values of 2.003 ± 0.001 which is very close to the free electron value of 2.0023. The linewidths for the spectra were quite narrow and equaled 0.45 G for $K^+(15C5)_2 \cdot e^-$ and 0.58 G for $Rb^+(15C5)_2 \cdot e^-$ and showed no evidence of hyperfine splitting. The g-value and linewidth indicate that the electron is fairly isolated in its environment and has little interaction with neighboring nuclei that would lead to a g-shift.

When the conduction electrons in metals give rise to an EPR signal, the lineshape of the spectrum is highly asymmetric and is referred to as Dysonian. For thick metal plates in which the skin depth, δ , is small compared to the

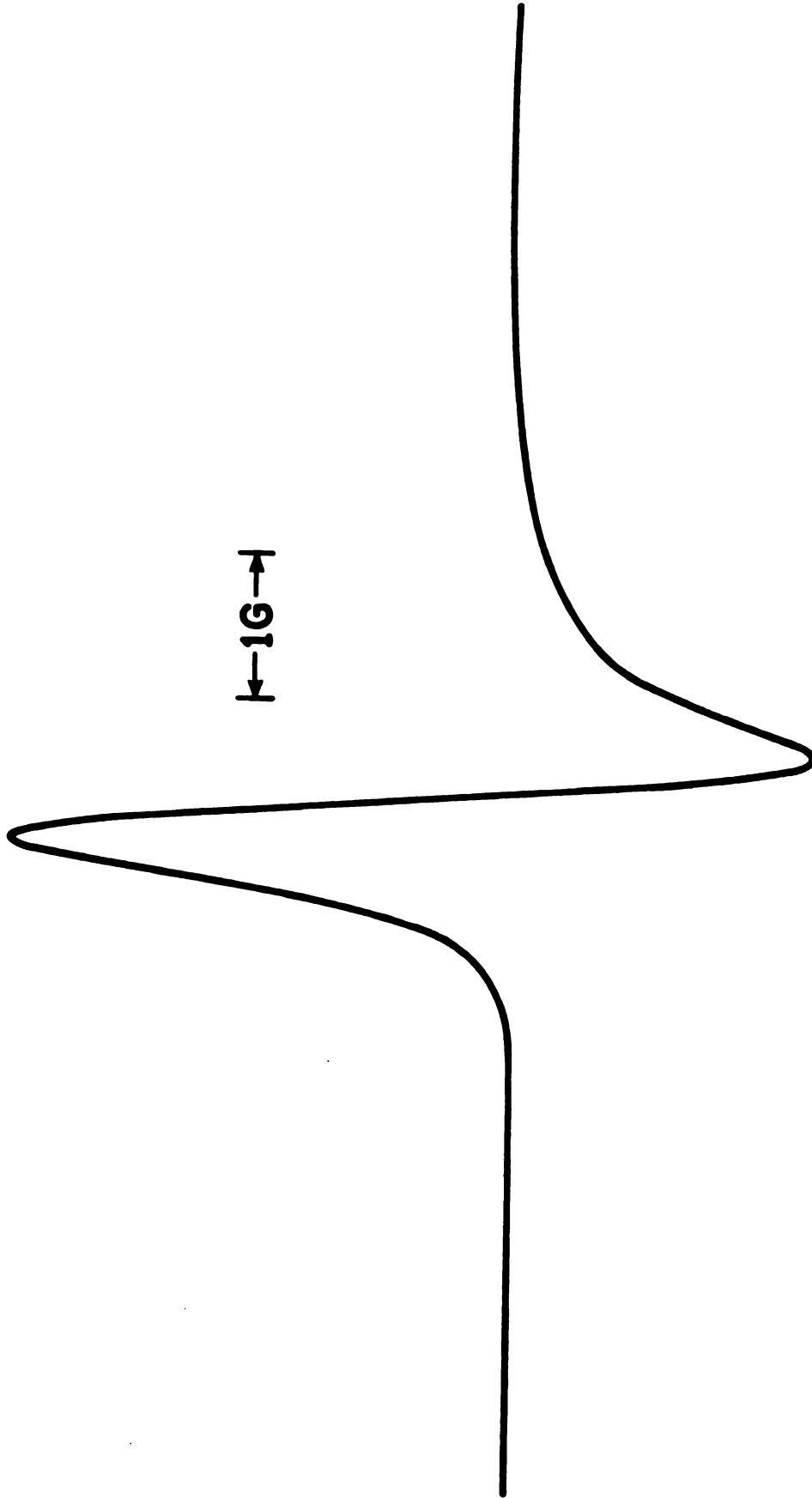


Figure 19. EPR Spectrum of $\text{Rb}^+(15\text{C}5)_2 \cdot \text{e}^-$ at -103°C .

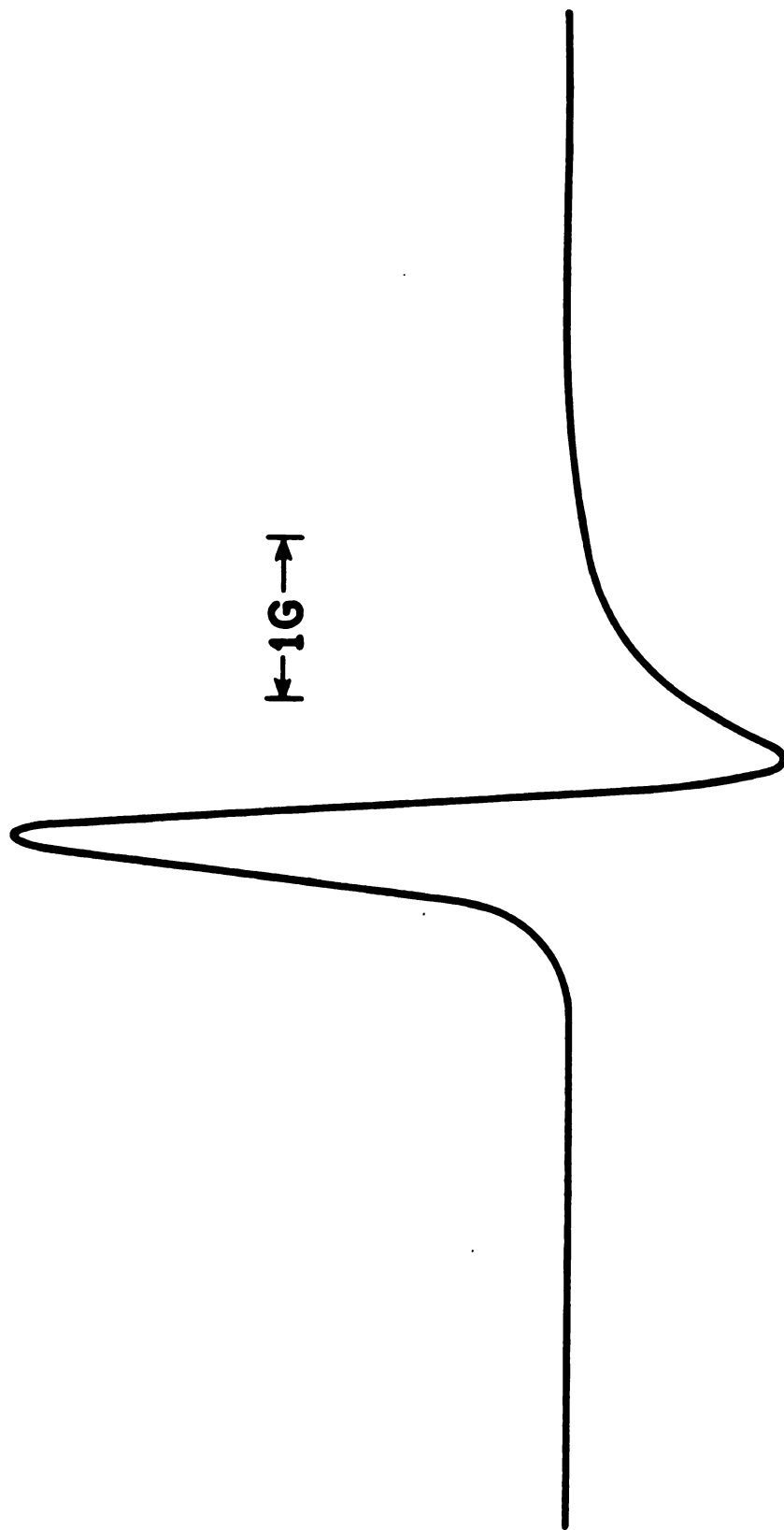


Figure 20. EPR Spectrum of $K^+(15C5)_2 \cdot e^-$ at $-97^\circ C$.

sample thickness, the A/B ratio exceeds 2.7 [62]. The A/B ratio will have a value between 1 and 2.7 for spherical metal particles in which the skin depth is on the order of the particle size. However, the packing density of powdered samples may also affect the A/B value [53].

The line shapes for both $K^+(15C5)_2 \cdot e^-$ and $Rb^+(15C5)_2 \cdot e^-$ were asymmetric with A/B ratios of 2.31 and 1.67 respectively. The asymmetry of the line may be due to the intrinsic conductivity of the sample even for nonmetallic samples. For small particles with high conductivity, a Dysonian line shape may be obtained where the skin depth is on the order of the particle size. The A/B ratio usually ranges between 1 and 2.7 for these types of samples.

The temperature dependence of the A/B ratio has been used to estimate the apparent band gap of $Cs^+(15C5)_2 \cdot e^-$ [53]. The band gap was estimated to be 0.1 eV from the EPR experiments and 0.9 eV from the pressed powder D.C. conductivity experiment. The cause of the difference of E_g between the two methods is not known. Perhaps this difference arises from intergrain resistance or the intrinsic differences in the methods of conduction. The microwave "conductivity" is really a measure of the AC impedance rather than the resistance only and the contributions of both resistance and capacitance components may give an usually small apparent band gap.

A number of additional EPR experiments should be done to permit us to understand the cause of the asymmetry of

the derivative of the signal. First, temperature studies need to be made to determine if there is a temperature dependence of the line shape. Temperature dependence would probably confirm the D.C. conductivity conclusions that $K^+(15C5)_2 \cdot e^-$ and $Rb^+(15C5)_2 \cdot e^-$ are semiconductors rather than metals. Second, the EPR spectra could be obtained for samples which have been diluted with an EPR inactive material. Diluted samples should have Lorentzian line shapes with $A/B = 1$ if the distortion is due to the bulk conductivity of the sample with conduction across the intergrain boundaries. Third, single crystal EPR could be used to study the effects of orientation on the line position and shape.

F. Magnetic Susceptibility

Pure paramagnetic materials have susceptibilities that are inversely proportional to the temperature. The proportionality constant, C , is called the Curie constant, named after the man who proposed this relationship. For a paramagnetic material with 100% unpaired spins in the state $S = 1/2$ and in the absence of orbital angular momentum of the electrons, $C = 0.3760$. This "law" was modified by P.R. Weiss to include the mean local field effects generated by ferromagnetic and antiferromagnetic materials above their transition temperature. The resultant relationship is given by

$$\chi = \frac{C}{T-\theta} \quad (10)$$

and is called the Curie-Weiss law where C is the Curie constant and θ is the Weiss constant. The high temperature susceptibility may be used to predict whether a material is ferromagnetic ($\theta > 0$), paramagnetic ($\theta = 0$) or antiferromagnetic ($\theta < 0$). For antiferromagnetic materials, a temperature, T_N , called the Néel temperature, may be approximated by $T_N = -\theta$. Below the Néel temperature the spins of the material will attempt to align perpendicular to the applied field. If the spins were completely free to move, a temperature independent susceptibility would result. However, this is never the case due to crystal field effects or other mechanisms which constrain the motion. In single crystal studies the crystals may be so oriented that the ideal behavior is observed. However, in powdered samples, deviations will be seen from Equation (10) near and below the Néel temperature [63]. Deviations from pure Curie law behavior may also be seen for systems where local interactions affect the environment of the electron but in which no distinct transitions occur. Many materials do not have the rigid spin lattice required for them to be classified as ferromagnetic or antiferromagnetic. For these materials, θ serves as a "catch all" correction parameter. Unfortunately, there is no straightforward way to analyze data that deviate from the simple Curie-Weiss law.

The temperature dependence of the susceptibility was measured for $\text{Rb}^+(\text{15C5})_2 \cdot \text{e}^-$ and $\text{K}^+(\text{15C5})_2 \cdot \text{e}^-$ up to 225 K. The data were fit, with the use of KINFIT [61], to a modified version of Equation (10) to which a temperature independent correction term, B, was added. Diamagnetic impurities, such as M^- , would give negative values for B and would decrease the observed value of the susceptibility. A correction for paramagnetic impurities, such as precipitated metal, can also be made by the use of the B correction term. The plot of $1/\chi_M$ versus T for $\text{Rb}^+(\text{15C5})_2 \cdot \text{e}^-$ is given in Figure 21 for measurements over a temperature range of 1.3 to 224 K. The susceptibility has been corrected to remove contributions from the bucket, crown ether molecules and nonvalence electrons of the rubidium so that only the electronic contribution to the magnetic susceptibility is reported. Two features of the $1/\chi_M$ versus T plot are remarkable. First, at temperatures of 20 K and below, the data deviate from the straight line expected for strict adherence to the Curie-Weiss law. This deviation is in a direction that suggests a decrease in the antiferromagnetic interaction at low temperature. The calculated value of θ , based upon all of the data, was -4.42 K, which indicates that $\text{Rb}^+(\text{15C5})_2 \cdot \text{e}^-$ exhibits antiferromagnetic interactions.

The second notable feature of the $1/\chi_M$ versus T plot for $\text{Rb}^+(\text{15C5})_2 \cdot \text{e}^-$ is the discontinuity in the slope observed between 120 and 140 K. Above 140 K, the plot is

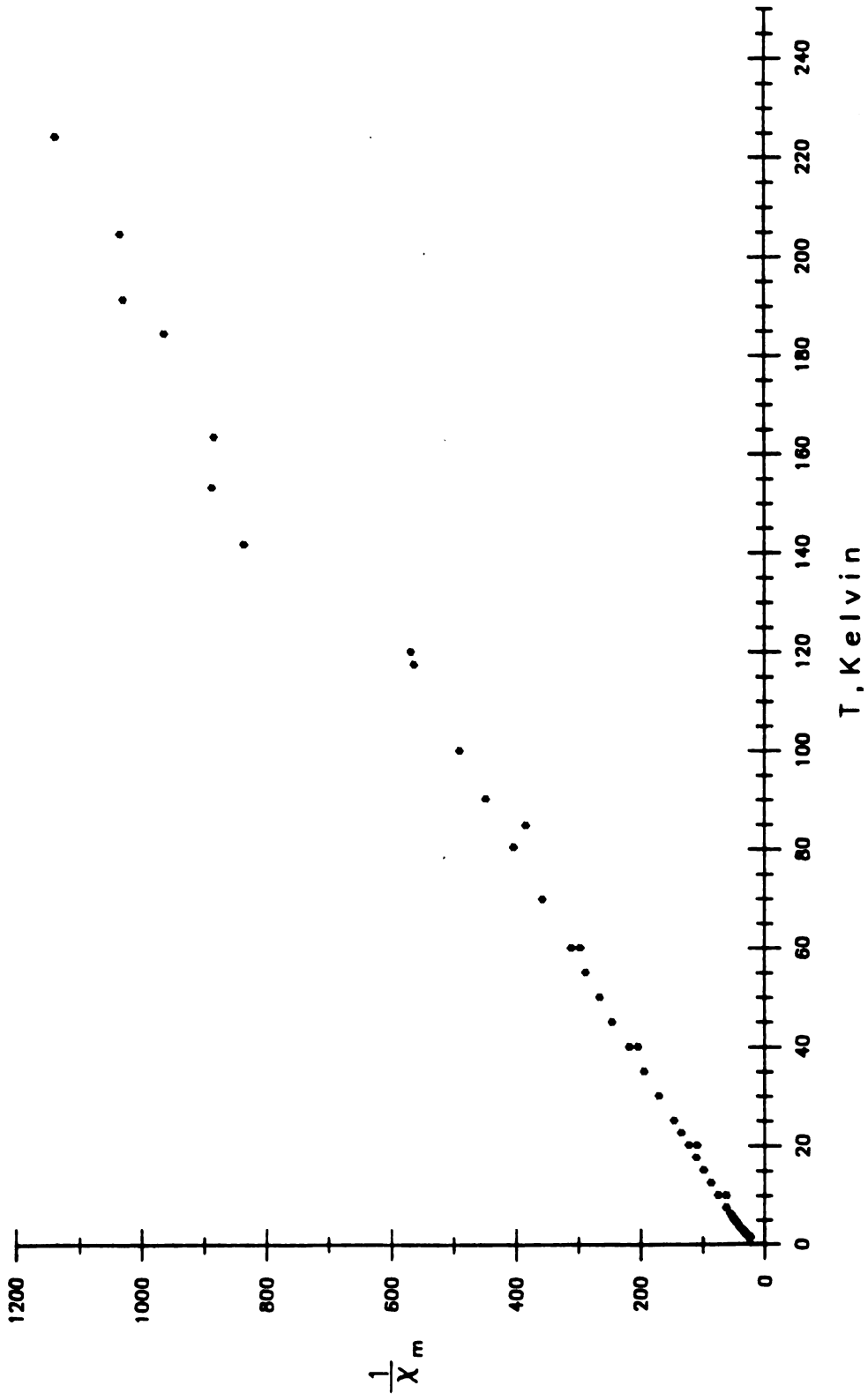


Figure 21. $1/X_m$ versus Temperature for $\text{Rb}^+(15\text{C5})_2 \cdot \text{e}^-$.

linear, but is displaced from the line observed in the 20 to 120 K temperature range. This change was observed as the temperature was decreased as well as increased, which is indicative of a reversible transition. The calculated Curie constant for the entire temperature range was 0.2068. Since the diamagnetic background has been subtracted, we can say $\text{Rb}^+(\text{15C5})_2 \cdot \text{e}^-$ behaves, to first order, as a compound with 55% free spins. The remaining spins may be associated with rubidium nuclei to form Rb^- , lie in diamagnetic ground states or be removed by decomposition of the sample. However the deviations suggest that the Curie-Weiss equation is not the correct one to use, so that one should not take the 55% figure too seriously. The correction term, B, was calculated to be $-65 \times 10^{-6} \text{ mol}^{-1}$ for this sample. These results might be used to imply the presence of Rb^- but, more likely, are a result of an inappropriate equation.

Instrument trouble prevented the measurement of the susceptibility of $\text{K}^+(\text{15C5})_2 \cdot \text{e}^-$ below 5 K. As in the case of $\text{Rb}^+(\text{15C5})_2 \cdot \text{e}^-$, the high temperature data points had good adherence to the Curie-Weiss law but no discontinuity in the slope was observed. The apparent Curie constant is 0.3548 for the electronic susceptibility of $\text{K}^+(\text{15C5})_2 \cdot \text{e}^-$ and corresponds to ~95% "unpaired spins". The experimental points deviate from the calculated line at $T \leq 15$ K as seen in the $1/\chi_M$ versus T plot given in Figure 22. The Weiss constant is -19.5 which, if real, corresponds to signifi-

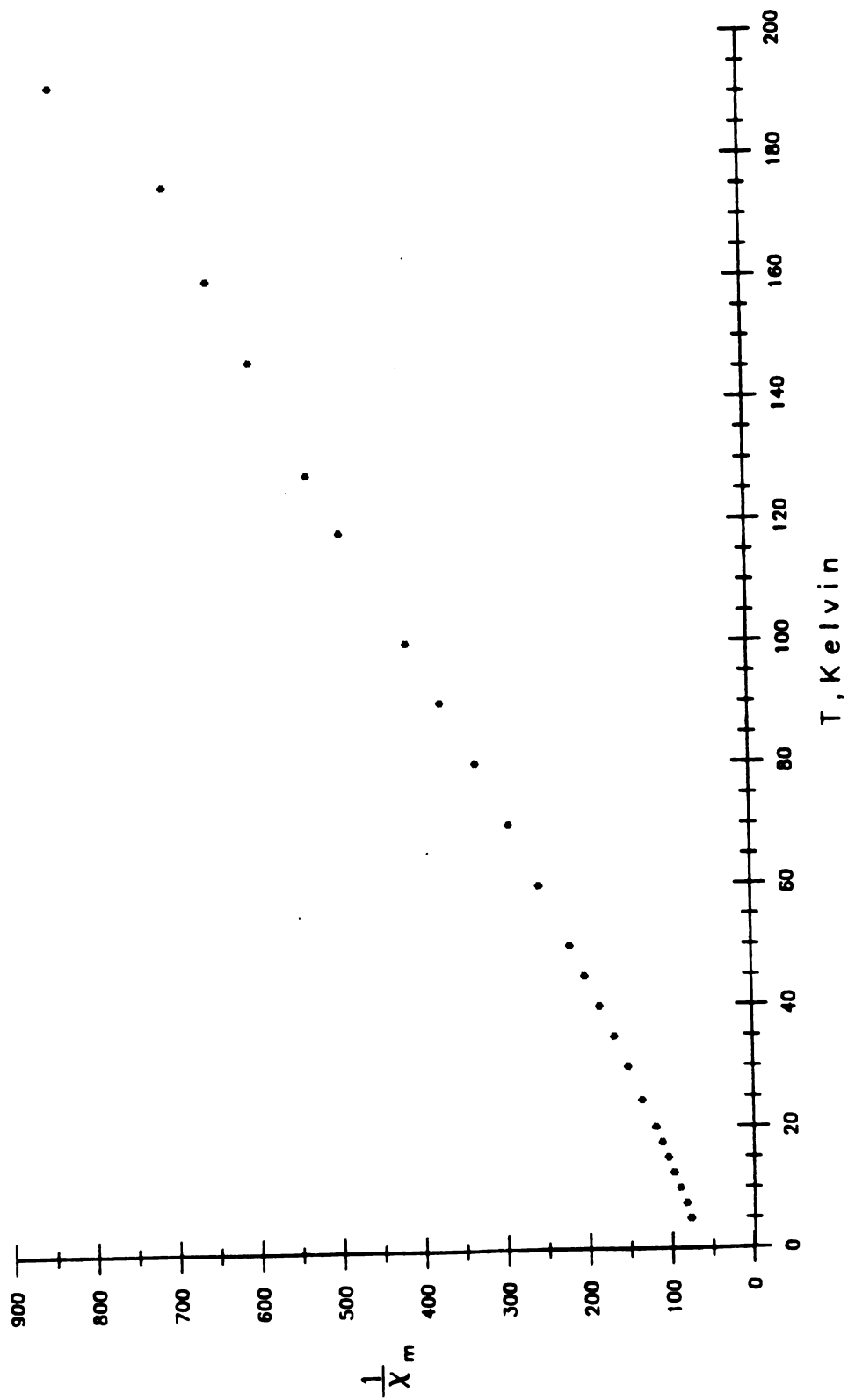


Figure 22. $1/X_m$ versus Temperature for $K^+(15C5)_2 \cdot e^-$.

cantly higher antiferromagnetic interactions for $K^+(15C5)_2 \cdot e^-$ than for $Rb^+(15C5)_2 \cdot e^-$. The temperature independent correction term is also much larger and is calculated to be $-500 \times 10^{-6} \text{ mol}^{-1}$ for $K^+(15C5)_2 \cdot e^-$. The magnitude of this correction term is too large to be attributed to K^- or other impurities. Although variations of the B term from one sample to another have been observed in the past, the values of the B term obtained for different samples of the same compound vary by no more than a factor of 2 and are on the order of $-40 \times 10^{-6} \text{ mol}^{-1}$ [44,50]. The magnitude of the correction term for $K^+(15C5)_2 \cdot e^-$ was such that it was first thought to be caused by a change of the zero in the susceptometer between the pristine and oxidized sample measurements. However neither data set, when considered individually, showed evidence of zero drift or discontinuity during the susceptibility measurements. A more plausible cause of the large B term is the low temperature susceptibility deviations from the Curie-Weiss law. The line fitting program probably overestimates the temperature independent correction terms in order to achieve a good fit with the wrong equation.

Careful studies of $Rb^+(15C5)_2 \cdot e^-$ and $K^+(15C5)_2 \cdot e^-$ should be made at low temperatures with varying field strengths in order to determine the extent of the antiferromagnetic behavior of $K^+(15C5)_2 \cdot e^-$ and $Rb^+(15C5)_2 \cdot e^-$. In addition, the susceptibility of $Rb^+(15C5)_2 \cdot e^-$ should be

carefully examined in the temperature range of 100 to 170 K in an attempt to verify the existence of the discontinuity. This transition may arise from the "quenching" procedure which occurs when the sample is loaded into the susceptometer at 5 K. Also, more samples of each electride need to be measured to get more reliable estimates of B. Care must be taken that only freshly prepared samples are used for susceptibility measurements due to the apparent decomposition with time during storage at -80°C .

G. Data From Other Sources

The unusually high thermal stability of the compounds reported in this chapter makes them ideal candidates for a variety of studies. The results of these types of studies, made by investigators other than the author, are included in this section in order to complete the presentation of information gathered for these new compounds. The reader is referred to the publications of the original investigator(s) for full experimental details and data manipulation techniques.

1. Differential Scanning Calorimetry -- The thermal stability of the new compounds that contain sodium is greater than that of the other new alkalides. In general, most sodides are stable up to their melting point (if heated rapidly) and decompose irreversibly at higher temperatures. Two of the new compounds, $\text{K}^+(\text{15C5})_2 \cdot \text{Na}^-$ and $\text{Rb}^+(\text{15C5})_2 \cdot \text{Na}^-$,

were studied by differential scanning calorimetry (DSC) by J.L. Dye at AT&T Bell Laboratories, Murray Hill, New Jersey [43]. The DSC trace for $\text{Rb}^+(\text{15C5})_2\cdot\text{Na}^-$ is given in Figure 23. There is a small endothermic transition at 35°C which may be due to the melting of excess crown ether, evaporation of remaining traces of solvent or the presence of electride. The compound melts at 75° and then decomposes irreversibly. $\text{Na}^+\text{C222}\cdot\text{Na}^-$ melts at 73°C and all other alkalides and electrides tested were observed to melt at temperatures below 70°C . Therefore, $\text{Rb}^+(\text{15C5})_2\cdot\text{Na}^-$ is the most stable alkalide to date. Rapid decomposition begins at $\sim 100^\circ\text{C}$ and is marked by the large exothermic peak at 121°C in the DSC trace. $\text{K}^+(\text{15C5})_2\cdot\text{Na}^-$ was observed to melt at 45°C with no prior endothermic peak. Decomposition was only 10% at 97°C and reached a maximum rate at 108°C . The thermal stability and ease of synthesis of $\text{Rb}^+(\text{15C5})_2\cdot\text{Na}^-$ and $\text{K}^+(\text{15C5})_2\cdot\text{Na}^-$ make these compounds the most feasible for possible utilization as two-electron donors for difficult reduction reactions.

2. X-ray Diffraction Studies -- The crystal structure of $\text{Rb}^+(\text{15C5})_2\cdot\text{Na}^-$ was determined by X-ray diffraction studies of a single crystal. Measurements were made by O. Fússá and D. Ward with a Nicolet P3F Diffractometer. The rubidium cation is sandwiched between two 15-crown-5 molecules as suggested by the stoichiometry. The crown ether rings are staggered such that the Rb^+ serves as an inversion center. The ten oxygen atoms are more-or-less at

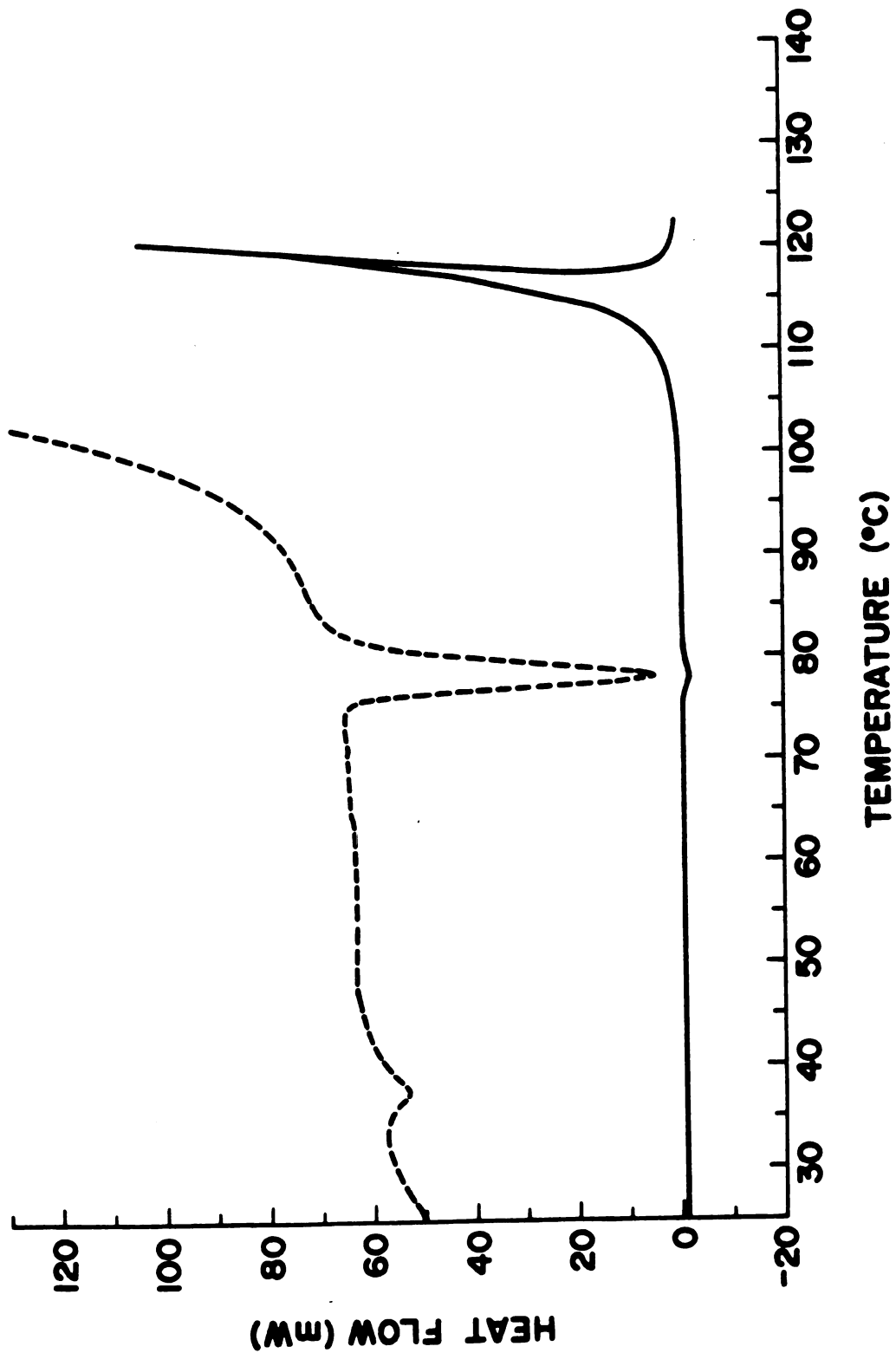


Figure 23. DSC Trace for $\text{Rb}^+(15\text{C}5)_2\cdot\text{Na}^-$.

equal distances from the Rb^+ and the ether rings lie planar and parallel to one another. The "expanded" cations are stacked in ABAB repeating layers with the crown ether rings tilted a few degrees from the column of stacking. The sodium anions are situated in the pseudo-octahedral hole with a radius of 2.4 to 2.6 Å. The reader is referred to a forthcoming paper for the full crystallographic description of $\text{Rb}^+(\text{15C5})_2 \cdot \text{Na}^-$.

3. EXAFS and XANES -- Extended X-ray Absorption Fine Structure (EXAFS) and X-ray Absorption Near Edge Structure (XANES) give information on the physical and electronic environment of a nucleus, respectively. The K-edge X-ray absorption spectrum of $\text{Rb}^+(\text{15C5})_2 \cdot \text{Na}^-$ is given in Figure 24. The spectrum has three features that were used to identify the environment of the rubidium nucleus. First, the location of the X-ray absorption edge can be used to distinguish between two oxidation states of a nucleus. Second, the relative area of the threshold resonances up to 40 eV from the edge may also be used to identify the electronic environment of the nucleus (XANES). Third, the modulations at 40 eV and beyond, after Fourier transformation may be compared to those of compounds with known structures. By the use of EXAFS, structural information may be obtained even when the crystals are too small or of too poor quality for single crystal X-ray diffraction studies. This information is usually limited to neighbors within a 4 Å distance from the nucleus under study.

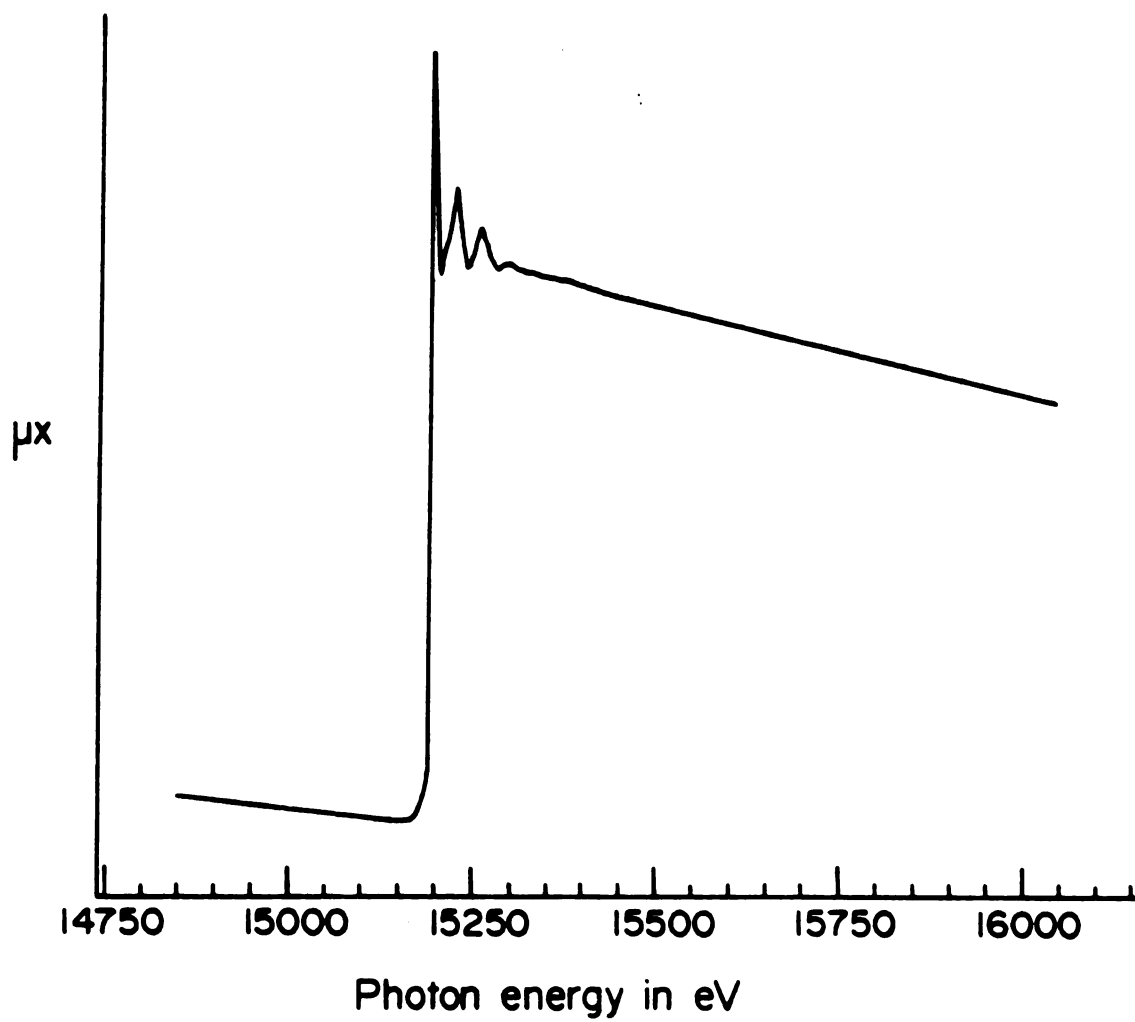


Figure 24. K-edge X-ray Absorption Spectrum of $\text{Rb}^+(\text{15C5})_2 \cdot \text{Na}^-$.

O. Fússá and coworkers [64,65] have studied the rubidium environment of $\text{Rb}^+(\text{15C5})_2 \cdot \text{e}^-$, $\text{Rb}^+(\text{15C5})_2 \cdot \text{Na}^-$, $\text{Rb}^+(\text{15C5})_2 \cdot \text{Rb}^-$ and $\text{RbK}(\text{15C5})_2$. The energy of the K-edge absorption threshold of Rb^- is only 2 eV lower than that of complexed Rb^+ salts. Therefore, the relative edge positions are not good indicators of the formal oxidation state of rubidium. XANES is used to assign the oxidation states. The area, A , of each absorption threshold resonance ("white line") was normalized to unit edge jump and compared to that of complexed rubidium model salts and known rubidides. The samples were allowed to react with air and the X-ray absorption of the decomposed sample was measured. The results of these studies are given in Table VI below.

Table VI. Relative Normalized Areas^a of Rubidium K-Edge Absorption Threshold Resonances.

<u>Compound</u>	<u>A (pristine)^b</u>	<u>A (oxidized)^b</u>
$\text{Rb}^+(\text{15C5})_2 \cdot \text{e}^-$	36	36
$\text{Rb}^+(\text{15C5})_2 \cdot \text{Na}^-$	29	34
$\text{Rb}^+(\text{15C5})_2 \cdot \text{Rb}^-$	18	29
$\text{Cs}^+(\text{15C5})_2 \cdot \text{Rb}^-$	1-6	36
$\text{K, Rb}(\text{15C5})_2$	16	34

^aRelative uncertainty is $\pm 4 \times 10^{-2}$ cm.

^bcm \times 100

The area of the white line for the complexed model salts and the oxidized alkalides and electriles ranged from 25 to 36. $\text{Rb}^+(\text{15C5})_2 \cdot \text{e}^-$ and $\text{Rb}^+(\text{15C5})_2 \cdot \text{Na}^-$ have areas equal to 37 and 29 respectively which indicates that the majority of the rubidium is in the +1 oxidation state in these compounds. This assignment is further confirmed by the small change in the area upon oxidation. On the other hand, the white line of $\text{Cs}^+(\text{15C5})_2 \cdot \text{Rb}^-$ has a very small area of only 1 to 6 which is on the order of that observed for the pure rubidide, $\text{Cs}^+ \text{18C6}_2 \cdot \text{Rb}^-$ ($\underline{\Lambda} = 1$). Upon oxidation the area changes to 36 for $\text{Cs}^+ \text{15C5})_2 \cdot \text{Rb}^-$ and to 30 for $\text{Cs}^+(\text{18C6})_2 \cdot \text{Rb}^-$.

The compound with stoichiometry $\text{Rb}(\text{15C5})$ was thought to have rubidium in both the +1 and -1 oxidation states. The white line area of 18 lies in between the values observed for pure rubidides and compounds with only complexed rubidium cations. The value of $\underline{\Lambda}$ increased to 29 upon decomposition thereby confirming the assignment of $\text{Rb}^+(\text{15C5})_2 \cdot \text{Rb}^-$ for this compound. It was hoped that the ambiguity over the anion assignment of $\text{RbK}(\text{15C5})_2$ could be resolved with rubidium XANES. Again, the area of the white line had an intermediate value of 16 which increased to 34 upon oxidation of the sample, indicative that there is a mixture of oxidation states as in $\text{Rb}^+(\text{15C5})_2 \cdot \text{Rb}^-$. From this result and the stoichiometry, it is evident that there is a mixture of crystals having both potassium and rubidium present as sandwich cations and anions.

The crystal structure of $\text{Rb}^+(\text{15C5})_2 \cdot \text{Na}^-$ allowed the EXAFS of this compound to serve as the model result. The Fourier transform of the spectrum of $\text{Rb}^+(\text{15C5})_2 \cdot \text{e}^-$ is virtually identical to that of $\text{Rb}^+(\text{15C5})_2 \cdot \text{Na}^-$ where the rubidium is sandwiched by two crown ether rings. The EXAFS and stoichiometry of this compound identify it as a true electride. Likewise, the EXAFS spectra of $\text{Rb}^+(\text{15C5})_2 \cdot \text{Rb}^-$ and the mixture, $\text{RbK}(\text{15C5})_2$, are consistent with the presence of both $\text{Rb}^+(\text{15C5})_2$ and Rb^- . The EXAFS spectrum of $\text{Cs}^+(\text{15C5})_2 \cdot \text{Rb}^-$ shows only very weak modulations as observed for krypton gas. Due to the large radius expected for Rb^- , the rubidium anion is expected to behave as an isolated ion in the extended X-ray absorption region. $\text{Cs}^+(\text{18C6})_2 \cdot \text{Rb}^-$ also has a very weak fine structure such that no structural information may be obtained for the Rb^- environment [64].

At this time EXAFS and XANES have been successfully applied to rubidium alkalides and electrides. Although sodium and potassium EXAFS studies are feasible, the K-edge of these elements lie at energies too low for the available experimental set up. Cesium K-edge X-ray absorption does not yield useful information due to fast core-relaxation effects. Some studies were made for the L-edge of cesium with fluorescence detection. The signal to noise ratio was, however, too low to provide useful information about alkalides and electrides. Although EXAFS and XANES can clearly identify rubidium compounds, another nuclear specific identification tool is needed for the other alkalides and electrides.

PART II:

Alkali Metal NMR Studies of Alkalides.

PART II

CHAPTER ONE -- INTRODUCTION

The identification of alkalides and electrides has traditionally been based on the stoichiometry and optical absorption spectrum of each compound. However, the species in the films which are used for optical studies, may or may not be the same as those present in the crystals. Recently, X-ray absorption near edge structure (XANES) studies have been used to identify crystalline alkalides and electrides that contain rubidium [64,65]. Unfortunately, due to instrument availability and other experimental limitations, this technique cannot be used to probe the environment of the other alkali metals.

Nuclear magnetic resonance provides a direct probe of the electronic environment of a nucleus since the resonance frequency of the nucleus is dependent on the shielding by the electrons. This chapter will cover some nuclear properties of the alkali metals, the application of alkali metal NMR to study alkali metal anions in solution, solid state NMR and finally, an example of magic angle spinning (MAS) NMR as an identification tool.

A. Nuclear Properties of Alkali Metals

Each alkali metal has at least one magnetically active isotope. Table VII gives some nuclear properties of the alkali metals. Most commonly, NMR studies involve the isotopes ${}^7\text{Li}$, ${}^{23}\text{Na}$, ${}^{39}\text{K}$ and ${}^{133}\text{Cs}$ due to their high natural abundances. In the case of rubidium, however, the less abundant isotope is the nucleus of choice. The relative sensitivity is dependent on the cube of the magnetic moment as well as the natural abundance and nuclear spin, so the larger μ_N for ${}^{87}\text{Rb}$ determines the larger sensitivity for that isotope than that of ${}^{85}\text{Rb}$.

The Sternheimer antishielding factor, $1+\gamma_\infty$, is a measure of the amplification of the field gradient of the nucleus produced as a result of polarization effects in the electron cloud induced when the atom, as a whole, is exposed to an electric field gradient. Values of $1+\gamma_\infty$ are determined from the fine structure in electron spectra of atoms by the use of quantum chemical calculations similar to those leading to electrical quadrupole moments. The values listed in Table VII refer to the free cations and will change, if the the electronic wavefunction becomes significantly altered by strong ion-ion or ion-solvent interactions.

For several of the alkali nuclei the quadrupole moments are large enough to make quadrupole effects dominate the NMR spectra. Linewidths are a reflection of the reaction

TABLE VII. Nuclear Properties of Alkali Metals.

Nucleus	Nuclear Spin, I	Natural Abundance, %	Magnetic Moment, μ_N	Quadrupole Moment (barns)	Relative Sensitivity ^{a,b}	Sternheimer ^c antishielding factor, $(1+Y_\infty)$
⁶ Li	1	7.4	0.822	4.6×10^{-4}	8.5×10^{-3}	0.74
⁷ Li	3/2	92.6	3.256	-0.042	0.29	0.74
²³ Na	3/2	100	2.216	0.10	9.25×10^{-2}	5.1
³⁹ K	3/2	93.1	0.391	0.049	5.08×10^{-4}	18.3
⁴⁰ K	4	0.012	-1.296	-0.07	6.2×10^{-7}	18.3
⁴¹ K	3/2	6.88	0.5047	0.067	8.4×10^{-5}	18.3
⁸⁵ Rb	5/2	72.2	1.348	0.26	1.05×10^{-2}	48.2
⁸⁷ Rb	3/2	27.8	2.741	0.13	0.17	48.2
¹³³ Cs	7/2	100	2.564	-0.003	4.74×10^{-2}	111

a) Reference 66.

b) Referred to the proton NMR signal of H₂O at the same magnetic field and with the same probe volume.

c) Reference 67.

rates and the efficiency of the quadrupole relaxation and depend upon the square of $Q(1+\gamma_{\infty})$. The quadrupole moment and Sternheimer antishielding factor are so small for ${}^7\text{Li}$ that the relaxation is relatively inefficient and the natural linewidths are often less than 1 Hz. In contrast to ${}^7\text{Li}$, the linewidths of ${}^{85}\text{Rb}$ and ${}^{87}\text{Rb}$ cations in aqueous solutions are on the order of 150 Hz. The extremely small quadrupole moment of ${}^{133}\text{Cs}$ makes the study of cesium as favorable as that for sodium.

Numerous NMR studies of alkali metals in solution have been made to investigate ion-ion and ion-solvent interactions [67-69]. These investigations also include the study of alkali metal complexation by organic macrocycles such as crown ethers and cryptands. Due to the low sensitivity of ${}^{39}\text{K}$ [70] and the large linewidth of ${}^{87}\text{Rb}$ [71], the majority of these studies have been made with ${}^7\text{Li}$, ${}^{23}\text{Na}$ and ${}^{133}\text{Cs}$.

B. NMR of Alkali Metal Anions in Solutions

The first direct proof of the centrosymmetric anion as the species with stoichiometry M^- in amines and ethers was obtained by ${}^{23}\text{Na}$ NMR studies of nonaqueous solutions that contained cryptand-2,2,2 and excess sodium metal [72,73]. Two signals were observed at ~ -10 and -62 ppm from $\text{Na}^+(\text{aq})$ at infinite dilution and were assigned to $\text{Na}^+\text{C222}$ and Na^- , respectively. The Na^- peak was shifted paramagnetically by only 1-2 ppm from the calculated values for the gaseous

atom [74]. Calculations based on Lamb's complete expression for atomic diamagnetic shielding [75] and analytic Hartree-Fock wavefunctions yielded a chemical shift for $\text{Na}^-(g)$ of -63.1 ppm [73]. Pyper and Edwards have combined the Hartree-Fock predictions with electron-electron correlation corrections to obtain chemical shift values for all alkali metals [76]. They predict a value of -63.3 ppm for the chemical shift of $\text{Na}^-(g)$.

The report of the first observation of Na^- by alkali metal NMR was followed by other studies of Na^- in non-aqueous solutions with and without cation complexants present [29,77-80]. Edwards and coworkers have observed Na^- in two component solutions of sodium metal in neat 12-crown-4 [29], in hexamethylphosphoric triamide (HMPA) [77] and in N,N-diethylacetamide (DEA) [78]. No cation signal was observed in any of these solutions due to the extreme broadening of the line by cation-solvent interactions and/or by interactions with solvated electrons. Both Na^+C and Na^- were observed in solutions of cryptand-2,2,2 and sodium metal in methylamine (MA), ethylamine (EA) and tetrahydrofuran (THF) [73]. For solutions of sodium metal and 18-crown-6 in MA, the two NMR signals collapsed into a single broad peak at a chemical shift intermediate to those of $\text{Na}^+(18C6)$ and Na^- . This temperature dependence of the spectrum is due to higher rates of exchange at higher temperatures. The kinetics of the sodium cation-sodium ion exchange has been investigated by Phillips, *et al.* [80].

The anions of rubidium and cesium have been observed by alkali metal NMR for solutions of cryptand 2,2,2 and excess metal [73]. In addition, the signal of $^{87}\text{Rb}^-$ has been obtained for rubidium in neat 12-crown-4 [29]. The complexed cation was not observed for either metal in these solutions, except for $\text{Cs}^+\text{C222}$ in THF [81]. This is not surprising in the case of Rb-C since the linewidth is extremely large for Rb^- and the cation is expected to be less shielded and therefore have broader peaks. The linewidth of Rb^- ranged from 15 Hz in THF to ~1000 Hz in 12C4. Khazaeli, *et al.* reported the absence of a Rb^+ signal when the complexant-rubidium ratio was sufficiently high to ensure complete complexation of Rb^+ [71]. The $^{87}\text{Rb}^+$ signal broadened as the complexant-rubidium ratio increased until it was too broad to measure.

The reason for the absence of a $^{133}\text{Cs}^+\text{C}$ signal in most solutions is not clear. $\text{Cs}^+\text{C222}$ was observed by ^{133}Cs NMR in an 0.08 M solution of $\text{Cs}^+\text{C222}\cdot\text{I}^-$ in methanol. The chemical shift of the Cs^+C was ~161 ppm more paramagnetic than the signal observed for a 0.08 M methanol solution of Cs^+I^- . The linewidths were <3 Hz for Cs^+ and ~30 Hz for $\text{Cs}^+\text{C222}$ and are indicative that the cation is truly complexed at 25°C. P. Smith [81] observed a $^{133}\text{Cs}^+\text{C222}$ signal in THF solutions of cryptand-2,2,2 and cesium metal at low temperatures (-64 to -86°C). The peak was probably broadened by rapid exchange between inclusive and exclusive complexation of the cation. The $^{133}\text{Cs}^+\text{C222}$ peak became

narrower as the temperature decreased, indicative of an exchange reaction.

Table VIII gives the calculated chemical shifts for $M(g)$ and $M^-(g)$ as well as the values observed for M^- in solution. All previous attempts to observed K^- have been unsuccessful [73,79,82]. The chemical shifts deviate from the calculated values of $M^-(g)$ as the atomic number increases. This deviation may be due to more polarization by the anion-solvent or anion-cation interactions or by greater mixing of p and/or d character into the ground state s function of M^- as the atomic number increases.

C. Solid State NMR

A notable feature of NMR is that the linewidths in the spectra of solids are much broader than those observed from solutions. An excellent example of the extreme difference that can occur between the solid state and solution linewidths is given by the proton spectra of H_2O . Liquid water has a linewidth of 0.1 Hz while that of ice is on the order of 10^5 Hz. This substantial difference arises from the static anisotropic interactions in solids which are averaged by rapid isotropic motions of the nuclei in fluid samples. Sometimes there is sufficient motion in solids to narrow the NMR signals, but these cases are the exceptions, not the rule [83].

TABLE VIII. Calculated Chemical Shifts for Gaseous Alkali Metal Atoms and Anions and Observed Chemical Shift of M⁺ in Solution.

Nucleus	Calculated ^b		Observed ^c		Solvent	Reference
	M ⁺ (g), ppm	M ⁺ (g), ppm	M ⁺ (solv), ppm	Chemical Shift		
²³ Na	-60.5 ± 1	-63.1	-61.7		HMPA	77
			-61.8		12C4	29
			-61.9		MA	73
			-62.1		EA	73
			-62.8		THF	73
			-62.9		DEA	78
³⁹ K	-101.1 ± .5	-103.4		not observed		
⁸⁷ Rb	-211.6 ± .1	-213.6	-185.4		EA	73
			-191		12C4	29
			-197.2		THF	73
¹³³ Cs	-344.3 ± 6	-346.4	-292		THF	73

a) Relative to M⁺ at infinite dilution.

b) Reference 74.

c) Reference 76.

Several experimental techniques have been implemented to reduce the anisotropic broadening in solids. One of these, which is called magic angle spinning (MAS), will be discussed in this section. The types of anisotropic nuclear interactions that are of interest are magnetic dipolar, chemical shift anisotropy and electronic quadrupolar interactions. Numerous review articles have been written on the NMR of solids and the magic angle spinning technique [84-88].

The truncated dipolar interaction Hamiltonian, for all nuclear pairs i, j in the solid is given by:

$$\mathcal{H}_D = \sum_{i < j} \frac{1}{2} \gamma_i \gamma_j \hbar^2 r_{ij}^{-3} (\mathbf{I}_i \cdot \mathbf{I}_j - 3 I_{iz} I_{jz}) (3 \cos^2 \theta_{ij} - 1) \quad (11)$$

where γ_i, γ_j are the nuclear magnetogyric ratios, r_{ij} is the internuclear distance, and θ_{ij} is the angle between r_{ij} and the direction of the field H_0 . The isotropic average of $\cos^2 \theta_{ij}$ is $1/3$, so that the rapid isotropic motion in fluids yields no net dipolar contribution.

When a solid specimen is rotated uniformly with angular velocity ω_r about an axis inclined to H_0 at an angle β , every internuclear vector, r_{ij} , may be described by the motion illustrated in Figure 25. The angle θ_{ij} may be expressed by other angles in the system as follows:

$$\cos \theta_{ij} = \cos \beta \cos \beta'_{ij} + \sin \beta \sin \beta'_{ij} \cos(\omega_r t + \phi_{oij}). \quad (12)$$

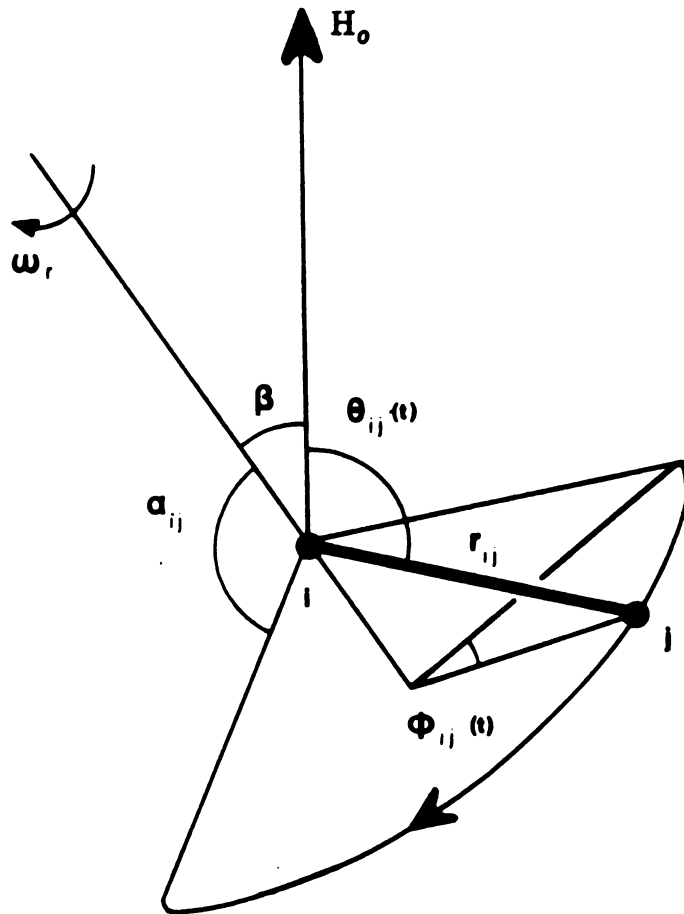


Figure 25. Diagram Illustrating the Motion of a Typical Internuclear Vector, r_{ij} , when a Solid is Rotated with an Angular Velocity, ω_r , about an Axis Inclined at Angle β to H_0 .

By substituting equation (12) into equation (11) we get, after rearrangement:

$$\begin{aligned} \mathcal{H}_D = & \sum_{i < j}^{1/2} \gamma_i \gamma_j \hbar^2 r_{ij}^{-3} (\underline{I}_i \cdot \underline{I}_j - 3 I_{iz} I_{jz}) \times \\ & \{ 1/2 (3 \cos^2 \beta - 1) (3 \cos^2 \beta'_{ij} - 1) \\ & + 3/2 \sin 2\beta \sin 2\beta'_{ij} \cos(\omega_r t + \phi_{oij}) \\ & + 3/2 \sin^2 \beta \sin^2 \beta'_{ij} \cos 2(\omega_r t + \phi_{oij}) \} \quad . \quad (13) \end{aligned}$$

Note that, the first term in the brackets is independent of time while the second and third are periodic with mean value of zero. If the angle of rotation, β , is chosen such that $3 \cos^2 \beta - 1 = 0$, then the dipolar effects will be seen only as rotational sidebands at multiples of ω_r from the central peak. The value of the appropriate angle is $54^\circ 44' 8''$ and is referred to as the magic angle. The effect of high speed rotation of the sample about an axis at the magic angle on chemical shift anisotropy and quadrupolar interactions is similar and is described below.

The electron shielding or shift interaction of nuclei in nonmetals may be written as:

$$\mathcal{H}_s = \hbar \sum_i (\gamma_i \sigma_{izz} H_o) \quad (14)$$

If the principal values of the chemical shift tensor are represented by σ_p ($p = 1, 2, 3$) and the direction cosines of its principal axis with respect to H_0 are represented by λ_p , then

$$\sigma_{zz} = \sum_p \lambda_p^2 \sigma_p \quad (15)$$

for nucleus i . The isotropic average of each λ_p^2 is $1/3$ so that the value of $\bar{\sigma}_{zz}$ in a normal fluid is simply σ , the scalar chemical shift encountered in the high resolution NMR spectra of fluids.

When a solid is rotated with angular velocity ω_r about an axis inclined at angle β to H_0 and at angles χ_p to the principal axis of σ , the direction cosines become

$$\lambda_p = \cos \beta \cos \chi_p + \sin \beta \sin \chi_p \cos(\omega_r t + \psi_p) \quad (16)$$

Substituting (15) and (16) into (14) gives an equation that is time independent and periodic in ω_r . The time independent chemical shift anisotropy becomes:

$$\bar{\sigma}_{zz} = 3/2 \sigma \sin^2 \beta + 1/2 (3 \cos^2 \beta - 1) \sum_p \sigma_p \cos^2 \chi_p. \quad (17)$$

When β is chosen to be the magic angle, $\bar{\sigma}_{zz}$ reduces to the scalar isotropic value σ and the shift anisotropy is removed from the central line. The periodic terms of \bar{K}_s contribute to the spinning side bands just as for the

dipolar time-dependent terms.

All alkali metal nuclei, except ${}^6\text{Li}$, are quadrupolar. The electric quadrupolar interaction Hamiltonian may be written as

$$\mathcal{H}_Q = \sum_i \frac{eQ_i}{6I_i(2I_i-1)} I_i \cdot V_i \cdot I_i \quad (18)$$

where eQ_i is the nuclear electric quadrupole moment of nucleus i and V_i is the electric field gradient tensor at the nucleus. V_i is a second rank tensor that is symmetric and traceless. The effect of high speed sample rotation on the quadrupolar interaction in solids has been treated by Cunningham and Day [89]. The first-order time-averaged diagonal terms of the quadrupolar Hamiltonian are given by

$$\overline{\mathcal{H}}_Q = \frac{e^2 Q_q}{16I(2I-1)} (3I_z^2 - I^2) (1+\eta) (1-3 \cos^2 \beta) (1-3 \cos^2 \theta) \quad (19)$$

where η is the asymmetry factor and θ is the angle between the principal axis of the electric field gradient tensor and H_0 . At an angle $\beta = 54^\circ 44'$, the first order quadrupole interaction becomes zero in the limit of infinite rotation frequency.

The second-order quadrupole effect is not averaged to zero in the MAS experiment. In fact, in some solid state

experiments, angles other than the magic angle are more effective in linewidth reduction [90]. The area of solid state NMR spectra of quadrupolar nuclei has been a field of great interest, especially for the study of inorganic salts [90-97].

D. Identification of a Ceside and an Electride by ^{133}Cs
MAS-NMR

Historically ^{23}Na was the first nucleus in crystalline alkalides to be studied by solid state NMR [23,98]. The results of these studies are given in Part II-Chapter Three of this dissertation. Later, Ellaboudy applied ^{133}Cs MAS-NMR to the identity problem surrounding the compound with stoichiometry $\text{Cs}(\text{18C6})$ [42,99]. This section describes the problem and the NMR results as an example of the usefulness of MAS-NMR as an identification tool.

The first $\text{Cs}(\text{18C6})$ crystals were isolated by Issa [41,52]. The optical absorption maximum was located at 6700 cm^{-1} , which corresponds to trapped electrons. The magnetic susceptibility data indicated that this compound was virtually diamagnetic with only 1% unpaired spins. The single crystal spectrum featured two lines, one temperature independent centered at $g = 2.0023$, the other, which broadened with increasing temperature, at $g = 2.0016$. The crystals were stable for hours at room temperature and

melted to a dark blue liquid at $\sim 65^{\circ}\text{C}$ before decomposing irreversibly. D.C. conductivity measurements yielded a small apparent band gap of ~ 0.6 eV.

The results obtained from the characterization studies of Cs(18C6) suggested that if this compound was the electrone, it had extensive spin pairing. Spin pairing had been observed for other electrone [48,55], so the nearly diamagnetic behavior was not surprising. This compound was considered a possible electrone because: (1) The single peak at 6700 cm^{-1} observed in the optical spectrum corresponds to e^{-} trapped. (2) Crystals of $\text{Cs}^{+}(\text{18C6})\cdot\text{Na}^{-}$ had been isolated and characterized [49]. Therefore, it was surmised that other cesium 18-crown-6 salts would have a Cs:18C6 ratio of 1:1. (3) The observed band gap was too small for a ceside salt.

Ellaboudy synthesized a second compound from solutions of cesium and 18-crown-6 which had the stoichiometry $\text{Cs}(\text{18C6})_2$. The optical absorption spectrum of films made from solutions of $\text{Cs}(\text{18C6})_2$ in methylamine featured a single maximum at 6700 cm^{-1} . As in the spectrum of Cs(18C6), this peak corresponded to the trapped electron. However, the magnetic susceptibility data were radically different. $\text{Cs}(\text{18C6})_2$ had a calculated Curie constant that corresponded to $\sim 75\%$ unpaired electron spins and a very small Weiss constant, indicative of weak electron-electron interactions. The EPR spectrum had a single intense signal with a g value of 2.0023 and a peak to peak width of only

0.48 gauss, independent of temperature. Based on these results the two compounds, $\text{Cs}(\text{18C6})$ and $\text{Cs}(\text{18C6})_2$, were tentatively assigned to $\text{Cs}^+(\text{18C6})_2 \cdot \text{Cs}^-$ and $\text{Cs}^+(\text{18C6})_2 \cdot e^-$, respectively.

Definite proof of these assignments was obtained by ^{133}Cs MAS-NMR. Figure 26 shows the spectra of $\text{Cs}^+(\text{18C6})_2 \cdot \text{Cs}^-$ and $\text{Cs}^+(\text{18C6})_2 \cdot e^-$. The former salt exhibits two cesium peaks at -61 and -228 ppm. The more paramagnetic chemical shift corresponds well with those observed for model salts with a Cs:18C6 ratio of 1:2. The second peak at -228 ppm is reminiscent of the Cs^- peak at -292 ppm observed in THF solutions [73]. The peak at -228 ppm was assigned to Cs^- . By contrast, the spectrum of $\text{Cs}(\text{18C6})_2$ had only a single peak at +81 ppm. The large paramagnetic shift is probably due to the high concentration of unpaired electrons in this compound. The identification of this compound is clearly $\text{Cs}^+(\text{18C6})_2 \cdot e^-$.

The ^{133}Cs MAS-NMR results proved unequivocally that $\text{Cs}(\text{18C6})$ was the ceside, $\text{Cs}^+(\text{18C6})_2 \cdot \text{Cs}^-$. The optical spectrum maximum must arise from the reaction during film deposition, such as



and suggests that the electride is thermodynamically favored. Extrapolation at the D.C. conductivity results to infinite temperature indicated that $\text{Cs}^+(\text{18C6})_2 \cdot \text{Cs}^-$ is an

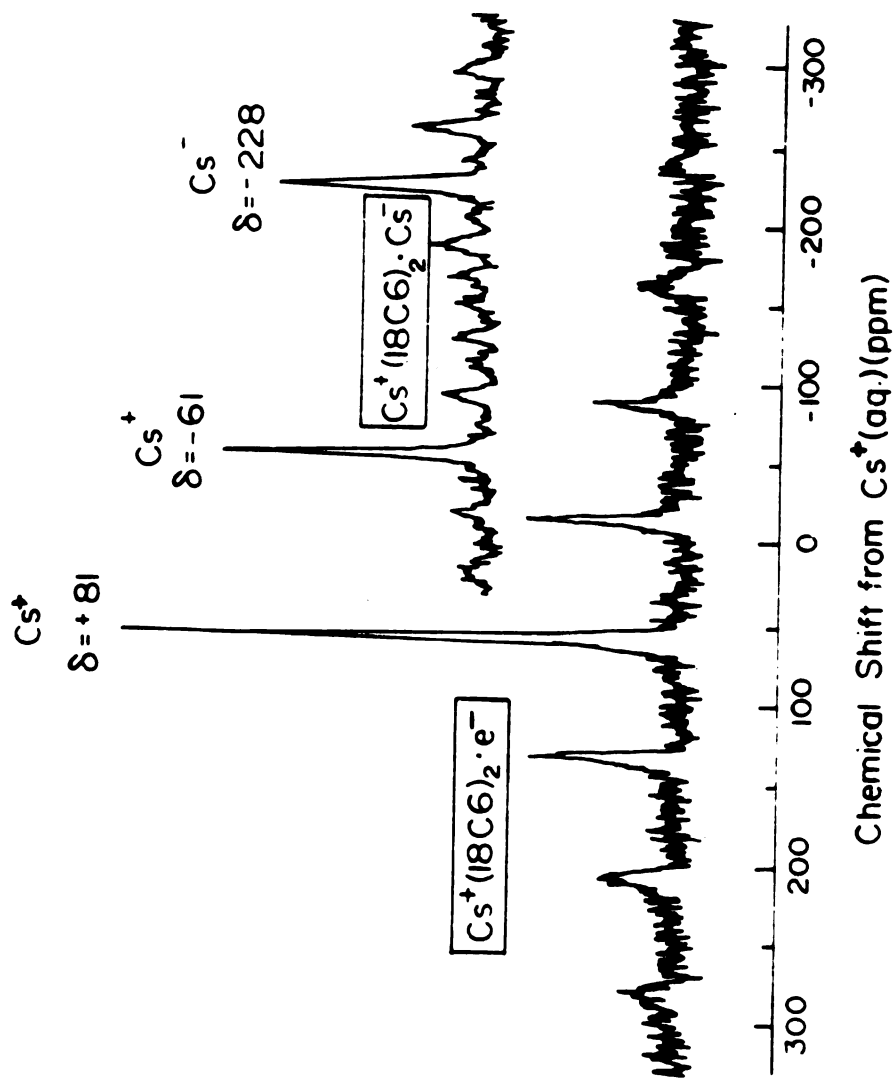


Figure 26. ^{133}Cs MAS-NMR Spectra of the Two Crystalline Compounds, $\text{Cs}^+(\text{18C6})_2 \cdot \text{Cs}^-$ and $\text{Cs}^+(\text{18C6})_2 \cdot \text{e}^-$ at 44.24 MHz.

extrinsic semiconductor and that the apparent band gap is due to the presence of trapped electrons as impurities. This resolution of the "identity crisis" for Cs(18C6) demonstrates the usefulness of MAS-NMR as an identification tool for alkalides and electrides.

PART II
CHAPTER TWO -- EXPERIMENTAL

A. Sample Preparation

The reagents, solvents and crystalline alkalide samples were prepared as previously described in Part I, Chapter Two of this thesis. The present chapter will describe the exact handling of the NMR samples starting with crystalline alkalides and the instrumentation used to record the spectra.

1. *Solution samples* - Crystalline alkalide samples were loaded through the stopcock of an evacuable 10 mm thin wall NMR tube under a dry nitrogen atmosphere. The apparatus was closed, removed to a vacuum line and evacuated to 2×10^{-5} torr. The scribed sample tube had been weighed before breaking so that a mass determination could be made. For samples in which an excess of 15-crown-5 was desired, the evacuated apparatus was brought into a helium-filled inert atmosphere dry box and a weighed amount of crown ether was pipetted through the stopcock onto the crystals. Dimethyl ether was distilled onto the crystals or crystal-crown ether mixture until a solution height of about 4 cm was reached. The walls of the apparatus were washed to

dissolve any crown ether or crystals adhered to them. The apparatus was then immersed in a dry ice-isopropanol bath at -78°C and opened to a rough vacuum. A flame seal-off was made at a constriction above the NMR tube at the vacuum of ca. 4×10^{-3} torr. The sealed tubes were stored at -80°C until use.

2. *Model salts* - Conventional alkali metal salts were complexed by crown ethers or cryptands by procedures similar to those of Pedersen [26]. The salts, together with stoichiometric amounts of complexant (mole ratio 1:1 or 1:2), were dissolved in either hot methanol or 2-propanol. The solutions were allowed to cool until crystals formed and were then filtered to yield the 18-crown-6 and cryptand-2,2,2 salts. The 15-crown-5 model salts were allowed to dry at room temperature. Model salts were further dried in a vacuum desiccator. Conventional salts without complexant were reagent grade and were used without further purification.

3. *Solid state samples* - Crystalline alkalides or electrides were loaded into either Andrew Beam type rotors made from Delrin or cylindrical Al_2O_3 rotors with Kel-F turbine and end caps. The cylindrical rotors required special Kel-F caps with holes in the centers and a Kel-F bolt and nut for low temperature experiments. Each type of rotor was loosely filled with crystals while cold under a dry nitrogen atmosphere. The rotors were then capped and brought slowly from static to spin rates of 1.2 to 4 kHz. This

allowed for centrifugal packing of the samples within the rotors. Model salts could be tightly packed in the cylindrical rotors prior to spinning by use of a plunger. Spin rates are significantly higher when the samples are uniformly packed.

B. Instrumentation

Spectra were recorded at three field strengths with instruments located at Michigan State University, Dow Chemical Corp. (Midland, Michigan) and the National Science Foundation Regional NMR Center (University of Illinois; Urbana, Illinois). Single 90° pulse sequences were used for all experiments. Downfield (paramagnetic) shifts are positive. A brief description of the instrumentation at each location follows.

1. *At Michigan State University* - A Bruker WH 180 superconducting multinuclear spectrometer equipped with a Nicolet 1180 computer system was used. All experiments for ^{39}K and ^{87}Rb in solution were made without a deuterium lock. The ^{39}K resonance was operated at a frequency of 8.403 MHz at a field strength of 4.227 Tesla. A Bruker 10 mm probe tunable in the range of 4.8 to 12.2 MHz was used for the ^{39}K solution studies. ^{89}Rb has a resonance of 58.9 MHz in this field strength and a homebuilt, broad band, 10 mm probe tunable in the range of 25 to 103 MHz was used for the solution studies.

Solid state samples were studied by the magic angle sample spinning (MAS) technique. A commercial MAS probe from Doty Scientific was used. This probe required cylindrical rotors with dimensions of 18 mm x 7 mm OD and was tunable to the 45 to 72 MHz range. Additional capacitors were used with the tuning impedance to bring the probe range to lower frequencies for measurements of ^{133}Cs at 23.62 MHz and ^{39}K at 8.403 MHz. An external standard was used to determine the chemical shift from the value of the reference salt in aqueous solution at infinite dilution. Spectral drift did not exceed 3 Hz during the time period of the experiment. The Doty MAS probe also featured proton decoupling capabilities at 180 MHz. Decoupling experiments could be studied only at low frequencies due to additional noise present at higher frequencies.

Samples were rotated at speeds up to 3 kHz by precooled nitrogen gas. Variable temperature experiments in the range of 160 to 300 K could be made with a Bruker variable temperature control unit. In the case of alkalide samples, spinning speeds were limited by sample packing and the effect of the center bolt of the low temperature turbine caps.

2. *At Dow Chemical Corporation* - A Bruker CXP-200 wide bore spectrometer equipped with an Aspect 2000 computer was used. Andrew-Beam type rotors with a volume of $\sim 0.4 \text{ cm}^3$ were used in a standard commercial MAS probe. Spectra were taken of ^{23}Na and ^{87}Rb at frequencies of 52.94 and 65.4 MHz

respectively, in a field strength of 4.7 Tesla. The spinning gas (nitrogen) was cooled by passing it through a copper cooling coil submerged in a dry ice-isopropanol bath. No temperature control was available and sample temperatures were in the range of -20 to -10°C. Spinning rates up to 4 kHz were achieved.

3. *At the NSF Regional NMR Center* - A "home built" Fourier transform NMR spectrometer with an 11.74 Tesla field strength was used. This system consisted of an Oxford 3.5 inch bore solenoid, a Nicolet 1280/293B computer system and a Control Data Corporation disk memory. Andrew-Beam type rotors were also used with this system. As at Dow Chemical Corporation, the spinning gas was cooled by a dry ice slush bath but temperature regulation was not available. Spin rates up to 4.5 kHz were observed.

PART II
CHAPTER THREE -- RESULTS AND DISCUSSION

Alkali metal nuclear magnetic resonance spectroscopy is a sensitive technique for the study of the ions present in alkalides and electrides. MAS-NMR has been demonstrated by Ellaboudy, et al. to be a powerful identification tool for cesium compounds [42,53]. This chapter covers the results of MAS-NMR studies that include the nuclei: ^{23}Na , ^{39}K , ^{87}Rb and ^{133}Cs . In addition, some advances in ^{39}K and ^{87}Rb NMR studies of solutions have been made and are reported.

A. ^{23}Na NMR Spectra

The 100 percent natural abundance of ^{23}Na and its relative NMR sensitivity permits easy data collection. The success of ^{23}Na NMR studies in solution made sodium a natural first choice for solid state NMR studies. The preliminary ^{23}Na NMR spectrum of $\text{Na}^+\text{C}_{222}\cdot\text{Na}^-$, obtained without spinning, consisted of a broad peak, with linewidth of ~2600 Hz, centered at ~-60 ppm relative to $\text{Na}^+(\text{aq})$ at infinite dilution [23,98]. A barely discernible, broad shoulder could also be seen on the low field side of the

peak at the peak location of $\text{Na}^+\text{C222}\cdot\text{I}^-$ (s) (\sim -13 ppm). These peak locations can be easily compared to the spectrum of $\text{Na}^+\text{C222}\cdot\text{Na}^-$ in various nonaqueous solvents, as described in Chapter One-Part II. The \sim -60 ppm peak and low field shoulder resolve into two clearly discernible peaks upon rotation of the sample at an angle of 54.74° from the direction of the field. Figure 27 demonstrates the drastic reduction of the linewidth of $\text{Na}^+\text{C222}\cdot\text{Na}^-$ upon spinning at this "magic angle". The two peaks at -22 and -61 ppm are assigned to $\text{Na}^+\text{C222}$ and Na^- , respectively. The location of the Na^- peak is within experimental error of the chemical shift calculated for $\text{Na}^-(\text{g})$ [73,76].

The ^{23}Na MAS-NMR spectra were recorded for several alkalides that contain sodium. Table IX gives the chemical shifts and linewidths of some conventional salts, both with and without complexing agents, and a number of crystalline alkalides. All heteronuclear alkalides had a single ^{23}Na NMR peak in the range of -56 to -63 ppm which corresponded to the peak at -61 ppm for Na^- in $\text{Na}^+\text{C222}\cdot\text{Na}^-$. The results prove that these compounds are all sodides. The concentration of Na^+ , either free or complexed, is too low in these salts to give a detectable NMR signal. The ^{23}Na MAS-NMR spectrum of crystals with stoichiometry $\text{Na}(\text{12C4})$ feature two peaks at -14 and -62 ppm. Analogous to the case of $\text{Na}^+\text{C222}\cdot\text{Na}^-$, these peaks correspond to the complexed cation, $\text{Na}^+(\text{12C4})_2$, and Na^- , respectively. The ^{23}Na MAS-NMR spectrum for $\text{Na}^+(\text{12C4})_2\cdot\text{Na}^-$ is given in Figure 28.

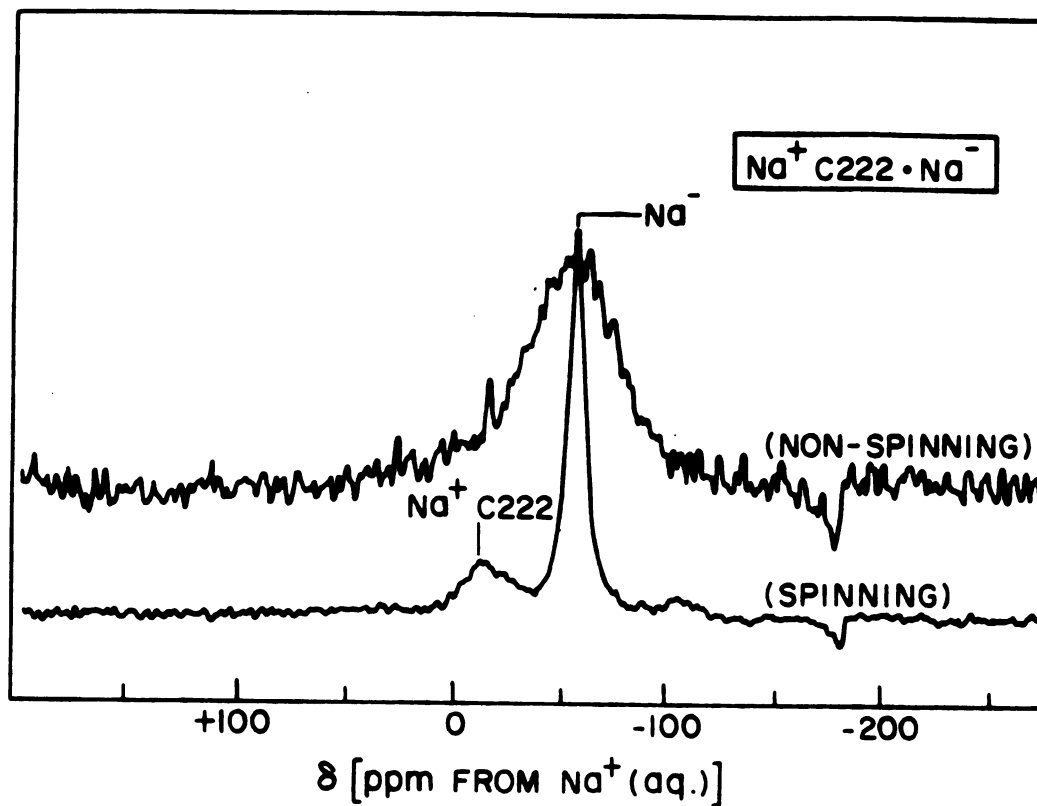


Figure 27. ^{23}Na NMR Spectra of Crystalline $\text{Na}^+ \text{C}_{222} \cdot \text{Na}^-$ at 52.94 MHz. Top - static spectrum; bottom - MAS spectrum.

TABLE IX. Results of ^{23}Na MAS-NMR Studies.

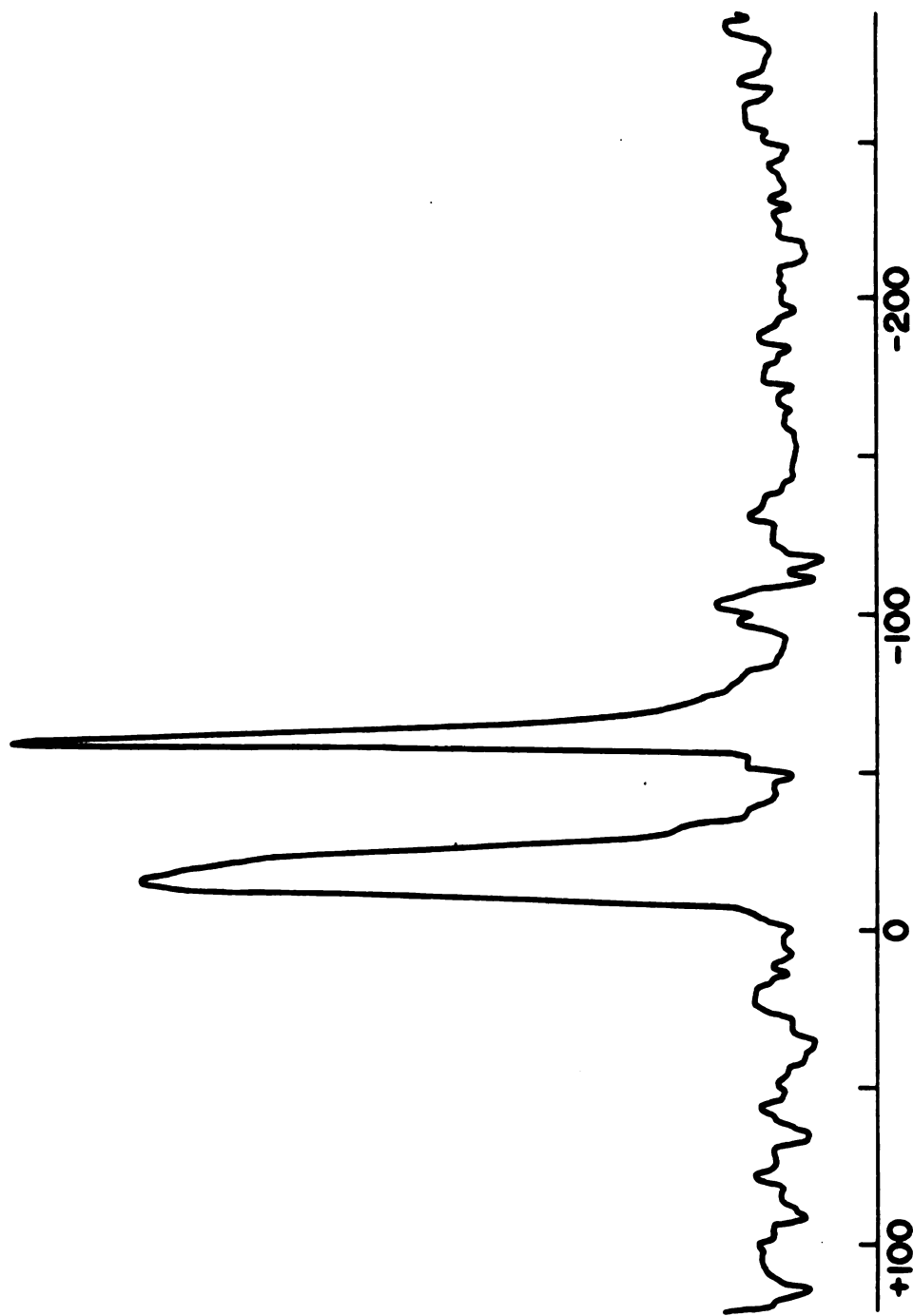
Compound	δ , ppm ^a	$\Delta\nu_{1/2}$, Hz	Reference
NaCl	+8	140	
NaBr	+6	200	
NaI	-3	160	
<u>Na⁺(12C4)₂·Na⁻</u>	-14 ^a	760	
Na ⁺ (12C4) ₂ · <u>Na⁻</u>	-62 ^b	170	
K ⁺ (12C4) ₂ ·Na ⁻	-61	51	38
Na ⁺ 15C5·Br ⁻	+4	580	
K ⁺ (15C5) ₂ ·Na ⁻	-61	90	
Rb ⁺ (15C5) ₂ ·Na ⁻	-61	90	
Cs ⁺ (15C5) ₂ ·Na ⁻	-61		
Na ⁺ 18C6·SCN ⁻	-22	500	
K ⁺ 18C6·Na ⁻	-56	120	
Rb ⁺ 18C6·Na ⁻	-60	90	
Cs ⁺ (18C6) ₂ ·Na ⁻ ^d	-63	75	53
Na ⁺ C222·SCN ⁻	-21	1120	
Na ⁺ C222·I ⁻	-21	1300	
<u>Na⁺C222</u> ·Na ⁻	-24 ^a	1200	
Na ⁺ C222· <u>Na⁻</u>	-61 ^b	290	
K ⁺ C222·Na ⁻	-61	400	
Rb ⁺ C222·Na ⁻	-61	360	

^aChemical shifts are referenced to Na⁺ aqueous at infinite dilution. Chemical shifts at separate samples were reproducible to ± 1 ppm.

^bAttributed to Na⁺L⁻.

^cAttributed to Na⁻.

^dFirst reported as Cs⁺18C6·Na⁻. Later analysis showed this compound had Cs⁺(18C6)₂·Na⁻ as the correct stoichiometry.



CHEMICAL SHIFT FROM Na^+ (aq), ppm

Figure 28. ^{23}Na MAS-NMR Spectrum of Na^+ (C_4O_4) $_2 \cdot \text{Na}^+$ at 47.61 MHz.

The chemical shift of Na^- is remarkably insensitive to the nature of the cation of the sodide salt. Of the eleven sodides examined, seven have identical shifts of -61 ppm, which is very close to the value of -63 ppm calculated for $\text{Na}^-(g)$ [76]. Nine of the sodides are within experimental error of the value of -62.3 ppm observed for Na^- in solution. The Na^- NMR peaks for $\text{K}^+(18C6)\cdot\text{Na}^-$ and $\text{Rb}^+(18C6)\cdot\text{Na}^-$ are shifted downfield to -56 and -60 ppm, respectively. The small paramagnetic shifts observed for these sodides might be caused by the presence of trapped electrons that have been detected by EPR spectroscopy [43,51,53]. The small deviations of the Na^- peak location from that of gaseous Na^- reflect the high degree of shielding of the 2p orbitals by the filled 3s orbital.

The environment of Na^+ affects its chemical shift much more than that of Na^- . The chemical shift ranges from -24 ppm for $\text{Na}^+\text{C}_{222}$ to +8 ppm for Na^+Cl^- . Most of the complexed sodium cations have more diamagnetic chemical shifts than uncomplexed sodium. The exception is $\text{Na}^+(15C5)\cdot\text{Br}^-$ with $\delta = +4$ ppm. This peak is most likely due to partially complexed Na^+ which would allow the cation to participate in more interactions with the environment. An extremely poor signal to noise ratio was obtained for this spectrum.

Oldfield has shown that only the central ($m = -1/2$, $m = 1/2$) spin transitions of ^{23}Na can be observed for solids when the quadrupolar coupling constant, e^2qQ/h , is appreciably larger than the sample spinning frequency

[90,100,101]. The residual linewidths and frequency shifts are determined by second order quadrupole effects [101]. These shifts could amount to 15-20 ppm for $\text{Na}^+\text{C222}$ and up to 8 ppm for Na^- . The narrow spread of the chemical shift values for Na^- and the good agreement with Na^- in solution and in the gas phase suggest that these effects are minimal.

Ellaboudy and Dye [102] have made line shape studies of ^{23}Na NMR spectra of solid $\text{Na}^+\text{C222}\cdot\text{Na}^-$. Their findings predict e^2qQ/h to be 1.2 ± 0.1 MHz with an asymmetry parameter, η , of about 0.1 for $\text{Na}^+\text{C222}$. Calculations of the quadrupolar line shapes indicate that the residual dipolar coupling contribution to the linewidths is approximately 300 Hz for a coupled MAS experiment. The dipolar contribution to the static linewidth was calculated to be 3340 Hz. Combination with the predicted quadrupolar effects yields a linewidth of 3670 Hz which is in good agreement with the observed linewidth of 3700 ± 300 Hz for $\text{Na}^+\text{C222}$.

The linewidths of the sodides that contain crown ethers when compared to Na^- in $\text{M}^+\text{C222}\cdot\text{Na}^-$ suggest greater asymmetry of the field gradient for Na^- in the cryptate salts. The relaxation processes may be enhanced by interaction of the hydrogen or nitrogen atoms in the cryptand with the sodium anion to give broader signals. The broadening of the line by greater relaxation rate enhancement of the signal is also indicated by results obtained by Ellaboudy [53]. Proton decoupling of the signal gave linewidths on

the order of 30-60 Hz for the cryptate sodides and 40-80 Hz for the crown ether sodides. The linewidths of the crown ether sodides are not drastically narrowed by proton decoupling as that of Na^- in $\text{M}^+\text{C222}\cdot\text{Na}^-$. This result further indicates a more symmetric environment and greater isolation from the neighboring atoms for Na^- in sodides which contain crown ethers.

In summary, ^{23}Na NMR has been shown to be a very effective identification tool for alkalides and electrides. One new homonuclear salt with stoichiometry $\text{Na}(\text{12C4})$ [54] was shown to be the sodide, $\text{Na}^+(\text{12C4})_2\cdot\text{Na}^-$, rather than the electride, $\text{Na}^+(\text{12C4})\cdot\text{e}^-$. In all, eleven compounds were examined and proven to be sodides. The chemical shift of Na^- at -56 to -63 ppm is in good agreement with the calculated value of $\text{Na}^-(\text{g})$ at -63 ppm and the observed value for Na^- in solution at -62 ppm. The chemical shift values reflect the shielding efficiency of the two 3s electrons for the 2p orbitals.

B. ^{39}K NMR Spectra

The relatively low NMR sensitivity of all potassium isotopes has caused potassium to be the least studied of the alkali metals by NMR. In addition, the potassium anion had never been observed by solution NMR studies. These two factors made the use of MAS-NMR for ^{39}K more challenging than for ^{23}Na or ^{133}Cs .

1. *Solution studies.* The previous failure to observe K^- in solution by ^{39}K NMR may have resulted from the equilibrium:



since K^- is more dissociated than Na^- , Rb^- or Cs^- [20,25]. Rapid equilibration to give paramagnetic solvated electrons (or intermediate species such as $K\cdot$) would substantially broaden the K^- NMR peak. Therefore, a solvent with low donicity, dimethyl ether, was chosen to dissolve crystalline $K^+(15C5)_2 \cdot K^-$ for solution NMR studies. Dimethyl ether (Me_2O) dissolves potassium metal only in the presence of a complexing agent and reaction (21) is expected to lie far to the left of these solutions.

The spectrum of a 0.06 M solution of $K^+(15C5)_2 \cdot K^-$ in Me_2O is shown in Figure 29. The peaks at -9.9 and -99.3 ppm from $K^+_{(aq)}$ at infinite dilution are assigned to $K^+(15C5)_2$ and K^- , respectively. The measured chemical shift for the gaseous potassium atom is -101 ± 5 ppm [74] and the anion is calculated to be slightly more diamagnetic at -107 ppm. The negligible solubility of potassium in Me_2O rules out the presence of uncomplexed potassium. The narrower linewidth of the K^- peak (20 Hz) compared with that of $K^+(15C5)_2$ (50 Hz) reflects a more spherical environment for K^- . Edwards and Ellaboudy have also recently observed K^- in solution by ^{39}K NMR [103]. Their

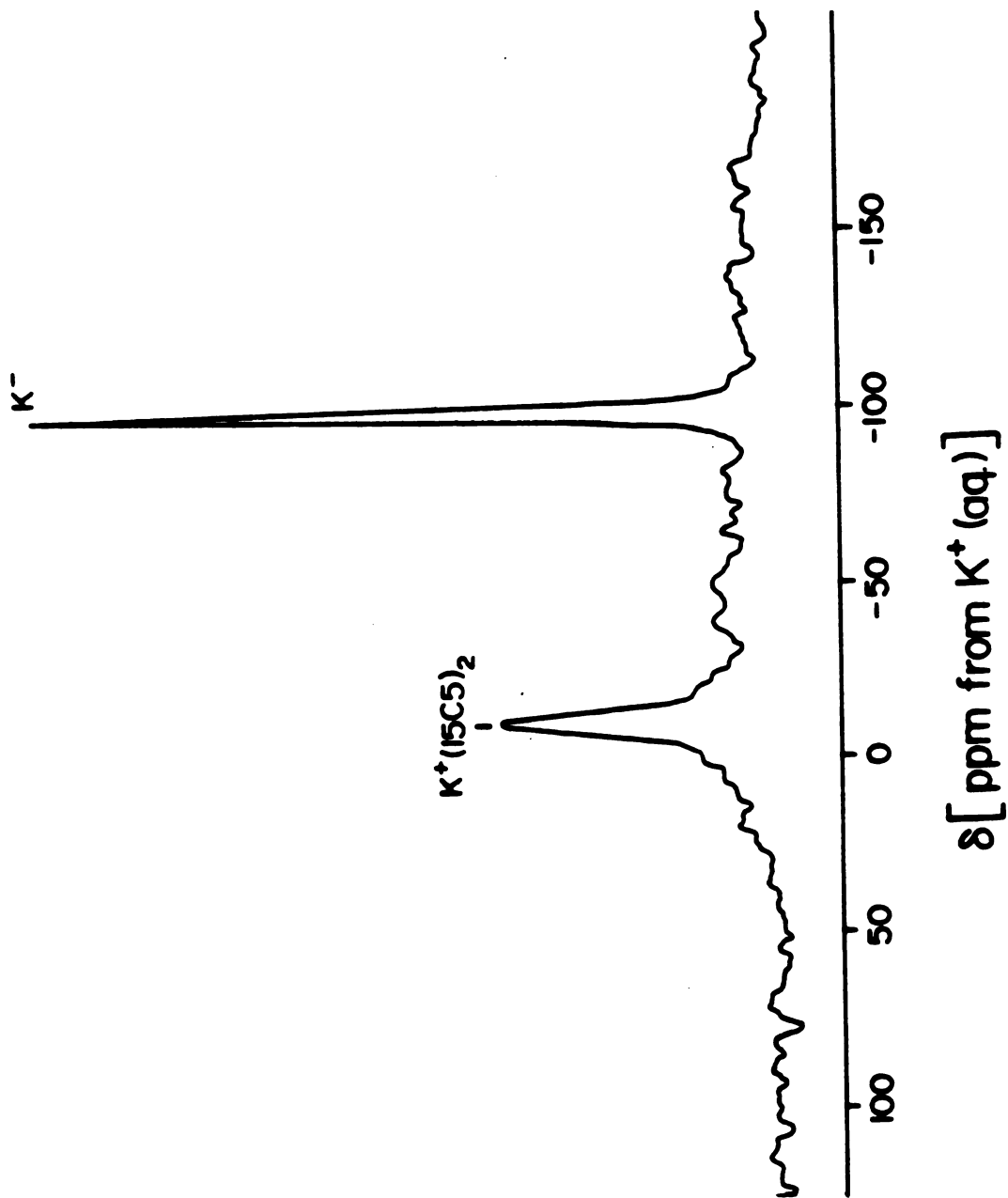


Figure 29. ^{39}K NMR spectrum of $K^+(15C5)_2 \cdot K^-$ in Dimethyl-ether (0.06 M) at 220 K and 8.40 MHz.

solutions consisted of a CsK alloy dissolved in mixtures of 12-crown-4 and tetrahydrofuran. The resultant spectrum featured a single peak at -98.2 ppm with a linewidth of 180 Hz, which corresponds to the K^- peak observed in this work for solutions of $K^+(15C5)_2 \cdot K^-$. The larger linewidths for the 12C4 solution indicates more interaction of the K^- with the environment than in the Me_2O solutions. The cesium cation is much too large to enter the cavity of the 12-crown-4. Even in a "sandwich" conformation, the cesium cation would be partially exposed and be able to participate in cation-anion interactions. Interactions that perturb the valence electrons of K^- would give broader lines rather than affect the chemical shift. The 15-crown-5 sandwich of K^+ should effectively shield the cation and minimize cation-anion interactions. Also, THF has higher donicity than Me_2O so the extent of solvent-anion interactions is greater in the THF solutions. Therefore, the greater linewidths observed for K^- in the THF solutions is probably due to the increased solvent- and cation-anion interactions. The observation of K^- in solution indicated that it might be possible to detect K^- in the solid state.

2. *MAS studies.* The first compound studied by ^{39}K MAS-NMR was $K^+(15C5)_2 \cdot K^-$, which was expected to give two ^{39}K NMR signals. Unfortunately, only the K^- signal was observed at -105 ppm. The static ^{39}K NMR spectrum without 1H decoupling and the decoupled static and MAS spectra of polycrystalline $K^+(15C5)_2 \cdot K^-$ are shown in Figure 30. The full

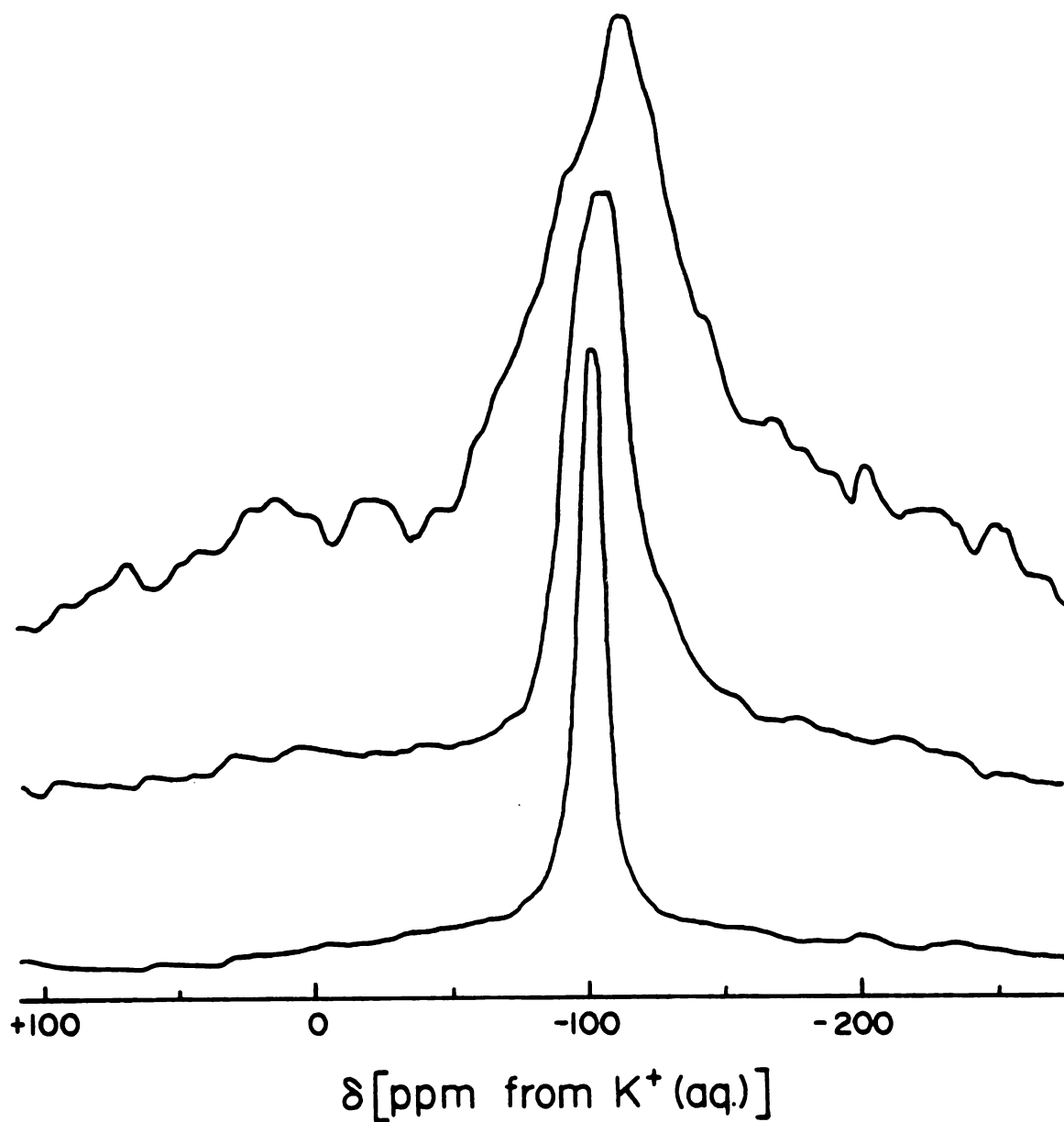


Figure 30. ^{39}K NMR Spectra of Polycrystalline $\text{K}^+(\text{15C5})_2\cdot\text{K}^-$ at 180 K. (Top) Static spectrum; (middle) static, ^1H decoupled spectrum; (bottom) MAS spectrum with ^1H decoupling. All spectra have 60 Hz exponential broadening.

widths at half height of the K^- peak are 300, 175 and 40 Hz, respectively. The residual width of the central transition ($m = 1/2$, $m = -1/2$) upon spinning and 1H decoupling give a *maximum* quadrupole coupling constant, e^2qQ/h , of about 0.1 MHz. This estimate is based on the calculation of the singular positions following the method of Kundla, *et al.* [92].

The ^{39}K MAS-NMR data for several other crystalline alkalides that contain potassium were collected and are presented in Table X. The chemical shifts of two conventional potassium salts are also presented. The chemical shifts observed for the alkalides are all within the experimental error of the value expected for $K^-(g)$. These compounds are therefore assigned to be potassides. The linewidths increase with cation size in $M^+(15C5)_2 \cdot K^-$, which suggests increasing cation-anion interactions. The increase in the interactions is probably due to the decrease in the ability of the two 15-crown-5 molecules to effectively shield the cation from the environment as the cation radius increases. The larger linewidth of K^- in $Cs^+(15C5)_2 \cdot K^-$ compared to that of $Cs^+(18C6)_2 \cdot K^-$ is also indicative of greater cation-anion interactions as was seen in the 15-crown-5 versus 12-crown-4 solution spectra.

Rubidium XANES indicated a mixture of Rb^+ and Rb^- for $KRb(18C6)$ and it was expected from the stoichiometry that a $^{39}K^-$ NMR signal would be observed. However, no signal was detected, possibly due to strong $Rb^+ - K^-$ or $K^+ - K^-$ interac-

TABLE X. Results of ^{39}K NMR-MAS Studies.

<u>Compound</u>	<u>δ, ppm from $\text{K}^+(\text{aq})^{\text{a}}$</u>	<u>$\Delta\nu_{1/2}$, Hz</u>
KCl	+46.7(5)	28
KBr	+54.5(5)	20
$\text{K}^+(\text{15C5})_2 \cdot \text{K}^-$	-105(1)	70
$\text{Rb}^+(\text{15C5})_2 \cdot \text{K}^-^{\text{b}}$	-105(2)	120
$\text{Cs}^+(\text{15C5})_2 \cdot \text{K}^-$	-105(5)	220
$\text{KRb}(\text{18C6})^{\text{b}}$	no signal	
$\text{Cs}^+(\text{18C6})_2 \cdot \text{K}^-$	-115(10)	150
$\text{K}^+\text{C222} \cdot \text{Rb}^-$	no signal	

^aUncertainty of the last digit given in parentheses.

^bProbably contain both K^- and Rb^- as indicated by rubidium XANES.

tions. The radius of the cavity of the 18-crown-6 molecule is large enough to accommodate K^+ and give axial symmetry with access to the K^+ from above and below the ring. A rubidium cation is slightly too large to enter the cavity of 18-crown-6 and therefore $Rb^+(18C6)$ may participate in cation-anion interactions to a larger extent than $K^+(18C6)$. In contrast to the 18-crown-6 compound, a K^- signal was observed for crystals with stoichiometry $KRb(15C5)_2$. Rubidium XANES also indicated a mixture of Rb^+ and Rb^- in $KRb(15C5)_2$ and the presence of $K^+(15C5)_2$ as well as K^- may be inferred from the stoichiometry. The observation of K^- for this compound indicates less cation-anion interaction due to the more effective shielding of the cation by the two 15-crown-5 molecules. The linewidth of $KRb(15C5)_2$ is reflective of more perturbation of the K^- in this compound than in the homonuclear potasside.

As in the case of $Na^+C222 \cdot Na^-$, the estimated quadrupole coupling constant for the complexed cation is much larger than that of the anion in the ^{39}K NMR studies. The absence of a peak signal for $K^+(15C5)_2$ indicates that e^2qQ/h is at least 0.5 MHz since a signal of linewidth ≤ 1000 Hz could be detected. This value is not unexpected since Na^+C222 has a quadrupole coupling constant of 1.2 MHz. The complexed cation was not detected by ^{39}K NMR for any complexing agent, even in the case of $K^+C222 \cdot Rb^-$. This compound was observed to be a pure rubidide by rubidium XANES and the environment of the cation should be more symmetrical than

that of the crown ether salts. In all cases the signal must be substantially broadened by quadrupole interactions.

The ^{39}K studies of K^- , both in solution and in potas-
side crystals, show that K^- is a "genuine" anion with two
electrons in the 4s orbital. The small chemical shift
range observed for K^- in solids and the proximity of the
peaks to that value calculated for $\text{K}^-(\text{g})$ indicates that the
filled 4s orbital effectively shields the 3p orbitals from
appreciable interaction with the surroundings. However,
the increase of linewidth with an increase of the accessi-
bility of the cation reflects that cation-anion interac-
tions do occur. A K^+C_n signal could not be detected in
crystalline samples. Therefore, ^{39}K MAS-NMR is useful for
the detection of K^- in crystals where the cation is effec-
tively shielded from the anion but this technique is in-
effective for the complete identification of alkalides that
contain potassium.

C. ^{87}Rb NMR Spectra

In contrast to previous potassium NMR studies, the
rubidium anion in solution was readily observed by ^{87}Rb NMR
[29,73]. The study of the complexed cation, however was
hindered by extreme line broadening of the NMR signal [71].
Rubidium X-ray absorption spectroscopy has proved to be
very useful in the identification of alkalides and elec-
trides [64,65] but the data must be collected and analyzed

at sites other than Michigan State University. The MAS-NMR studies of crystalline alkalides and electrides were extended to include ^{87}Rb in the hope of providing an "in house" identification technique.

1. *Solution studies.* The first objective of the ^{87}Rb NMR studies was to observe a signal for Rb^+C_n in solution. The absence of a signal for the complexed cation in earlier studies was thought to be due to either exchange broadening with the use of 18-crown-6 as a complexant or asymmetry of the Rb^+ environment in $\text{Rb}^+\text{C}_{222}$. Since linewidths observed for species in solution are generally much smaller than those from the same species in the solid state, it was presumed that if Rb^+C_n could not be observed in solution, then it would be impossible to observe a complexed cation signal in crystalline samples. Analogous to the procedures used for ^{39}K NMR solution studies, crystalline $\text{Rb}^+(\text{15C5})_2 \cdot \text{Rb}^-$ was dissolved in dimethyl ether. To ensure the complete complexation of Rb^+ , excess 15-crown-5 was added to the samples. The spectrum of a 0.068 M $\text{Rb}^+(\text{15C5})_2 \cdot \text{Rb}^-$ in Me_2O in the presence of excess 15-crown-5 (mole ratio $15\text{C5}/\text{Rb}^+ = 14$) is given in Figure 31. The peaks at +33 and -192 ppm are assigned to $\text{Rb}^+(\text{15C5})_2$ and Rb^- , respectively. The Rb^- peak position with the chemical shift range of -185 to -197 ppm has been observed previously [29,73]. The linewidth of $\text{Rb}^+(\text{15C5})_2$ is ~5000 Hz and demonstrates the much lower symmetry of the cation environment relative to Rb^- with a linewidth of 170 Hz.

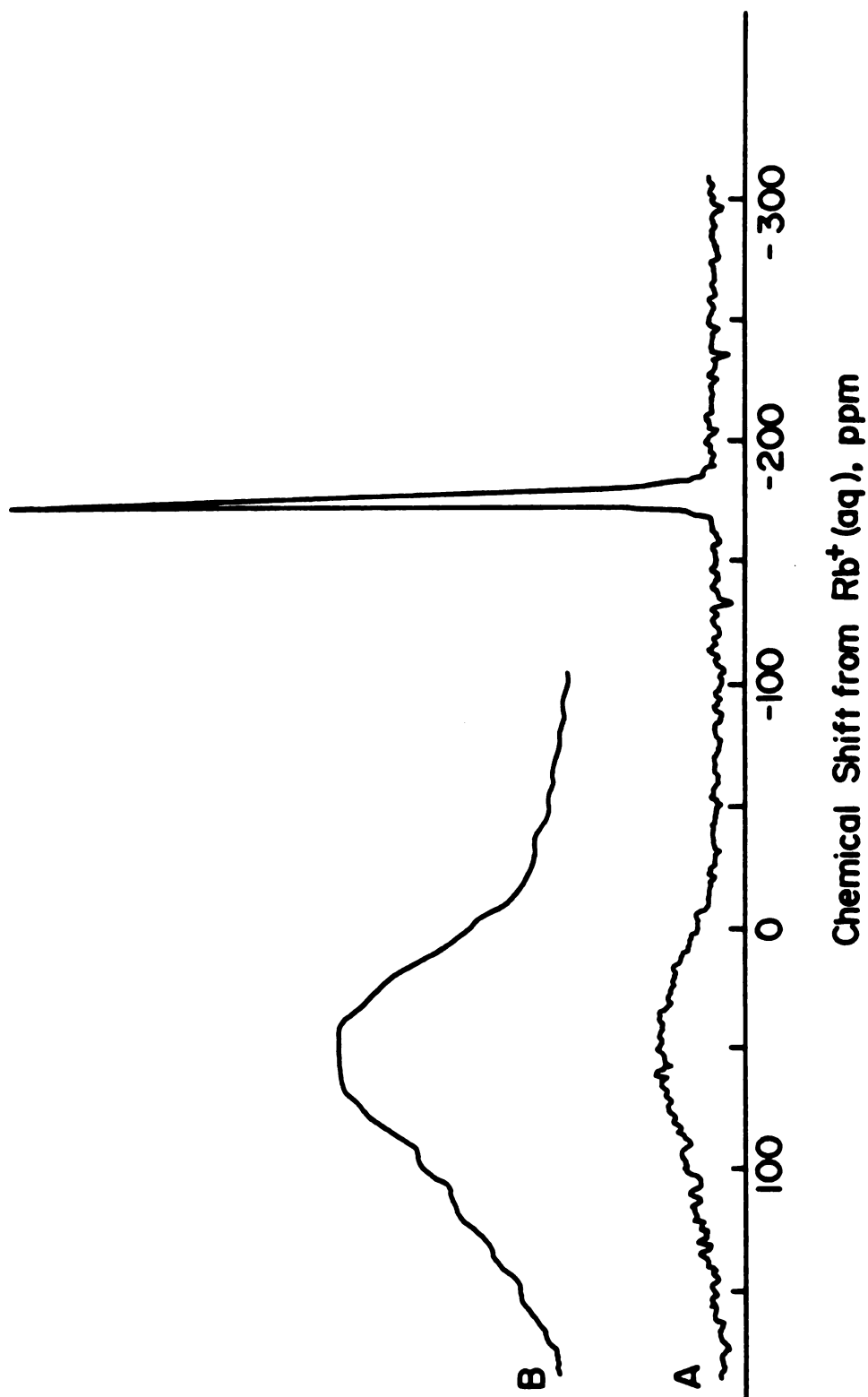


Figure 31. ^{87}Rb NMR Spectrum of $\text{Rb}^+(15\text{C5})_2\cdot\text{Rb}^-$ in Dimethylether (0.068 M) at 235 K. A has 40 Hz exponential broadening while B has 500 Hz exponential broadening.

The negligible solubility of rubidium metal in dimethyl ether rules out the possibility of uncomplexed rubidium in the solvent. This study provides the first observation of Rb^+C_n by ^{87}Rb NMR [104]. The extremely large linewidth observed for $\text{Rb}^+(\text{15C5})_2$ makes the prospect of the observation of Rb^+C_n by ^{87}Rb MAS-NMR doubtful (see later calculations).

2. *MAS studies.* Several crystalline alkalides were examined by ^{87}Rb MAS-NMR at one or more Larmor frequencies (58.90, 65.44 and 163.6 MHz). Table XI gives the chemical shifts and full widths at half height for the spectra of three simple rubidium salts and six alkalides that contain Rb^- . All alkalides had frequency dependent signals in the range of -185 to -199 ppm which correspond to Rb^- . Only for the simple salts could the signal of Rb^+ be detected. Extreme quadrupolar broadening or other mechanisms prevented its detection in model salts such as $\text{Rb}^+(\text{18C6})\cdot\text{SCN}^-$ or in the sodide $\text{Rb}^+(\text{15C5})_2\cdot\text{Na}^-$. The latter compound is known from the crystal structure to contain the sandwich cation $\text{Rb}^+(\text{15C5})_2$. In some cases, even the expected signal of Rb^- known to be present in the salt, was not detected. For example, rubidium XANES studies indicate the presence of Rb^- in compounds of stoichiometry $\text{Rb}_2(\text{C222})$ and $\text{KRb}(\text{C222})$; yet no ^{87}Rb signal could be detected in the MAS studies of these systems. As expected, the electride, $\text{Rb}^+(\text{15C5})_2\cdot\text{e}^-$, showed no signal of either Rb^+ or Rb^- .

TABLE XI. Results of ^{87}Rb MAS-NMR Studies at Three Frequencies. ^a

Compound	δ , ppm ^b	$\Delta\nu_{1/2}$, Hz	δ , ppm ^b	$\Delta\nu_{1/2}$, Hz	δ , ppm ^b	$\Delta\nu_{1/2}$, Hz
RbCl	+125(.5)	150(10)	+127(.5)	170(10)	+128(.5)	240(10)
RbI	+179(.5)	820(30)	+178(.5)	1400(30)	---	---
RbSCN	---	---	---	---	-20.5(.5)	c
					-29.8(5)	
K, Rb(15C5) ₂	-198(1)	855(30)	-191(1)	370(30)	-187(1)	550(10)
Rb ⁺ (15C5) ₂ ·Rb ⁻	-199(1)	850(30)	-191(1)	460(30)	-188(1)	300(10)
Cs ⁺ (15C5) ₂ ·Rb ⁻	-196(2)	800(30)	-189(2)	490(30)	-187(1)	560(10)
Cs ⁺ (18C6) ₂ ·Rb ⁺	---	---	-194(1)	650(30)	-187(1)	420(10)
Rb18C6	-197(2)	920(30)	---	---	no signal	no signal
K, Rb18C6	---	---	no signal	---	-185(1)	520(10)
					-193(1)	400(10)

^aUncertainty given in parentheses.

^bChemical shift from Rb⁺ aqueous of infinite dilution.

^cPeak overlap prevents measure of full width at half height

Salts that contain rubidium and 18-crown-6 with and without potassium appear to be mixed systems that are preparation dependent. Although XANES data indicate that these alkalides contain both $\text{Rb}^+(\text{18C6})$ and Rb^- [64,65], not all samples yielded ^{87}Rb MAS-NMR spectra. For example, one preparation of stoichiometry $\text{KRb}(\text{18C6})$ gave two Rb^- signals at 163.6 MHz indicating, perhaps, the presence of mixtures of $\text{K}^+(\text{18C6})\cdot\text{Rb}^-$, $\text{Rb}^+(\text{18C6})\cdot\text{Rb}^-$ and probably the corresponding potassides. However no Rb^- signal was observed with subsequent preparations, nor was any ^{39}K signal observed. Likewise, only one preparation of nominal stoichiometry $\text{Rb}(\text{18C6})$ showed the ^{87}Rb peak of Rb^- and crystals of stoichiometry $\text{Rb}_2(\text{18C6})$ showed no ^{87}Rb peaks. However, every sample prepared from rubidium and 18-crown-6 showed evidence in the XANES studies of the presence of Rb^- . Thus, the absence of the NMR peak cannot be used as evidence that the rubidide ion is not present. The variability from one preparation to the next in these systems (18C6 with Rb and/or K) indicates that the factors that determine which crystalline phases precipitate from solution were not under control in these cases. In contrast, the compounds $\text{Rb}^+(\text{15C5})_2\cdot\text{Rb}^-$, $\text{Cs}^+(\text{15C5})_2\cdot\text{Rb}^-$ and $\text{Cs}^+(\text{18C6})_2\cdot\text{Rb}^-$ yield no such ambiguities.

The ^{87}Rb MAS spectrum of the compound $\text{KRb}(\text{15C5})_2$ indicates the presence of Rb^- . This result agrees with the rubidium XANES data, optical spectrum and ^{39}K MAS-NMR studies, all of which indicate this system to be a mixture.

The crystal quality was too poor to visibly detect two or more types of crystals.

In addition to species identification, ^{87}Rb MAS-NMR studies of crystalline rubides yield information about the isotropic chemical shift and quadrupolar coupling constants of Rb^- . As for ^{23}Na and ^{39}K , only the central transition ($m = 1/2$, $m = -1/2$) can be observed. The second-order quadrupolar shift of this transition affects both the linewidth and the chemical shift observed by MAS-NMR. For the axially symmetric case, the frequency difference between the singularities is given by

$$\Delta\nu = \frac{9}{224} \frac{\nu_Q^2}{\nu_L} \left[I(I+1) - 3/4 \right] , \quad (22)$$

in which ν_Q , the nuclear quadrupole frequency, is related to the nuclear quadrupole moment Q and the electric field gradient eq by

$$\nu_Q = \frac{3e^2qQ}{2I(2I-1)h} = 1/2 \left[\frac{e^2qQ}{h} \right] . \quad (23)$$

Equation (22) may be used with the linewidth to estimate the maximum value of ν_Q . Of course, incomplete removal of proton dipolar coupling and chemical shift anisotropy by spinning at the magic angle will also contribute to the linewidth. The absence of well-defined singularities suggests a distribution of quadrupolar coupling constants. The linewidths of the ^{87}Rb MAS-NMR peaks of Rb^- in the

various rubidides given in Table XI yield a maximum quadrupolar coupling constant $2\nu_Q$, of 1.3 MHz, with a standard deviation of ± 0.3 MHz.

The chemical shifts of Rb^- decrease with increasing Larmor frequency, as expected from the quadrupolar shift of the central transition. For ^{87}Rb with nuclear spin $3/2$ the shift in ppm is related to the Larmor frequency by [91]

$$\delta = \delta_0 - 10^5 \left[\frac{\nu_Q}{\nu_L} \right]^2, \quad (24)$$

in which δ_0 is the isotropic chemical shift. The data in Table XI (excluding $\text{RbK}(\text{l8C6})$) yield $\delta_0 = -186 \pm 2$ ppm and $2\nu_Q = 1.2 \pm 0.2$ MHz.

A quadrupole coupling constant (e^2qQ/h) of 1.2 MHz for Rb^- is consistent with the estimates of ≤ 0.23 MHz for Na^- and > 0.5 MHz for K^- as discussed earlier in this chapter. If the external field gradient is assumed to be the same for Rb^- as for Na^- , then correction for the quadrupole moment and Sternheimer antishielding factor (of the cations) yields an estimate of ≤ 2.2 MHz for Rb^- .

The absence of a signal for complexed Rb^+ is not surprising in view of the large quadrupolar broadening. Based upon the quadrupole-broadened MAS-NMR signal of Na^+ in $\text{Na}^+(\text{l8C6}) \cdot \text{SCN}^-$, the MAS linewidth of $\text{Rb}^+(\text{l5C5})_2$ is estimated to be $\sim 60,000$ Hz which is too broad to detect with the available instrumentation. Another method to estimate the linewidth for Rb^+C_n is to examine the ^{87}Rb NMR results

from solutions. The linewidth of 150 Hz for Rb^- in solution, together with a nuclear quadrupole coupling constant of 1.2 MHz estimated from the solid state spectra, yield an approximate correlation time of $\sim 10^{10}$ s for this species. This estimation is extremely rough since the field gradient in solution may differ appreciably from that in the solid. The complexed cation, being larger, probably has a longer correlation time than the anion. However, if the same correlation time is used for the cation as for Rb^- , the linewidth yields a quadrupole coupling constant of ~ 7 MHz for $\text{Rb}^+(\text{15C5})_2$. This, in turn, would give a MAS linewidth of $\sim 24,000$ Hz, which is also too broad to measure.

The static and MAS spectra of Rb^- , with and without proton decoupling, were measured at 65.4 MHz. The results for four compounds are given in Table XII. The quadrupolar contribution is expected to increase by a factor of 2.7 to 3.6, depending upon the asymmetry parameter, η , from MAS to static spectra [96]. The static coupled and MAS coupled spectrum of $\text{Rb}^+(\text{15C5})_2 \cdot \text{Rb}^-$ is given in Figure 32. Since the linewidths observed by MAS-NMR were essentially unchanged upon proton decoupling, the dipolar contributions from coupling to protons must have been removed by spinning. The increase in linewidth from spinning to static-decoupled spectra falls within the range expected from the quadrupolar contribution. This indicates that the contribution from chemical shift anisotropy is small.

TABLE XII. Results of ^{87}Rb NMR with and without Proton Decoupling at 65.4 MHz.

Compound	δ , ppm from Rb $^+$ infinite ^a Dilution	$\nu_1/2$, Hz ^a			
		^1H Coupled Static	^1H Decoupled Static	^1H Coupled MAS	^1H Decoupled MAS
KRb(15C5) ₂	-191(1)	1400(30)	1040(30)	370(30)	350(30)
Rb $^+$ (15C5) ₂ •Rb $^-$	-191(1)	1830(30)	1400(30)	460(30)	480(30)
Cs $^+$ (15C5) ₂ •Rb $^-$	-189(2)	1830(30)	1160(30)	490(30)	490(30)
Cs $^+$ (18C6) ₂ •Rb $^-$	-194(1)	2450(30)	2210(30)	650(30)	680(30)

^aUncertainty given in parentheses.

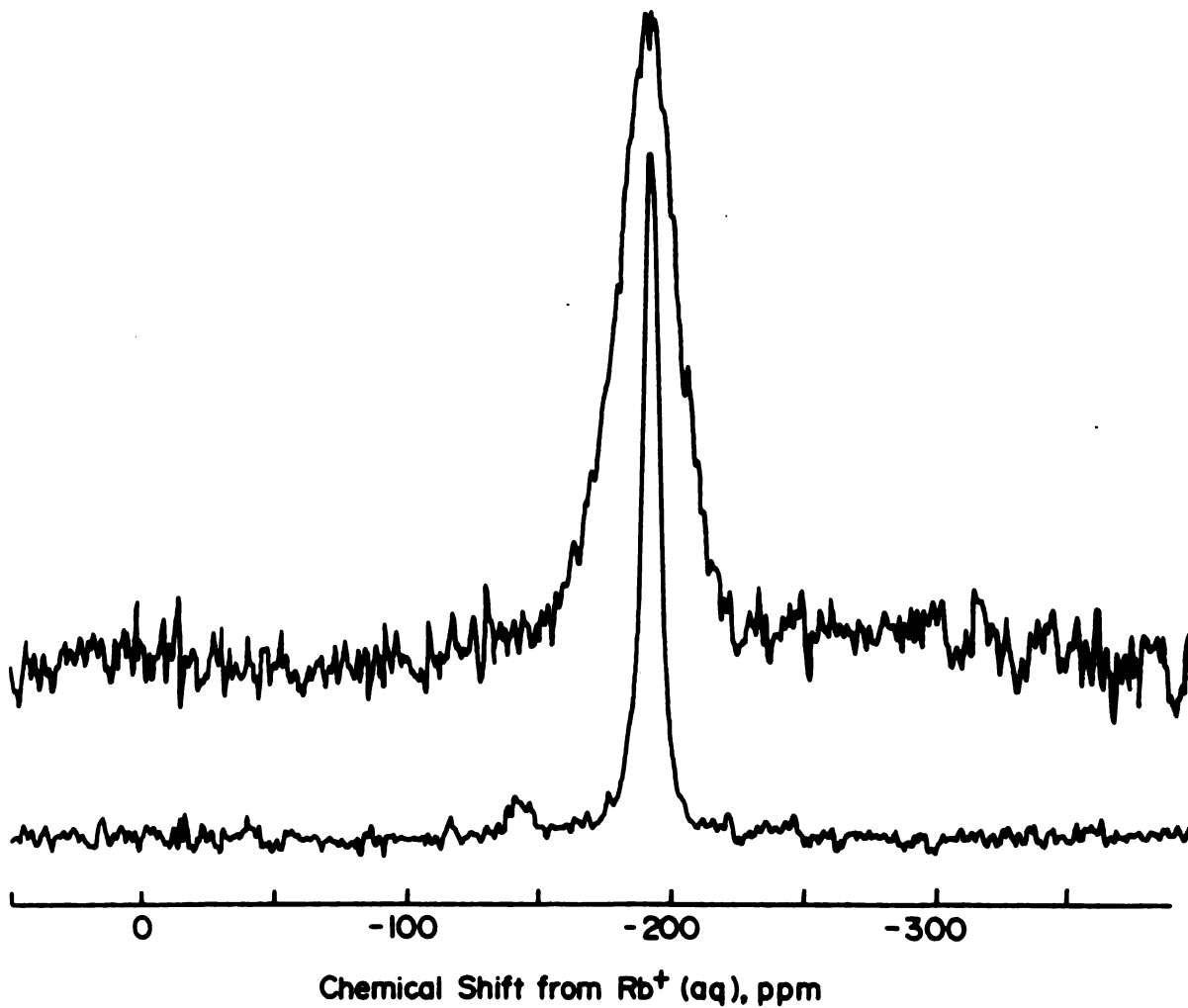


Figure 32. ^{87}Rb NMR Spectra of Polycrystalline $\text{Rb}^+(\text{15C5})_2 \cdot \text{Rb}^-$ at 65.4 MHz. Top, static coupled spectrum; bottom, MAS coupled spectrum.

Reduction of the static linewidth of Rb^- upon proton decoupling ranged from ~250 Hz for $\text{Cs}^+(\text{18C6})_2 \cdot \text{Rb}^-$ to ~650 Hz for $\text{Cs}^+(\text{15C5})_2 \cdot \text{Rb}^-$. Calculation of the expected dipolar contribution by the method of Van Vleck [105] would require knowledge of the crystal structures, which are not available for these compounds. However, an estimate can be made by increasing the known Na^- to H distances for $\text{Cs}^+(\text{18C6})_2 \cdot \text{Na}^-$ [57] to accommodate the larger size of Rb^- . These calculations yielded a dipolar contribution of ~900 Hz which is much larger than that observed for $\text{Cs}^+(\text{18C6})_2 \cdot \text{Rb}^-$. This suggests, as with the sodides [57], rapid motion of the CH_2 protons of the 18-crown-6 molecule at the temperatures at which the NMR measurements were made.

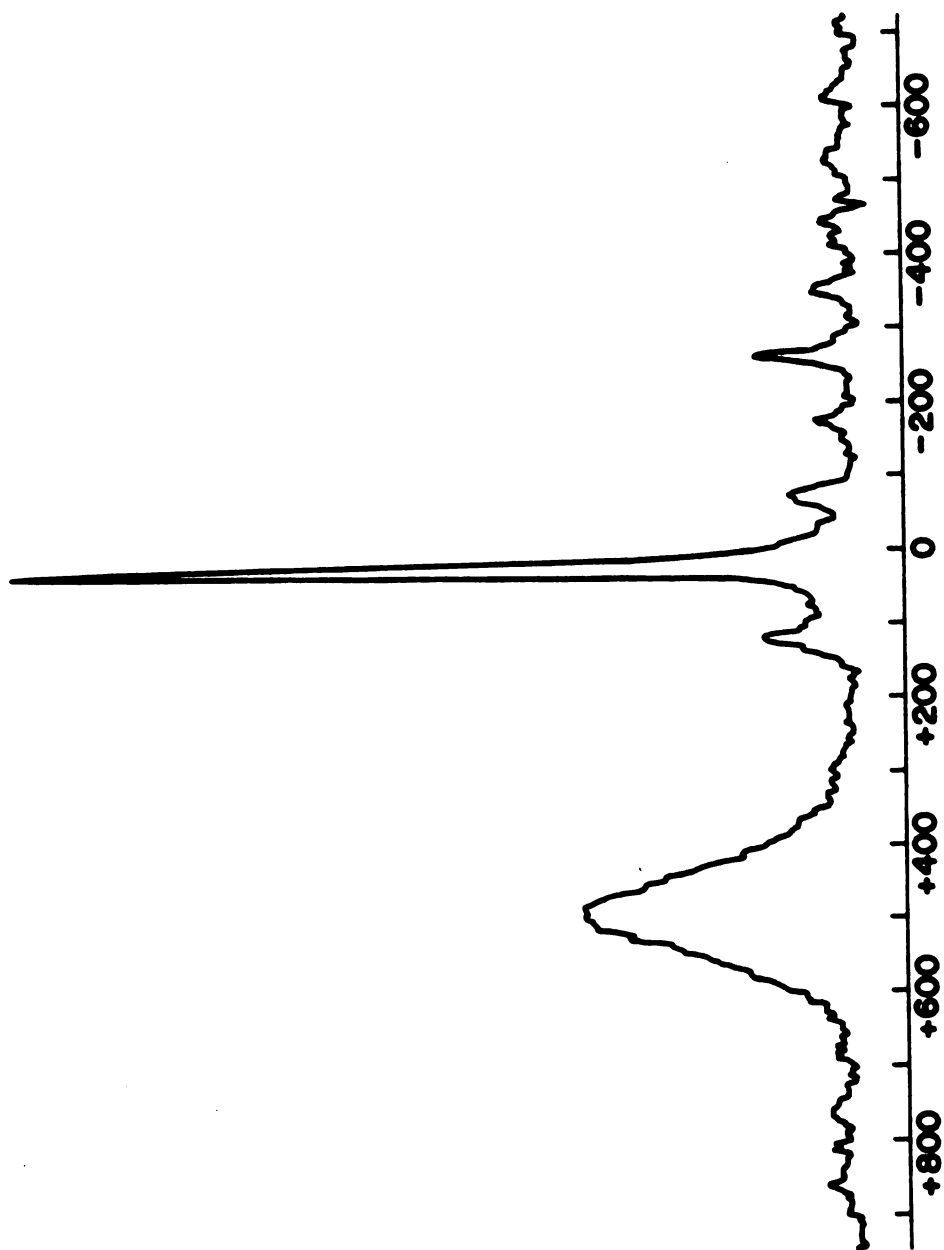
The use of ^{87}Rb MAS-NMR provides an excellent confirmation of the presence of Rb^- in crystalline alkalides. However, the absence of a signal does not necessarily mean that Rb^- is absent. The signal of complexed Rb^+ in the solid is too broad to detect but both $\text{Rb}^+(\text{15C5})_2$ and Rb^- were detected in Me_2O solutions. The quadrupole coupling constant of Rb^- in crystals is 1.2 ± 0.2 MHz, while that of complexed Rb^+ is probably at least an order of magnitude larger. Comparison of proton-coupled and proton-decoupled static linewidths indicated the presence of $-\text{CH}_2$ motion in the complexant, even in the solid state. Extrapolation of the chemical shift to infinite frequency gives an isotropic chemical shift of -186 ± 2 ppm for Rb^- in crystalline

rubidides, which falls within the range of Rb^- chemical shifts in solution.

D. ^{133}Cs NMR Spectra

Extensive ^{133}Cs MAS-NMR studies have been done by Ellaboudy and coworkers [42,53,99] and Dawes [57] as described in Part II-Chapter One of this dissertation. In the present work, ^{133}Cs MAS-NMR was used to identify the compounds whose synthesis and characterization were described in Part I. The unusually small electric quadrupole moment of $-3 \times 10^{-27} \text{ cm}^2$ and 100 percent abundance of ^{133}Cs provide ideal conditions for NMR studies. The chemical shifts of Cs^- , $\text{Cs}^+(\text{18C6})_2 \cdot \text{e}^-$ and $\text{Cs}^+(\text{18C6})_2 \cdot \text{X}^-$, where X^- is a diamagnetic anion, are separated by several hundred ppm [53]. It was hoped that the peaks of the corresponding 15-crown-5 complexes would be similarly separated from Cs^- and each other so that exact identification could be made.

The ^{133}Cs MAS-NMR spectrum of $\text{CsRb}(\text{15C5})_{2.5}$ represented in Figure 33 clearly shows the separation of the various cesium signals. The peaks at +505, +29 and -263 ppm from $\text{Cs}^+(\text{aq})$ at infinite dilution are assigned to $\text{Cs}^+(\text{15C5})_2 \cdot \text{e}^-$, $\text{Cs}^+(\text{15C5})_2 \cdot \text{X}^-$ and Cs^- , respectively. This sample had a ^{87}Rb MAS-NMR peak at -194 ppm which indicates that Rb^- was also present. Obviously, this sample consisted of a mixture of $\text{Cs}^+(\text{15C5})_2 \cdot \text{e}^-$, $\text{Cs}^+(\text{15C5})_2 \cdot \text{Rb}^-$ and probably $\text{Rb}^+(\text{15C5})_2 \cdot \text{Rb}^-$ with some Cs^- contamination. Another sam-



CHEMICAL SHIFT FROM Cs^+ (aq), ppm

Figure 33. ^{133}Cs MAS-NMR Spectrum of an Impure Sample of $\text{Cs}^+ (15\text{C}5)_2 \cdot \text{Rb}^-$.

ple, without excess 15-crown-5, gave a cleaner spectrum. The ^{133}Cs MAS-NMR spectrum of $\text{Cs}^+(\text{15C5})_2\cdot\text{Rb}^-$ is shown in Figure 34. The major peak at -29 ppm corresponds to $\text{Cs}^+(\text{15C5})_2\cdot\text{X}^-$. A small but discernible peak at -265 ppm indicates a small amount of Cs^- in the sample.

The results of the ^{133}Cs MAS-NMR studies of the 15-crown-5 alkalides that contain cesium are given in Table XIII. Each compound has a chemical shift in the range of 24-29 ppm which corresponds to diamagnetic $\text{Cs}^+(\text{15C5})_2$ salts. Often a small peak at ~260 ppm would be observed in the spectrum of $\text{Cs}^+(\text{15C5})_2\cdot\text{K}^-$ or $\text{Cs}^+(\text{15C5})_2\cdot\text{Rb}^-$ and indicated a small amount of Cs^- in these samples. The narrowness of the $\text{Cs}^+(\text{15C5})_2$ peak (130-270 Hz) compared to that of Cs^- in $\text{Cs}^+(\text{18C6})_2\cdot\text{Cs}^-$ (350 Hz) is unexpected for a cesium cation in an environment with axial symmetry. Temperature studies by S. Dawes show an increase of the linewidth for $\text{Cs}^+(\text{15C5})_2$ with a decrease in temperature [57]. The unusual narrowness of the complexed cation peak may be due to molecular motion at higher temperatures as in the case of Rb^- previously observed.

The frequency dependence of ^{133}Cs MAS-NMR spectra studied by Ellaboudy indicates that the quadrupole interactions are minimal and that the chemical shift anisotropy and magnetic dipole interactions are the main source of line broadening in $\text{Cs}^+(\text{18C6})_2$ compounds [53]. In contrast to the ^{87}Rb MAS-NMR studies, the chemical shifts were independent of the Larmor frequency. The quadrupole coupling

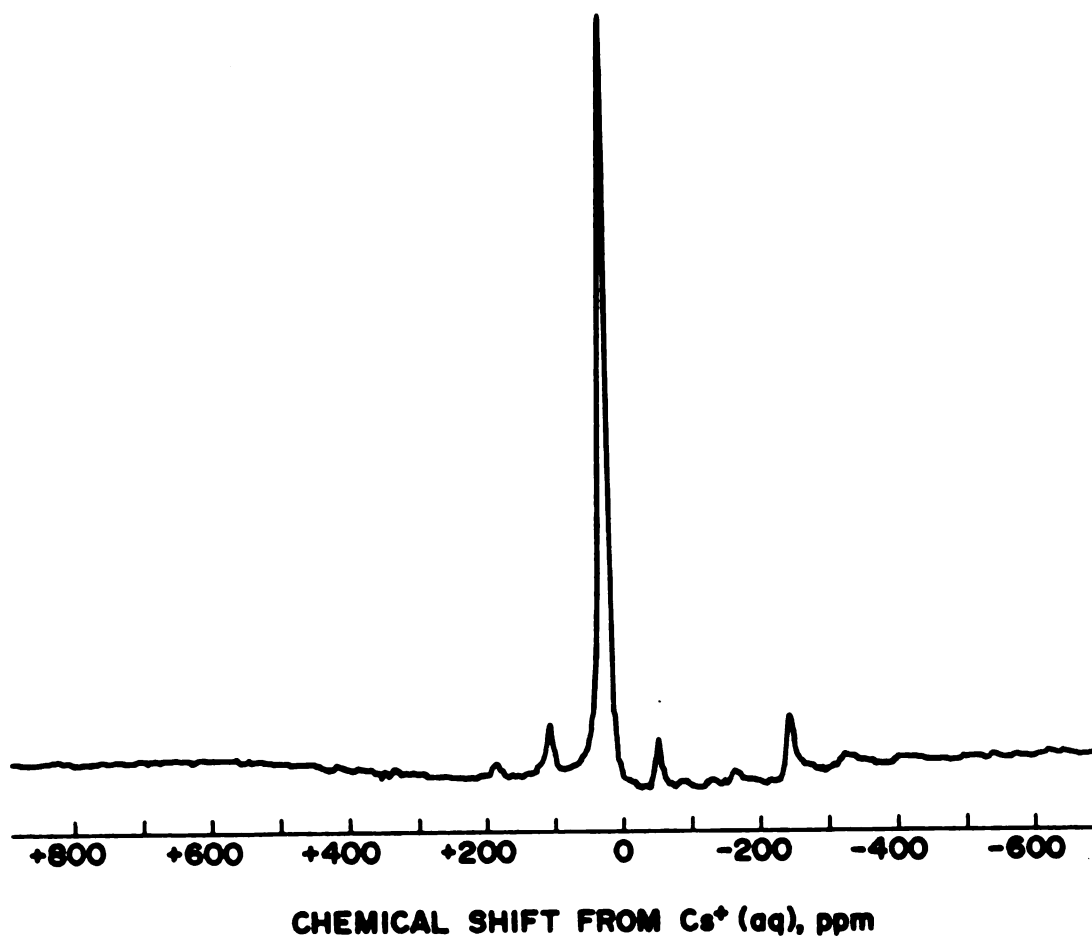


Figure 34. ^{133}Cs MAS-NMR Spectrum of $\text{Cs}^+(\text{15C5})_2 \cdot \text{Rb}^-$ at 23.62 MHz.

TABLE XIII. Results of ^{133}Cs MAS NMR Studies.

<u>Compound</u>	<u>δ, ppm from Cs^+ at Infinite Dilution</u>	<u>$\Delta\nu_{1/2}$, Hz</u>
CsI	+284	---
$\text{Cs}^+(\text{15C5})_2 \cdot \text{Na}^-$	+24	130
$\text{Cs}^+(\text{15C5})_2 \cdot \text{K}^-$	+24	270
$\text{Cs}^+(\text{15C5})_2 \cdot \text{Rb}^-$	+29	250

constants for $\text{Cs}^+(\text{18C6})_2$ and $\text{Cs}^+(\text{15C5})_2$ were calculated from the location of the satellite peaks with respect to the central transition for each spectrum.

In conclusion, ^{133}Cs MAS-NMR is very useful for the identification of alkalides and electriles since the complexed cation as well as the anion are easily observed. The chemical shift of $\text{Cs}^+(\text{15C5})_2$ is independent of the anion as long as the anion is diamagnetic. Impurities such as trapped electrons cause large paramagnetic shifts which are indicative of cation-anion interactions. Small amounts of Cs^- could be detected in some samples. The chemical shift of Cs^- was ~ -260 ppm in contrast to the calculated value of -346 ppm for $\text{Cs}^-(\text{g})$ [76]. The large paramagnetic shift of Cs^- from the gaseous anion indicates strong interaction of Cs^- with the environment and the less effective shielding of the ^{133}Cs nucleus by the ns^2 electrons than that observed for ^{23}Na and ^{39}K .

SUMMARY AND SUGGESTIONS FOR FUTURE WORK

Ten new crystalline systems were isolated from solutions of alkali metals and 15-crown-5. Elemental analysis and optical absorption spectroscopy identified two of these compounds as the electrides, $K^+(15C5)_2 \cdot e^-$ and $Rb^+(15C5)_2 \cdot e^-$. The remaining compounds are alkalide salts. In all cases the alkali metal cation is thought to be "sandwiched" between two 15-crown-5 molecules. This configuration has been confirmed for Rb^+ in $Rb^+(15C5)_2 \cdot Na^-$ by single crystal X-ray diffraction studies. The use of optical absorption spectroscopy as an identification tool was found to yield ambiguity in the case of systems with the stoichiometry $KRb(15C5)_2$ and $CsRb(15C5)_2$. The assignments of these salts as a mixed alkalide and $Cs^+(15C5)_2 \cdot Rb^-$, respectively were based on rubidium XANES data. In general, only the sodide salts could be identified by optical absorption spectroscopy with a fair degree of certainty; the other alkalides had very broad absorption peaks and it was difficult to make exact assignments of the anions.

Pressed powder conductivity measurements indicate that all of the new compounds behave as semiconductors with relatively small apparent band gaps. The calculated resis-

tivities are much larger than those expected for intrinsic semiconductors with the observed band gaps. The conductivity arises from impurities in the crystal. The electrider salts, $K^+(15C5)_2 \cdot e^-$ and $Rb^+(15C5)_2 \cdot e^-$, both had higher conductivities than the alkalides salts, indicative of the presence of more carriers in the electrideres.

Preliminary EPR and magnetic susceptibility studies were used to probe the environment of the electron in $K^+(15C5)_2 \cdot e^-$ and $Rb^+(15C5)_2 \cdot e^-$. The EPR spectra of each electrider had very narrow, single lines at the free electron g-value. The narrowness of the line and the absence of a g-shift indicate that the electrons have very few interactions with neighboring atoms and undergo rapid exchange. The lines were asymmetric with A/B ratios less than 2.7. This lineshape is consistent with those observed for small particles with high conductivity where the skin depth is on the order of the particle size. Spectra were recorded at only one temperature.

The molar susceptibility of each electrider deviated substantially from Curie-Weiss behavior at low temperatures. The apparent Curie constants at high temperature correspond to 94 percent unpaired spins for $K^+(15C5)_2 \cdot e^-$ and 55 percent unpaired spins for $Rb^+(15C5)_2 \cdot e^-$. Each electrider had a temperature independent contribution to the observed susceptibility. In the case of $Rb^+(15C5)_2 \cdot e^-$, a small amount of Rb^- may be present. The temperature independent contribution for $K^+(15C5)_2 \cdot e^-$ is too large to be

attributed to K^- . A probable cause of the magnitude of this term is the use of an inappropriate equation to describe the magnetic behavior.

In general, the new alkalides and electriles are relatively stable. Most of the new compounds may be handled at room temperatures for time periods up to 10 minutes. The stability makes characterization studies relatively easy to complete. Differential scanning calorimetry studies determined the melting points of $Rb^+(15C5)_2 \cdot Na^-$ and $K^+(15C5)_2 \cdot Na^-$ to be 75 and 45°C, respectively. The higher melting point of $Rb^+(15C5)_2 \cdot Na^-$ makes it the most stable alkalide characterized to date. The ease of preparation and stability indicates that $Rb^+(15C5)_2 \cdot Na^-$ is the most likely candidate to be used as a two electron reductant. For the alkalides, the stability decreases with an increase in anion size. The electriles are sufficiently stable to resist decomposition at room temperature for short periods of time. However, decomposition of the crystals occurs at a very slow rate when stored at -80°C.

Identification of alkalides and electriles without ambiguity has been a major problem. Alkali-metal magic angle spinning NMR is a technique that can be applied to each alkali metal for the identification of alkalides and electriles. The MAS-NMR spectra have been recorded for several alkalides. The generalizations, which can be made from these spectra, are as follows:

^{23}Na NMR can be used to detect the presence of both the complexed sodium cation and the sodium anions in the solid. The chemical shift range observed for Na^- is -56 to -63 ppm, which indicates very effective shielding of the 2p orbitals by the filled 3s orbital.

Potassium 39 was used for the NMR studies. The first NMR observation of K^- , both in solution and in the solid state was made. The chemical shifts observed were -99.3 ppm for K^- in dimethylether and -105 to -115 ppm for K^- in crystalline potas-sides. These shifts are in good agreement with the calculated value of $\text{K}_{(g)}^-$ at -107 ppm and are reflective of highly efficient shielding of inner orbitals by the two 4s electrons. No signal was observed for the complexed cation, presumably due to the large quadrupolar coupling constant.

^{87}Rb MAS-NMR can detect Rb^- in crystalline alkali-lides but the absence of a signal does not necessarily mean that Rb^- is absent. The signal of complexed Rb^+ in the solid was too broad to detect even though both $\text{Rb}^+(\text{15C5})_2$ and Rb^- were detected in Me_2O solutions. The chemical shift of Rb^- in the solid state was dependent on frequency and extrapolation to infinite frequency yielded an isotropic chemical shift of -186 ± 2 ppm. The

calculated chemical shift value of $\text{Rb}^-_{(g)}$ is -214 ppm. Therefore, Rb^- is slightly more deshielded than Na^- or K^- .

-The chemical shifts observed by ^{133}Cs MAS-NMR for $\text{Cs}^+(\text{15C5})_2 \cdot \text{e}^-$, $\text{Cs}^+(\text{15C5})_2 \cdot \text{X}^-$ and Cs^- are sufficiently separated so that these species can be readily identified. Therefore, ^{133}Cs MAS-NMR can be used to check the purity of a given alkalide system. Three alkalides were identified by ^{133}Cs NMR. The chemical shift observed for Cs^- was -260 ppm compared to the calculated value of -348 ppm for $\text{Cs}^-_{(g)}$. This value indicates even further deshielding of Cs^- relative to Rb^- .

-The deviation of the chemical shift of $\text{M}^-_{(s)}$ from the calculated value for $\text{M}^-_{(g)}$, calculated increases with the atomic number for the alkalide anions. This could be caused by less effective shielding of p and/or d electrons by the valence s electrons or by an admixture of p and/or d character with the ground-state s wave functions.

Finally, seven of the new crystalline alkalides, which were described in Part I, have been identified without ambiguity by alkali metal NMR. They are $\text{K}^+(\text{15C5})_2 \cdot \text{Na}^-$, $\text{K}^+(\text{15C5})_2 \cdot \text{K}^-$, $\text{Rb}^+(\text{15C5})_2 \cdot \text{Na}^-$, $\text{Rb}^+(\text{15C5})_2 \cdot \text{Rb}^-$, $\text{Cs}^+(\text{15C5})_2 \cdot \text{Na}^-$, $\text{Cs}^+(\text{15C5})_2 \cdot \text{K}^-$ and $\text{Cs}^+(\text{15C5})_2 \cdot \text{Rb}^-$. The eighth system, which had the stoichiometry $\text{KRb}(\text{15C5})_2$, was

shown to be a mixture with K^- , Rb^- , $Rb^+(15C5)_2$ and $K^+(15C5)_2$ present.

The work presented in this dissertation can serve as a springboard for several other experiments. First, the electriles, $K^+(15C5)_2 \cdot e^-$ and $Rb^+(15C5)_2 \cdot e^-$, appear to have fascinating magnetic properties. Careful, low field, low temperature susceptibility measurements are needed to determine the exact types of localized magnetic interactions. The EPR studies of the electriles should also be continued to include the temperature and dilution dependencies of the line shape.

Second, a need for crystal structures is present and these compounds, for the most part, have sufficient stability so that X-ray diffraction studies are feasible. These studies require high quality single crystals and therefore, the crystallization techniques need to be improved. Besides X-ray diffraction studies, high quality single crystals could be used in investigations of the orientation dependence of the EPR and MAS-NMR spectra and AC and DC conductivity experiments.

Third, the presence of a Cs^- signal in the ^{133}Cs MAS-NMR spectra indicates that the final alkalide in the series, $Cs^+(15C5)_2 \cdot Cs^-$, may be synthesized.

Fourth, the field dependence of the K^- signal should be checked by ^{39}K MAS NMR at higher field strengths. The availability of appropriate instruments is limited by the low Larmor frequency of the ^{39}K nucleus and these studies

would have to be done at other NMR facilities at this time.

Finally, the synthesis of new alkalides and electriles should be pursued with other complexants such as 12-crown-4, 21-crown-7 or "lariat" ethers. The most easily available may be those compounds that contain 12-crown-4 due to its relatively low cost and commercial availability. New electriles are especially desirable for the study of magnetic properties and the understanding of the nature of the trapped electron.

LIST OF REFERENCES

1. P.P. Edwards, *Adv. Inorg. Chem. Radiochem.* 25, 135 (1982).
2. W. Weyl, *Annalen der Physik und Chemie* 197, 601 (1864).
3. G. Lepoutre and M.J. Seinko, Eds., "Metal-Ammonia Solutions, Colloque Weyl I", W.A. Benjamin, New York, 1964.
4. J.J. Lagowski and M.J. Seinko, Eds., "Metal-Ammonia Solutions, Colloque Weyl II", IUPAC Butterworth, London, 1970.
5. J. Jortner and N.R. Kestner, Eds., "Electrons in Fluids, Colloque Weyl III", Springer-Verlag, Berlin, 1973.
6. J.L. Dye, Conference Organizer, "Colloque Weyl IV, Electrons in Fluids -- The Nature of Metal-Ammonia Solutions", *J. Phys. Chem.* 79(26), (1975).
7. B. Webster, Conference Organizer, "Colloque Weyl V, The Fifth International Conference on Excess Electrons and Metal-Ammonia Solutions," *J. Phys. Chem.* 84 (10), (1980).
8. J. C. Thompson, Conference Organizer, "Colloque Weyl VI, Le Dernier Colloque Weyl, The Sixth International Conference on Excess Electrons and Metal-Ammonia Solutions," *J. Phys. Chem.* 88 (17), (1984).
9. C. A Kraus, *J. Chem. Educ.* 30, 83 (1953).
10. W. L. Jolly, *Prog. Inorg. Chem.* 1, 235 (1959).
11. M. C. R. Symons, *Q. Rev.* 13, 99 (1959).

12. U. Schindewolf, *Angew Chem.* 80, 165 (1968); *Angew Chem. Int. Eng. Ed.* 7, 190 (1968).
13. T. P. Das, *Adv. Chem. Phys.* 4, 303 (1962).
14. J. L. Dye, *Sci. Amer.* 216 (77), (Feb. 1967).
15. M. H. Cohen and J. C. Thompson, *Adv. Phys.* 17, 847 (1968).
16. R. Catterall and N.F. Mott, *Adv. Phys.* 18, 665 (1969).
17. L. Kevan and B. Webster, Eds., "Electron-Solvent and Anion-Solvent Interactions", New York, 1976.
18. M.C. R. Symons, *Chem. Soc. Rev.* 5, 337 (1976).
19. J. C. Thompson, "Electrons in Liquid Ammonia", Oxford University Press, Oxford, 1976.
20. J. L. Dye, *Prog. Inorg. Chem.* 32, 237 (1984).
21. J. T. Lin, G. P. Hagen and J. E. Ellis, *J. Am. Chem. Soc.* 105, 2296 (1983).
22. P. P. Edwards and M. J. Sienko, *Acc. Chem. Res.* 15, 87 (1982).
23. B. Van Eck, Ph.D. Dissertation, Michigan State University, 1983.
24. R. R. Dewald and J. L. Dye, *J. Phy. Chem.* 68, 128 (1964).
25. J. L. Dye, *Angew Chem. Int. Ed., Eng.* 18, 587 (1979).
26. C. J. Pedersen, *J. Am. Chem. Soc.* 89, 7017 (1967); 92, 386 (1970).
27. B. Dietrick, J.-M. Lehn and P. J. Sauvage, *Tetrahedron Lett.* 34, 2885 (1969).
28. R. R. Dewald, S. R. Jones and B. S. Schwartz, *J. Chem. Soc., Chem. Commun.* 1980, 272 (1980).
29. D. M. Holten, P. P. Edwards, D. C. Johnson, C. J. Page, W. McFarlane and B. Wood, *J. Chem. Soc., Chem. Commun.* 1984, 740 (1984).
30. J. D. Lamb, R. M. Izatt, C. S. Swain and J. J. Christensen, *J. Am. Chem. Soc.* 102, 475 (1980).

31. J. L. Dye, J. M. Ceraso, M. T. Lok, B. L. Barnett and F. J. Tehan, *J. Am. Chem. Soc.* 96, 608 (1974).
32. F. J. Tehan, B. L. Barnett and J. L. Dye, *J. Am. Chem. Soc.* 96, 7203 (1974).
33. J. L. Dye, *J. Chem. Ed.* 54, 332 (1977).
34. U. Schindewolf and M. Werner, *J. Phys. Chem.* 84, 1123 (1980).
35. M. Werner and U. Schindewolf, *Ber. Bunsenges. Phys. Chem.* 84, 547 (1980).
36. W. Gross and U. Schindewolf, *Ber. Bunsenges. Phys. Chem.* 85, 112 (1981).
37. U. Schindewolf, L. D. Le and J. L. Dye, *J. Phys. Chem.* 86, 2284 (1982).
38. F. N. Tientega, M.S. Dissertation, Michigan State University, 1984.
39. J. L. Dye, C. W. Andrews and S. E. Mathews, *J. Phys. Chem.* 79, 3065 (1975).
40. B. Van Eck, L. D. Le, D. Issa, and J. L. Dye, *Inorg. Chem.* 21, 1966 (1982).
41. D. Issa and J. L. Dye, *J. Am. Chem. Soc.* 104, 3781 (1982).
42. A. Ellaboudy, J. L. Dye and P. B. Smith, *J. Am. Chem. Soc.* 105, 6490 (1983).
43. J. L. Dye, *J. Phys. Chem.* 88, 3842 (1984).
44. D. Issa, A. Ellaboudy, R. Janakiraman and J. L. Dye, *J. Phys. Chem.* 88, 3847 (1984).
45. J. L. Dye, M. R. Yemen, M. G. DaGue and J.-M. Lehn, *J. Chem. Phys.* 68, 1665 (1978).
46. M. G. DaGue, J. S. Landers, H. L. Lewis and J. L. Dye, *Chem. Phys. Lett.* 66, 169 (1979).
47. J. L. Dye, M. G. DaGue, M. R. Yemen, J. S. Landers, and H. L. Lewis, *J. Phys. Chem.* 84, 1096 (1980).
48. J. S. Landers, J. L. Dye, A. Stacy and M. J. Sienko, *J. Phys. Chem.* 85, 1096 (1981).

49. L. D. Le, D. Issa, B. Van Eck and J. L. Dye, *J. Phys. Chem.* 86, 7 (1982).
50. M. K. Faber, Ph.D. Dissertation, Michigan State University, 1985.
51. M. L. Tinkham, M.S. Dissertation, Michigan State University, 1982.
52. D. Issa, Ph.D. Dissertation, Michigan State University, 1982.
53. A. S. Ellaboudy, Ph.D. Dissertation, Michigan State University, 1984.
54. F.N. Tientega, unpublished results.
55. M. G. DaGue, Ph.D. Dissertation, Michigan State University, 1979.
56. J. S. Landers, Ph.D. Dissertation, Michigan State University, 1981.
57. S. B. Dawes, unpublished results.
58. DISNMR, Disk Interactive Spectroscopy on the Aspect 2000 minicomputer, version 81091, Bruker instrument, Inc., 1981.
59. M. R. Yemen, Ph.D. Dissertation, Michigan State University, 1982.
60. J. Papaioannou, unpublished results, this laboratory.
61. J. L. Dye and V. A. Nicely, *J. Chem. Ed.* 48, 43 (1971).
62. R. S. Alger, "Electron Paramagnetic Resonance: Techniques and Applications", Interscience Publishers, New York, 1968.
63. D. C. Mattis, "The Theory of Magnetism", Harper & Row, New York, 1965.
64. O. Fussá, S. Kauzlarich, J. L. Dye and B. K. Teo, *J. Am. Chem. Soc.* 107, 3727 (1985).
65. O. Fussá, B. K. Teo and J. L. Dye, to be submitted to *J. Am. Chem. Soc.*
66. R. K. Harris, "Nuclear Magnetic Resonance Spectroscopy", Pitman Books, Ltd., London, 1983.

67. B. Lindman and S. Forsén, "NMR and the Periodic Table", (R. K. Harris and B. Mann, eds.), p. 129, Academic Press, New York, 1978.
68. F. W. Wehrli, "Annual Reports on NMR Spectroscopy", (G.A. Webb, ed.), p. 126, Academic Press, New York, 1979.
69. S. Forsén and B. Lindman, *Meth. Biochem. Anal.* 27, 270 (1981).
70. K. J. Neurohr, T. Drakenberg, S. Forsén and H. Lilja, *J. Magn. Reson.* 51, 460 (1983).
71. S. Khazaeli, J. L. Dye and A. I. Popov, *Spectrochimica Acta* 39A, 19 (1983).
72. J. M. Ceraso and J. L. Dye, *J. Chem. Phys.* 61, 1585 (1974).
73. J. L. Dye, C. W. Andrews and J. M. Ceraso, *J. Phys. Chem.* 79, 3076 (1975).
74. A. Beckmann, K. D. Böklen and D. Elke, *Z. Phys.* 270, 173 (1975).
75. W. Lamb, *Phys. Rev.* 60, 817 (1941).
76. N. C. Pyper and P.P. Edwards
77. P. P. Edwards, S. C. Guy, D. M. Holton and W. McFarlane, *J. Chem. Soc., Chem. Commun.*, 1185 (1981).
78. P. P. Edwards, S. C. Guy, D. M. Holton, D. C. Johnson, M. J. Sienko, W. McFarlane and B. Wood, *J. Phys. Chem.* 87, 4362 (1983).
79. P. P. Edwards, *J. Phys. Chem.* 88, 3772 (1984).
80. R. C. Phillips, S. Khazaeli and J. L. Dye, *J. Phys. Chem.* 89, 606 (1985).
81. P. B. Smith, Ph.D. Dissertation, Michigan State University, 1978.
82. J. L. Dye, in "Progress in Macrocyclic Chemistry", (R. M. Izatt and J. J. Christensen, eds.), Wiley-Interscience, New York, Vol. 1, p. 63, (1979).
83. E. R. Andrew, W. S. Hinshaw and A. Jasinski, *Chem. Phys. Lett.* 24, 399 (1974).
84. E. R. Andrew, *Prog. NMR Spectrosc.* 8, 1 (1971).

85. P. Mansfield, *Prog. NMR Spectrosc.* 8, 41 (1971).
86. U. Haeberlen, *Adv. Magn. Reson., Suppl.* (1) (1976).
87. M. Mehring, *NMR Basic Principles & Prog.* 11 (1976).
88. "NMR Spectroscopy in Solids", (Proceedings of a Symposium), The Royal Society (London) (1981).
89. A. C. Cunningham and S. M. Day, *Phys. Rev.* 152 (287), (1966).
90. S. Ganapathy, S. Schramm and E. Oldfield, *J. Chem. Phys.* 77, 4360 (1982).
91. K. Narita, J.-I. Umeda and H. Kusumoto, *J. Chem. Phys.* 44, 2719 (1966).
92. E. Kundla, A. Samoson and E. Lippmaa, *Chem. Phys. Lett.* 83, 229 (1981).
93. V.D. Müller, *Annalen der Physik* 7, 451 (1982).
94. D. Freude, J. Haase, J. Klinowski, T. A. Carpenter and G. Ronikier, *Chem. Phys. Lett.* 119, 365 (1985).
95. A. Samoson, *Chem. Phys. Lett.* 119, 29 (1985).
96. H.-J. Behrens and B. Schnabel, *Physica* 114B, 185 (1982).
97. E. Oldfield and R. J. Kirkpatrick, *Science* 227, 1537 (1985).
98. A. Ellaboudy, M. L. Tinkham, B. Van Eck, P. B. Smith and J. L. Dye, *J. Phys. Chem.* 88, 3852 (1984).
99. J. L. Dye and A. Ellaboudy, *Chem. Br.* 20, 210 (1984).
100. E. Oldfield, S. Schramm, M. D. Meadows, K. A. Smith, R. A. Kinsey and J. Ackerman, *J. Am. Chem. Soc.* 104, 919 (1982).
101. M. D. Meadows, K. A. Smith, R. A. Kinsey, T. M. Rothgeb, R. P. Sarjune and E. Oldfield, *Proc. Nat. Acad. Sci. USA* 79, 1351 (1982).
102. A. Ellaboudy and J. L. Dye, *J. Magn. Reson.*, in press.
103. P. P. Edwards and A. Ellaboudy, *Nature*, 317, 242 (1985).

104. M. L. Tinkham, A. Ellaboudy, P. B. Smith and J. L. Dye, *J. Phys. Chem.*, in press.
105. J. H. VanVleck, *Phys. Rev.* 74, 1168 (1948).

MICHIGAN STATE UNIVERSITY LIBRARIES



3 1293 03177 8594